



BRNO UNIVERSITY OF TECHNOLOGY

VYSOKÉ UČENÍ TECHNICKÉ V BRNĚ

FACULTY OF ELECTRICAL ENGINEERING AND COMMUNICATION

FAKULTA ELEKTROTECHNIKY
A KOMUNIKAČNÍCH TECHNOLOGIÍ

DEPARTMENT OF RADIO ELECTRONICS

ÚSTAV RADIOELEKTRONIKY

SIGNAL INTEGRITY OPTIMIZATION TECHNIQUES FOR HIGH-SPEED CHIPS SIGNALING

METODY OPTIMALIZACE PRO ZAJIŠTĚNÍ INTEGRITY SIGNÁLŮ PRO VYSOKORYCHLOSTNÍ PŘENOS DAT
MEZI ČIPY

DOCTORAL THESIS

DIZERTAČNÍ PRÁCE

AUTHOR

AUTOR PRÁCE

Ing. Břetislav Ševčík

SUPERVISOR

ŠKOLITEL

prof. Ing. Lubomír Brančík, CSc.

BRNO 2016

ABSTRACT

The doctoral thesis deals with signal integrity problems in modern chip circuits. Based on the simulation and practical experiments an optimized second order pre-emphasis signaling technique is proposed. High bandwidth efficiency of signal pre-emphasis together with a minimum voltage swing during signal emphasizing and still lower power dissipation are the main features respected in the proposal. The performed analysis clearly shows that proposed pulse shaping method due to the spectral efficiency can increase the transmission bandwidth of low cost wire channels. The performance of proposed signaling technique is demonstrated on various type channels with higher order transfer function. Additional channel impairments which can occur during transmission channel design are discussed too.

KEYWORDS

High-speed communications, inter-chip interconnects, transmission lines, equalization, pre-emphasis, pulse shaping methods, signal integrity

ABSTRAKT

Tato disertační práce je obsahově zaměřená na problematiku integrity signálů v moderních čipových obvodech. Na základě provedených simulací a praktických experimentů byl proveden návrh equalizační techniky druhého řádu pro efektivnější vysokorychlostní komunikaci. Předložený návrh respektuje současné požadavky na vyvíjené signalizační techniky, které zahrnují efektivnější využití šířky pásma přenosového kanálu a energetickou úsporu. Provedené analýzy podrobně ukazují možnost zvýšení přenosové rychlosti při přenosu signálu skrz nízkonákladové přenosové kanály s využitím navržené signální metody. Výkonnost navrhované signalizační techniky je demonstrována na různých typech přenosových kanálů s přenosovou funkcí vyššího řádu. Diskutovány jsou rovněž možnosti omezení rušivých vlivů na přenosové kanály během návrhu.

KLÍČOVÁ SLOVA

Vysokorychlostní komunikace, komunikace mezi čipy, přenosové vedení, ekvalizace, preemfáze, metody tvarování pulsů, integrita signálu

ŠEVČÍK, B. *Signal Integrity Optimization Techniques for High-Speed Chips Signaling*. Brno: Vysoké učení technické v Brně, Fakulta elektrotechniky a komunikačních technologií. Ústav radioelektroniky, 2016. 111 s. Disertační práce. Vedoucí práce: prof. Ing. Lubomír Brančík, CSc.

PROHLÁŠENÍ

Prohlašuji, že svou disertační práci na téma Signal Integrity Optimization Techniques for High-Speed Chips Signaling jsem vypracoval samostatně pod vedením vedoucího disertační práce a s použitím odborné literatury a dalších informačních zdrojů, které jsou všechny citovány v práci a uvedeny v seznamu literatury na konci práce.

Jako autor uvedené disertační práce dále prohlašuji, že v souvislosti s vytvořením této disertační práce jsem neporušil autorská práva třetích osob, zejména jsem nezasáhl nedovoleným způsobem do cizích autorských práv osobnostních a/nebo majetkových a jsem si plně vědom následků porušení ustanovení § 11 a následujících zákona č. 121/2000 Sb., o právu autorském, o právech souvisejících s právem autorským a o změně některých zákonů (autorský zákon), ve znění pozdějších předpisů, včetně možných trestněprávních důsledků vyplývajících z ustanovení části druhé, hlavy VI. díl 4 Trestního zákoníku č. 40/2009 Sb.

V Brně dne

.....

(podpis autora)

PODĚKOVÁNÍ

Děkuji vedoucímu disertační práce prof. Ing. Lubomíru Brančíkovi, CSc. za účinnou metodickou, pedagogickou a odbornou pomoc a další cenné rady při zpracování mé disertační práce.

V Brně dne

.....

(podpis autora)



Faculty of Electrical Engineering
and Communication
Brno University of Technology
Technická 12, CZ-616 00 Brno
Czech Republic
<http://www.six.feec.vutbr.cz>

Research described in this doctoral thesis has been implemented in the laboratories supported by the SIX project; reg. no. CZ.1.05/2.1.00/03.0072, operational program Research and Development for Innovation.

Brno

.....
(author's signature)



EVROPSKÁ UNIE
EVROPSKÝ FOND PRO REGIONÁLNÍ ROZVOJ
INVESTICE DO VAŠÍ BUDOUCNOSTI



ACKNOWLEDGMENT

Research described in this doctoral thesis has been supported by Czech Science Foundation under grant no. 15-18288S, *Research of signal integrity at high-speed interconnects*.

CONTENT

1 INTRODUCTION	13
2 STATE OF THE ART	14
2.1 High-Speed Interconnect	14
2.2 Channel Measurements Results	19
2.3 Performance of pulse-width adjusting	26
2.4 Basic Concept of Equalization	28
2.5 Solutions from Literature	29
2.5.1 Transmitter Equalization	29
2.5.2 Receiver Equalization	32
3 DISSERTATION OBJECTIVES	34
4 TIME-DOMAIN PRE-DISTORTION TECHNIQUES	35
4.1 Pulse-Width Modulation Scheme	35
4.2 PWM-RC Pre-Distortion Technique	38
4.3 Frequency Spectrum Analysis	42
4.4 Equalized Channel Transfer Functions	45
4.5 Eye Diagram Analysis	48
4.6 Signal spectrum analysis	51
4.7 Optimization of raised-cosine pulse	53
4.8 Simulation Results	54
4.9 Summary	59
5 EXTENSION OF PWM-RC TECHNIQUE FOR SECOND ORDER CHANNELS	60
5.1 Second Order Pulse-Width Modulation Scheme	60
5.2 Frequency Domain Behavior	65
5.3 Transfer function analysis	69
5.4 Equalized channel transfer function	70
5.5 Summary	73
6 SIGNAL INTEGRITY PROBLEMS IN DIGITAL SYSTEMS	74
6.1 RMS Surface Roughness	74
6.2 Impact of Vias and Open Stubs on Signal Integrity	79
6.3 Summary	85
7 IMPLEMENTATION OF BOTH PWM AND PWM-2 SIGNALING TECHNIQUES	86
7.1 Channel Properties	86
7.2 Signal Generation Circuits	88
7.3 Performance of Equalization	89
7.4 Summary	95
8 RESEARCH CHALLENGES AND CONCLUSION	96
REFERENCES	99

LIST OF FIGURES

Fig. 2.1:	PCI-Express communication system realized in ADS Agilent development studio.	15
Fig. 2.2:	Channel losses: a) the variation of the conductive and dielectric losses on the geometry of the coplanar strips at frequency 5 GHz, b) the variation of conductor, dielectric and total losses versus frequency.....	16
Fig. 2.3:	Crosstalk variations for various defined parameters of transmission lines (MathCad simulation).	17
Fig. 2.4:	Channel losses: a) measured magnitude of the transfer function S21, b) Measured transient input and output channel response.....	18
Fig. 2.5:	Experimental results: a) Two analyzed backplane prototypes (taken from [31]), b) experimental backplane measurements.....	19
Fig. 2.6:	Losses calculation: a) dielectric losses (DL) for different frequencies, even and odd mode listed, b) Computational model for crosstalk estimation realized in MathCAD environment, c) propagation delay (t_{pd}) for red - isolated microstrip line, blue- even mode, green- odd mode.....	21
Fig. 2.7:	Transmitter output eye diagram and channel output eye diagram: a) channel outputs for two analyzed backplanes prototypes upper eye: higher distance between transmission lines, lower eye - significant transmission line distance reduction, b) optimal pre-emphasis setting: upper eye - transmitter output, lower eye - channel output, c) strong pre-emphasis setting: upper eye - transmitter output, lower eye - channel output.	23
Fig. 2.8:	High-speed interconnect: a) measured transfer functions of real transmission channels, b) simple schematic of proposed/modeled communication chain....	24
Fig. 2.9:	Eye diagram performance: a) output eye diagram analysis, conventional pulse b) histogram of eye height improvement.....	25
Fig. 2.10:	Output eye diagram analysis, optimized pulse	27
Fig. 2.11:	Transmitter (TX) pre-emphasis versus receiver (RX) equalization	28
Fig. 2.12:	FIR filter at the transceiver side as FFE - principle.....	30
Fig. 2.13:	FIR filter at the transmitter side as FFE - frequency responses.....	31
Fig. 2.14:	Single RC-degenerated stage (taken from [16]).....	32
Fig. 4.1:	Eye diagram outputs a) TX pulse shapes ($T_b = 200$ ps) of FIR filter (dashed line) and PWM filter (solid line) and simulated channel pulse responses for transmission line bandwidth $BW_{3dB} = 0.35$ GHz, b) output eye diagrams for optimal coefficients setting and second order channel response for PWM.....	37
Fig. 4.2:	Raised cosine pulse shaping: a) spectral analysis of raised cosine function, b) raised cosine impulse response.....	40
Fig. 4.3:	Time-domain analysis: a) PWM-RC pulse shaping - strong pre-emphasis, b) PWM-RC pulse shaping -weak pre-emphasis, c) band-limited channel output, PWM-RC scheme enabled.....	41
Fig. 4.4:	Spectrum analysis: a) analysis of PSD for different signal types, b) frequency spectrum analysis of conventional PWM pulse vs. PWM-RC pulse.	42
Fig. 4.5:	PWM-RC frequency domain analysis: a) calculated magnitude of PWM-RC filter transfer function ($\beta_S = 0.4$) b) high- frequency compensation settings for different values of β_S parameter.	44

Fig. 4.6:	Equalization performance: a) equalized first order channel transfer function (strong preemphasis), b) pre-emphasis techniques overall losses compensation performance analysis.	46
Fig. 4.7:	Performance of higher order equalization: a) equalized higher order channel transfer function (strong pre-emphasis) b) pre-emphasis techniques overall losses compensation for higher-order channel.	47
Fig. 4.8:	Eye diagram analysis ($BW_{3dB} = 350$ MHz): a) transmitter output at 5 Gbps, b) channel output, c) transmitter output for PWM-RC signalling, d) channel output for PWM-RC signalling, e) transmitter output for PWM signalling, f) channel output for PWM-RC signalling, g) transmitter output for FIR signalling, h) channel output for FIR signalling.....	50
Fig. 4.9:	Channel output frequency spectrum analysis if random data pattern is transmitted at 5 Gbps ($BW_{3dB} = 150$ MHz, strong pre-emphasis enabled $dc = 50$ %): a) PWM-RC scheme b) PWM scheme.....	51
Fig. 4.10:	Channel output frequency spectrum analysis if LF data pattern is transmitted at 5 Gbps ($BW_{3dB} = 350$ MHz, optimal pre-emphasis enabled): a) PWM-RC scheme b) PWM scheme.	52
Fig. 4.11:	Impulse response of all compared pulses t.....	54
Fig. 4.12:	Dependence of β_x when variables α_x and $T_{b_{opt}}$ are linearly swept.....	55
Fig. 4.13:	Impulse response and eye diagram performance for various α_x	55
Fig. 4.14:	Impulse response and eye diagram performance for various T_b	56
Fig. 4.15:	Eye diagram performance of all analyzed pulses.....	58
Fig. 4.16:	ISI error probability.....	59
Fig. 5.1:	Time-domain analysis: a) impulse responses for FIR, PWM and PWM-2 pulse shaping, b) eye diagrams to evaluate signalling performance after passing through the channel with significant bandwidth restriction.....	62
Fig. 5.2:	Time-domain analysis: a) PWM-2 pulse shaping with channel output bit stream demonstration, b) the relevant eye diagrams for both PWM and PWM-2 signalling technique.	62
Fig. 5.3:	Duty cycle variation: a) amplitude variations of PWM signal during duty-cycle changing, b) amplitude variations of PWM-2 signal during duty-cycle changing.....	64
Fig. 5.4:	PSD calculation for PWM-2 pulse.....	67
Fig. 5.5:	PSD calculations normalized in dB	68
Fig. 5.6:	Detailed view of the signal spectrum.....	68
Fig. 5.7:	Calculated magnitude of PWM-2 filter transfer. Note that f_N is at 0.5 on the x-axis	69
Fig. 5.8:	Second order pulse responses	71
Fig. 5.9:	Equalized transfer function, second order channel used: a) FIR filter, b) PWM filter, c) PWM-2 filter.....	72
Fig. 5.10:	LF compensation comparison for PWM and PWM-2 filter.....	73
Fig. 6.1:	Conductive losses, without RMS surface roughness - green (3 GHz), red (6 GHz), light blue (9 GHz), yellow (12GHz), with RMS surface roughness - gray (3 GHz), orange (6 GHz), purple (9 GHz), blue (12GHz).....	75
Fig. 6.2:	Channel pulse responses comparison for various channel losses effects.....	76
Fig. 6.3:	Output eye diagram for conventional FIR filtering: a) transmission channel without RMS surface roughness, b) channel with RMS surface roughness ...	77

Fig. 6.4:	Output eye diagram for PWM filtering: a) transmission channel without RMS surface roughness, b) channel with RMS surface roughness.	78
Fig. 6.5:	Output eye diagram for PWM-2 filtering: a) transmission channel without RMS surface roughness, b) channel with RMS surface roughness.	78
Fig. 6.6:	Two configurations of simulated model: a) differential signal jumps across a reference ground plane, b) differential signal jumps across a reference power plane.	81
Fig. 6.7:	Input dynamic impedances: red - jumping across a power plane, blue jumping across a ground plane.	82
Fig. 6.8:	Frequency domain analysis: a) channel response, b) pulse frequency content. Note that the black colour represent input pulse, red colour show pulse affected by jumping across a power plane, blue colour pulse represent effect of jumping across a ground plane.	83
Fig. 6.9:	Pulse responses extracted directly from the frequency responses, red pulse represent input pulse, black pulse represent the pulse affected by jumping across a power plane, pulse marked by dashed line represent effect of jumping across ground plane.	84
Fig. 6.10:	Eye diagram analysis: a) output eye pattern when signal jumping across a ground plane, b) output eye pattern when signal jumping across a power plane.	84
Fig. 7.1:	Channel transfer function of analyzed low cost coaxial cable.	86
Fig. 7.2:	Channel output eye diagrams: a) 300 Mbps data transfer rate enabled, b) 450 Mbps data transfer rate enabled, c) input signal definition - conventional signalling.	87
Fig. 7.3:	Principle of PWM-2 equalization technique: a) signalling circuit concept for FPGA implementations, b) signal diagram.	88
Fig. 7.4:	Eye diagrams for PWM signalling (200Mbps): a) input signal, b) channel output signal.	90
Fig. 7.5:	Eye diagrams for PWM-2 signalling (200Mbps): a) input signal, b) channel output signal.	90
Fig. 7.6:	Eye diagrams for PWM signalling (450Mbps): a) input signal, b) channel output signal.	91
Fig. 7.7:	Eye diagrams for PWM-2 signalling (450Mbps): a) input signal, b) channel output signal.	92
Fig. 7.8:	Eye diagram for PWM signalling (450Mbps) - strong pre-emphasis $dc = 50\%$	93
Fig. 7.9:	Eye diagram for 3-TAP FIR signalling (450Mbps) - optimal setting.	94
Fig. 7.10:	Practical implementation - eye diagram for PWM signalling (450Mbps) - weak pre-emphasis $dc = 85\%$	95

LIST OF TABLES

Tab. 2.1: Optimized pulse parameters	28
Tab. 4.1: BER analysis, raised cosine pulse.....	57
Tab. 4.2: BER analysis, exponential pulse.....	57
Tab. 4.3: BER analysis, exponential-optimized pulse.	57
Tab. 6.1: Performance of equalization techniques, surface roughness	79
Tab. 7.1: Performance of analyzed equalization techniques - 200 Mbps	94
Tab. 7.2: Performance of analyzed equalization techniques - 450 Mbps	94

LIST OF SYMBOLS, PHYSICAL CONSTANTS AND ABBREVIATIONS

BW	bandwidth
BW_{3dB}	bandwidth, 3dB in signal level reduction
DFE	decision feedback equalizer
FIR	finite impulse response
FFE	feed forward equalizer
TX	transceiver, transmitter
RX	receiver
t_r	risetime, the main pulse parameter
t_{pd}	propagation delay
T_b	bit period
T_s	symbol period
PWM	pulse-width modulation
PWM-RC	pulse-width modulation with raised cosine pulse shaping
PWM-2	pulse width modulation of second order extension
DL	dielectric losses
α	losses, usually conductive or dielectric losses
β_s	pulse roll-off parameter
β_x	parameter for inverse exponential function
dc	duty cycle
PCIe	Peripheral Component Interconnect Express
ISI	intersymbol interference
PCB	printed circuit board
CMOS	Complementary Metal–Oxide–Semiconductor
SERDES	Serializer/Deserializer, digital blocks used in high speed communications
V_{DD}	supply voltage
V_{RX}	receiver sensitivity
Z_0	characteristic impedance of transmission line
$H(f), H(s)$	transfer function f -domain, s -domain
BER	bit error rate
W	transmission line width
h	transmission line height

d	transmission line thickness
RMS	root mean square
f_N	Nyquist frequency
Γ_n	definition of reflection
ρ_s	source reflection coefficient
A	pulse amplitude
EQ	equalizer
PE	pre-emphasis
UI	unit interval
LVDS	low-voltage differential signaling
$u(t)$	unit step function
NRZ	Non Return to Zero, one type of signalling binary code
f, w_n	FIR filter coefficient definition
$W(z)$	FIR filter definition in z -domain
DAC	digital to analog converter
SSF	symbol spaced filter
PAM	pulse amplitude modulation
LF	low-frequency
HF	high-frequency
SNR	signal to noise ratio
LMS	least mean square

1 INTRODUCTION

Today's high-speed multi-core microprocessors and memory interfaces require ever-increasing interconnect bandwidth for modern applications such as computing and graphic systems, networking and other high-speed systems. Stringent requirements for reduced board space, miniature connectors, efficient printed circuit board (PCB) design and low susceptibility to noise are associated with serial communications links architecture. Many existing serial I/O standards operate at multi-Gbps speeds such as well known PCI Express (PCIe). Next generation of the standard PCIe Gen 3 is able to operate at 8 Gbps in a single lane. As data rates are increasing, their susceptibility to damage is more critical. It is caused by the nonideal aspects of transmission lines, such as crosstalks and losses as well as energy dissipation caused by reflections and radiation. All these issues can cause significant problems in signal integrity and timing. These impacts dominate at multi-Gb/s speeds where the unwanted signal distortion can cause that signal energy is spread over multiple bit positions, a phenomenon known as intersymbol interference (ISI) [1]. This leads to increase in the jitter that degrades the timing margin as well as a distortion in the signal levels is the main cause of voltage margin degradation of the inter-chip signaling link [3]. In such severe environments, sophisticated pulse-shaping techniques such as equalization or pre-emphasis (equalization at the transmitter is often called transmitter pre-emphasis to reflect the effect of the filter operation), need to be employed to increase the data rates [4]. Equalization is a circuit technique that reduces the ISI-induced timing jitter and voltage margin loss by compensating for nonideal aspects, in particular the loss of interconnects at high speed [5]. For instance, the significant frequency-dependent losses of transmission lines which can cause system degradation are effectively overcome by using pre-emphasis or equalization techniques, the maximum signaling rate is significantly extended [6], [7], [8].

The transmitter equalization filter is commonly realized as finite impulse response (FIR) filters [9], [10], [11]. Various types of equalizers are also commercially available [12], [13]. The purpose of this operation is to increase (decrease for de-emphasis [14]) amplitude for the first bit after a logic transition relative to successive bits. However, the conventional FIR pre-emphasis techniques for recent CMOS technology trends are mainly restricted by its supply voltage, which will decrease according to CMOS scaling [2]. A time-domain pre-emphasis method does not change the pulse amplitude as for conventional FIR pre-emphasis, but a timing resolution is used to signal pre-distortion [15], [16]. This method is able to better adapt to current requirements in CMOS technology trends where higher switching speeds and lower supply voltage dominate. Actual research is primarily focused on the analysis and development of effective transmitter pre-distortion method for PCB channels where ISI and crosstalk noise are dominant factors of losses. In the dissertation thesis a modified signaling scheme to minimize these factors is proposed. Current time-domain pre-distortion methods use conventional rectangular pulse. This causes that many undesirable harmonic high frequency components are contained in a pre-distorted signal at the transmitter output. Such a system is very susceptible to crosstalk noise.

2 STATE OF THE ART

In this Chapter, the concept of equalization is explained. First section offers a very brief introduction to high-speed interconnect issues. Furthermore, the basic principle of equalization for loss compensation is described. Finally, the conventional equalization methods available in the literature are presented. This part of doctoral thesis is complemented by results from simulation of own models for signal integrity problems and also outputs from practical measurements realized during the study of undesirable channel effects are presented.

2.1 High-Speed Interconnect

A basic inter-chip communication system can be schematically described as in Fig. 2.1, in detail described in [17]. The three main parts including the transmitter, the channel, and the receiver are shown. As the bandwidth requirement of communication systems at board-to-board, and chip-to-chip levels increases, interconnect topologies have been moving away from multi-point and toward high-speed point-to-point link [18]. In this case a high-speed serial communications for data transmission over the channel is used. This principle is based on the use of device known as SERDES (serializer/deserializer) which form data format into the serial stream, details in [19]. It provides an ability to easier equalization techniques implementation. The channel can take the form of a microstrip on a printed circuit board (PCB), or some form of connector/cable assembly for inter-PCB communication. Figure 2.1 shows the analyzed transmission channel which is representative of today's high-speed computing and networking systems. These systems have several channel parts with different lengths, and number of additional components as packages and connectors. In this case the channel performance at multi-gigahertz frequencies is strongly affected by using low cost package and PCB technologies and secondary sources such as via discontinuities. The output of the channel is connected to a receiver. One of the main parameter, receiver sensitivity can be used to calculate a transmitted voltage swing. The signaling power can be expressed as [18]

$$P_{\text{SIGNALING}} = \frac{V_{DD} \cdot V_{RX}}{Z_0 \cdot H(f)} \quad (2.1)$$

where V_{DD} is I/O supply voltage, V_{RX} represents receiver sensitivity, $H(f)$ is channel frequency response, the transmitted swing is defined as $V_{TX} = V_{RX} / H(f)$ and Z_0 represents the characteristic impedance.

The expression shows that the minimum transmitted signal swing depends on the receiver sensitivity and the channel's frequency response [20]. In our case, the signal swing requirement assumes inter-symbol interferences (ISI) compensation by equalization techniques such as pre-emphasis at the transmitter. Ideally for minimum bit error rate (BER) which is typically 10^{-9} - 10^{-1} . The design of perspective pre-distortion method for high-speed inter-chip data signaling for PCB interconnect is strongly dependent on two main factors. Firstly, it is necessary to compensate losses that need to be considered in PCB design. These high-frequency effects can be summarized as conductor (dispersion, skin-effect, surface roughness) losses and dielectric losses.

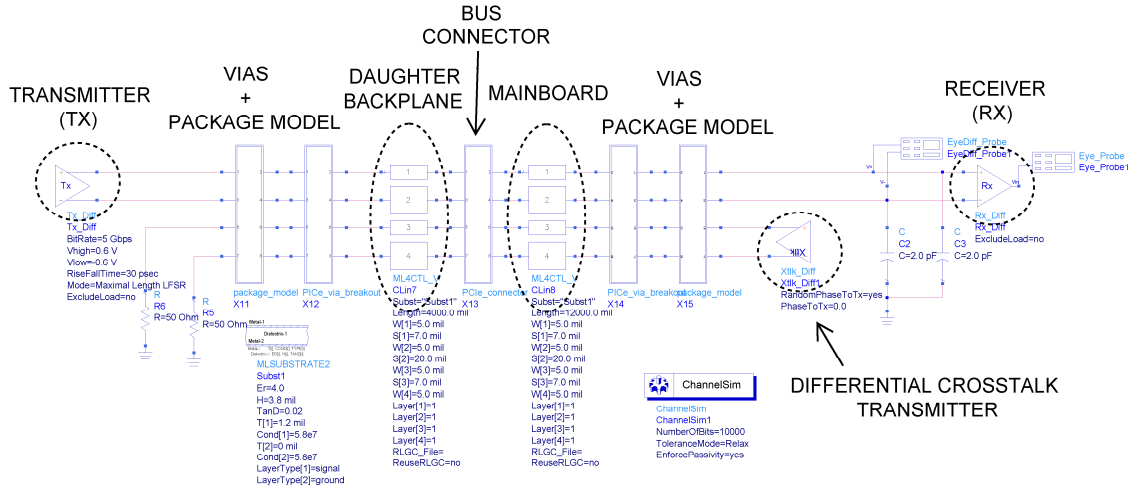
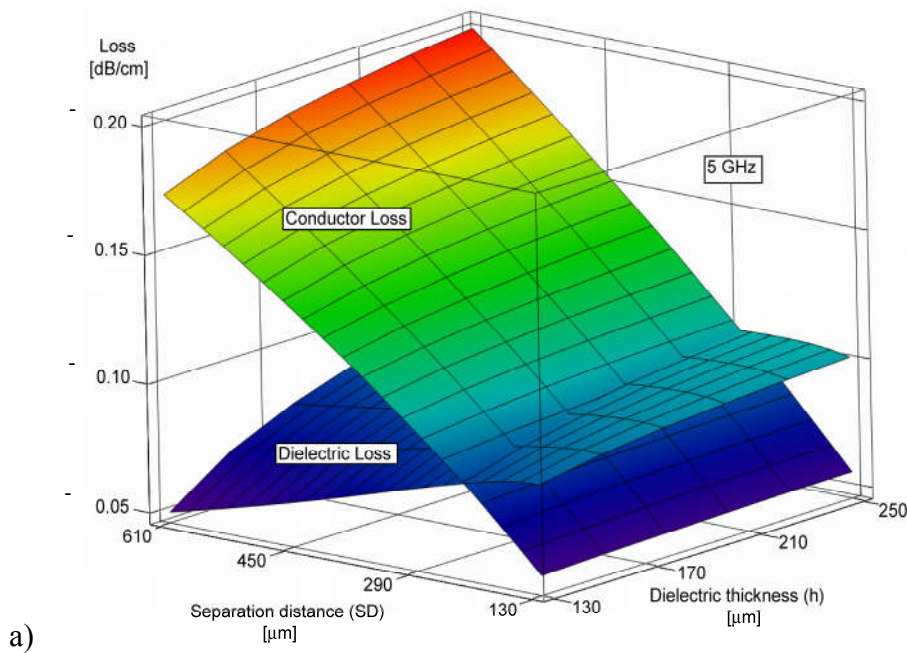


Fig. 2.1: PCI-Express communication system realized in ADS Agilent development studio.

In many research papers is shown that the channel bandwidth is predominantly limited by the PCB losses caused by the use of low-cost laminate materials. In this case low-loss laminate materials are often used in backplanes to extend the link data rates. The optimal foil roughness to optimize conductor loss for robust packaging is dependent on maintaining a good dielectric/foil adhesion [21], [22]. In [14], [23] is shown that the dispersive effects of the dielectric material forming a microstripline can cause reduction transmission bandwidths that are manifested as reduced received pulse amplitudes for the pulses propagating down the line. The following surface plots show the variation of the conductive, dielectric and total losses on the geometry of the coplanar strips at frequency 5 GHz. Differential stripline pair is analyzed in Fig. 2.2a. Finally Fig. 2.2b shows total losses estimation.



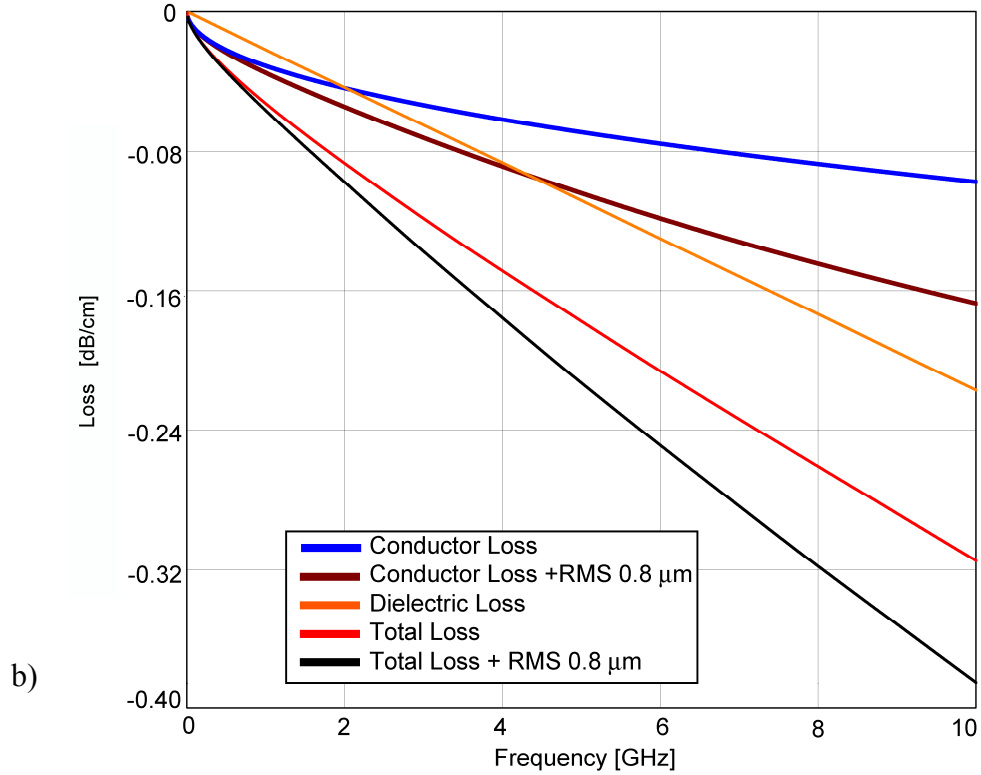


Fig. 2.2: Channel losses: a) variation of the conductive and dielectric losses on the geometry of the coplanar strips at frequency 5 GHz, b) variation of conductor, dielectric and total losses versus frequency.

It is clearly seen that the dielectric losses dominate at higher data rates (frequencies). The effect of copper roughness is not included in this analysis. Further analysis is focused on determining the total channel losses, and the effect of copper roughness is included. Typical values for RMS roughness could be $0.8 \mu\text{m}$ (0.03 mils) for stripline, $1.6 \mu\text{m}$ (0.06 mils) for surface microstrip [14], [25]. It is obvious how the total losses are increasing if the RMS roughness is set to $0.8 \mu\text{m}$. Other results in [14] show how dispersion affects the effective propagation delays. The higher frequencies will propagate with larger delays than the lower frequencies. The spreading of the propagation delays is maximized for large h and large W . For example, the spread in propagation delays for $h = 1.524 \text{ mm}$ and $W = 0.381 \text{ mm}$ is about 2 ps/cm between 1 GHz and 10 GHz. More information can be found in [14], [23], [24]. The dispersive effects appear to be much more sensitive to changes in conductor heights (h) than to changes in conductor widths (W). In addition to these undesirable effects, dispersion can cause reductions in the intended characteristic impedances of the microstripline. Differential transmission lines, that are typical for high-speed communication systems design, can be designed to match the typically 100Ω . This reduction in the impedance can be as high as about 5Ω up to 10 GHz, which corresponds to a rise time of about 50 ps [14]. The problems at higher frequencies can be observed in the signal as a distortion of the leading edges, see Fig. 2.3. The measured magnitude of the transfer function S_{21} is shown in Fig. 2.4a. In this case the chip to chip communication system based on PCIe platform consists of differential transmitter, differential receiver (both with optimal 100Ω impedance load), vias and PCIe connector is used. For printed

circuit boards (PCBs), the problem of impedance discontinuities is more complicated than for cables. This can cause additional deep notches (spectral nulls) in the channel transfer function at higher frequencies.

Signal degradation factors described above can cause significant ISI and crosstalk. Thus the second important factor for PCB pre-distortion technique design is crosstalk noise. The conventional pulse shaping scheme based on the square wave approaches can induce higher frequency content into a signal. This situation is shown in Fig. 2.3. It can be determined that crosstalk occurs along the rising and falling edges. From the simulations in MathCAD development environment it is possible to expect that smaller rise-times would produce more crosstalk. Two parameters, coupling length (*length*) and isolation distance (*distance*), are varied. Note the significant reduction in the peak crosstalk for larger isolation distance.

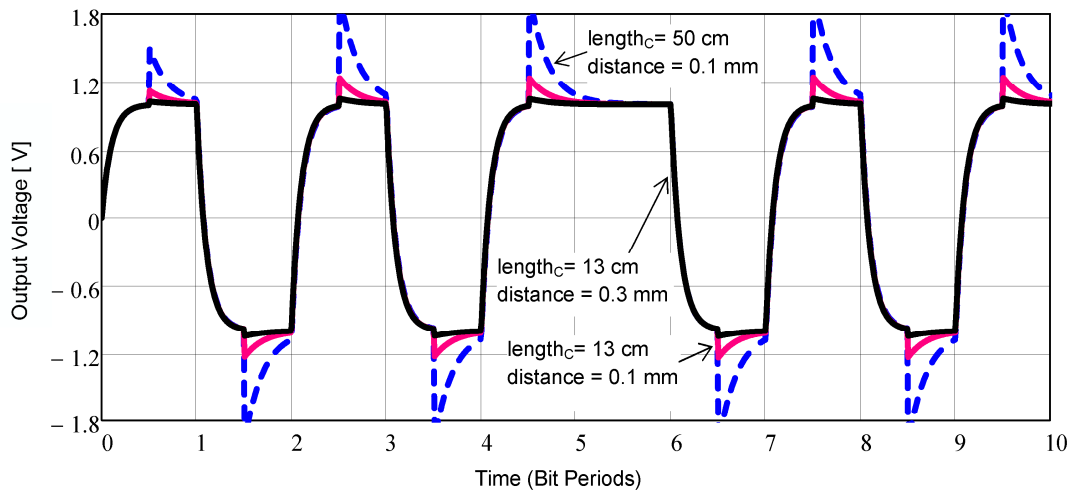


Fig. 2.3: Crosstalk variations for various defined parameters of transmission lines (MathCad simulation).

Efficient channel (transmission lines) modeling is necessary in both time-domain [26]-[29] and frequency domain [14], [30]. The attenuation and dispersion effects described above can be seen in the time domain as inter-symbol interference (ISI). From the transient response shown in Fig. 2.4b, we can roughly estimate the channel attenuation at Nyquist frequency (f_N) for 2 Gbps data rate by looking at the fastest transitions, e.g. from 47 ns to 48 ns. Their amplitudes are approximately 300 mV. Seeing that the amplitude of the channel input signal is approximately 700 mV, the channel attenuation at f_N is $300 \cdot 10^{-3} / 700 \cdot 10^{-3} = 0.43$, which corresponds to 7 dB loss. (Compare this with the frequency-domain measurement of 8 dB in Fig. 2.4a. Additional 6 dB loss is sufficient to close the eye completely. This means that if the slope of the loss curve is such that high-frequency bit patterns (101010) are attenuated by 6 dB or more relative to low-frequency bit patterns (11110000), the eye will be closed.

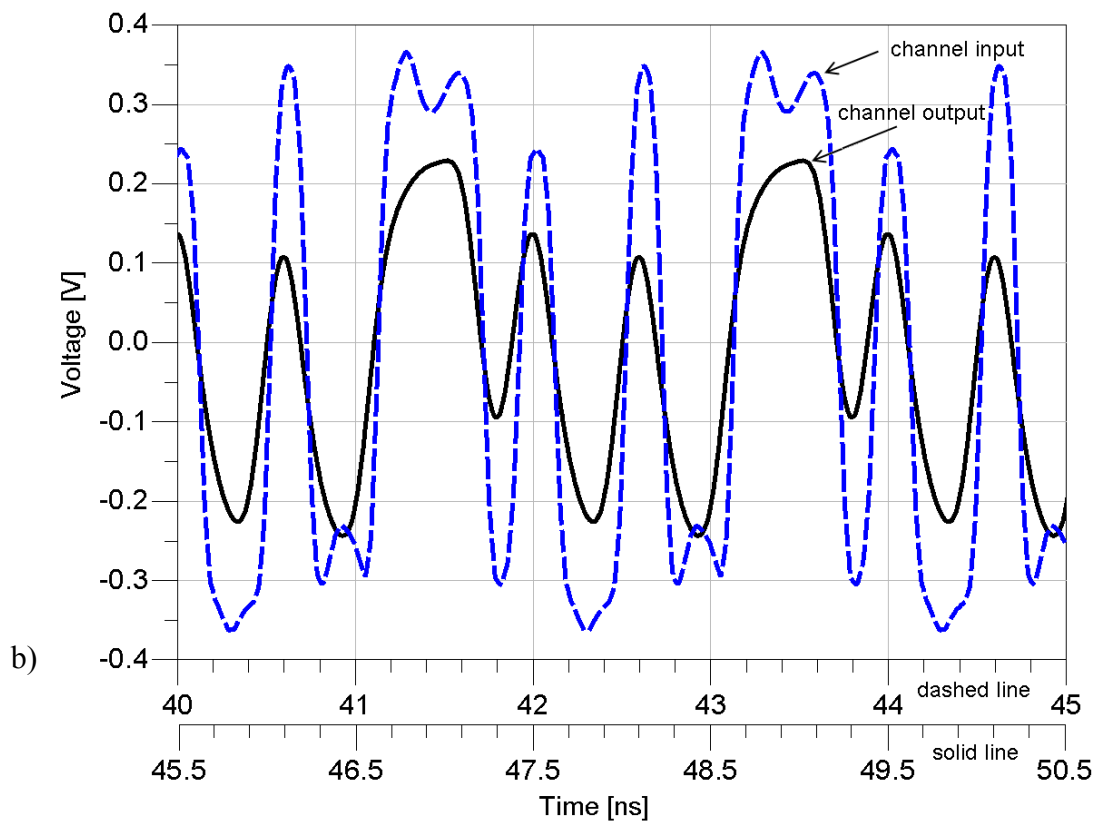
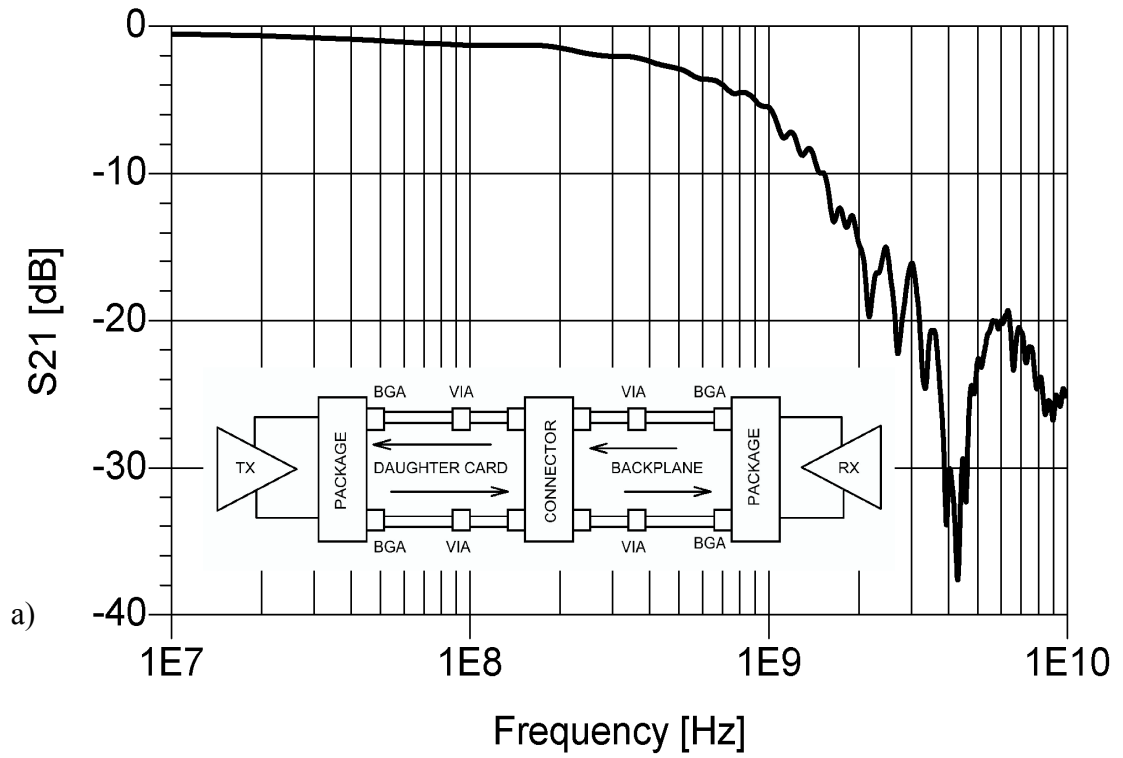


Fig. 2.4: Channel losses: a) measured magnitude of the transfer function S_{21} , b) measured transient input and output channel response.

Most high-speed designs use the eye diagram results to evaluate system performance. The typical result is that the transmission channel with limited bandwidth closes the data “eye”. In this case the signal crosses the threshold and the bit will be detected wrongly, resulting in a bit error. An eye diagram is constructed by superimposing numerous consecutive bits in a data stream. The opening of the eye is a qualitative metric to assess the quality of the signal integrity. The eye opening (eye height) and eye width can be used to estimate the voltage margin and timing margin respectively. The horizontal axis of the eye diagram represents time and is typically one or two symbols wide, while the vertical axis represents the amplitude of the signal [1].

2.2 Channel Measurements Results

For the experimental measurements two types of 30 cm long backplanes created within diploma thesis [31] was used, see Fig. 2.5a. The first backplane prototype was designed with relatively large distance between transmission lines, $d = 6$ mm.

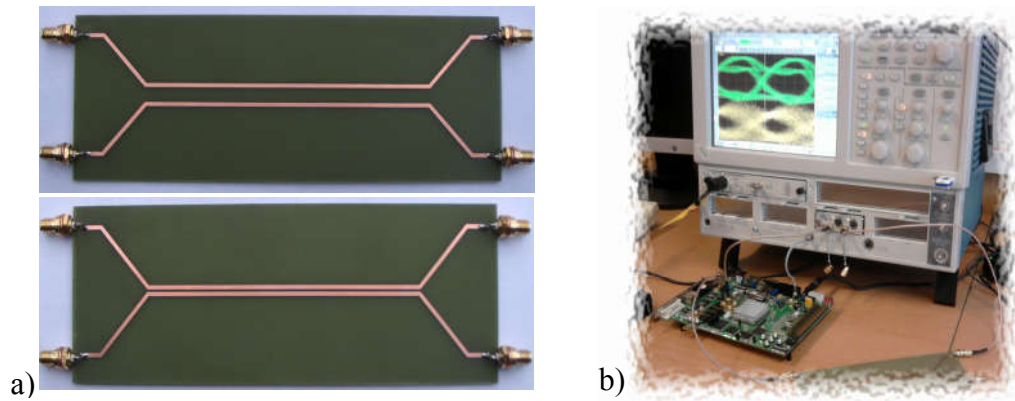
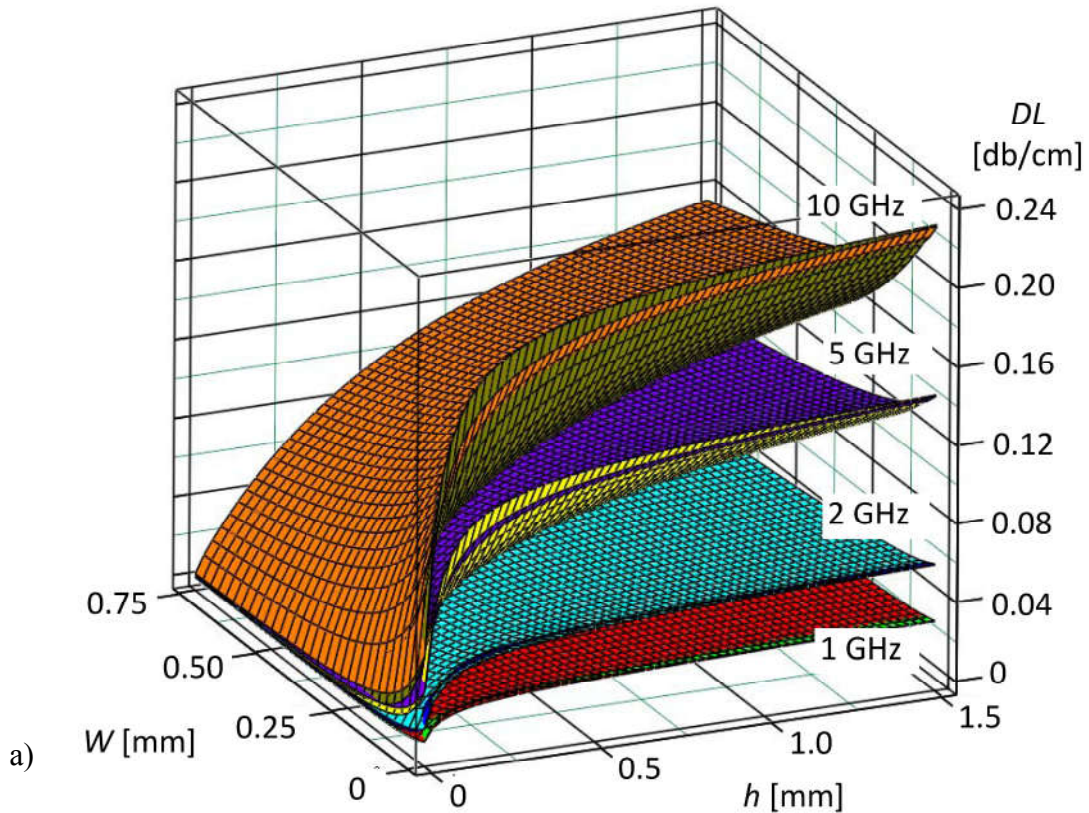


Fig. 2.5: Experimental results: a) two analyzed backplane prototypes (taken from [31]), b) experimental backplane measurements.

In this case the microstrip conductor and dielectric losses are dominant factors that must be taken into account. It is quite possible in multi conductor transmission line systems that two and more independent microstrip conductors may be close enough to each other to induce mutual coupling effect. In Fig. 2.6a are calculated dielectric losses for simple coplanar coupled microstrip configuration. In this case the effect of odd and even mode is compared over the various frequency settings. This situation represents a practical use of transmission lines in various modes where two conductors are driven differentially or driven with the identical signals with the same polarity. All calculations are swept with different parameters for width of the signal trace marked as W and the thickness of the PCB dielectric marked as h . In practice the PCB contains a solder mask, a third medium which affects the overall dielectric losses. Thus, it should be considered in the calculation of dielectric losses alongside the first medium substrate under the trace and the second medium the air above the trace. It is obvious that significant reduction in W parameter critically increase dielectric losses similarly as the enlargement of microstrip distance from the reference plane.

The second backplane prototype is designed with significant distance reduction between transmission lines, $d = 0.5$ mm. Due to the electromagnetic field, the victim line is influenced by an inductive and a capacitive coupling and a significant crosstalk effect should be taken into account in real communication systems. In Fig. 2.7a a significant impact of crosstalk effect on output signal data quality is obvious. In this case coupling length is about 20 cm. The simulation results realized in MathCAD simulation environment show significant increase in crosstalk for relatively long coupling lengths (this corresponds with realized backplane prototypes measurements) and decreasing in aggressor distance, see Fig. 2.6b. The aggressor represents separated single ended circuit. There is far more parameters that should be monitored to assure good signal quality. One of them is propagation delay parameter marked in Fig. 2.6c as t_{pd} . During increasing the data transmission rate the effect of transmission line propagation delay has significant impact on additional amount of intersymbol interference in transmitted signal because of more stringent timing and skew requirements. From fig. 2.6c is clearly seen that both even and odd mode propagation delay calculations are fold smaller than the propagation delays for the isolated microstripline.



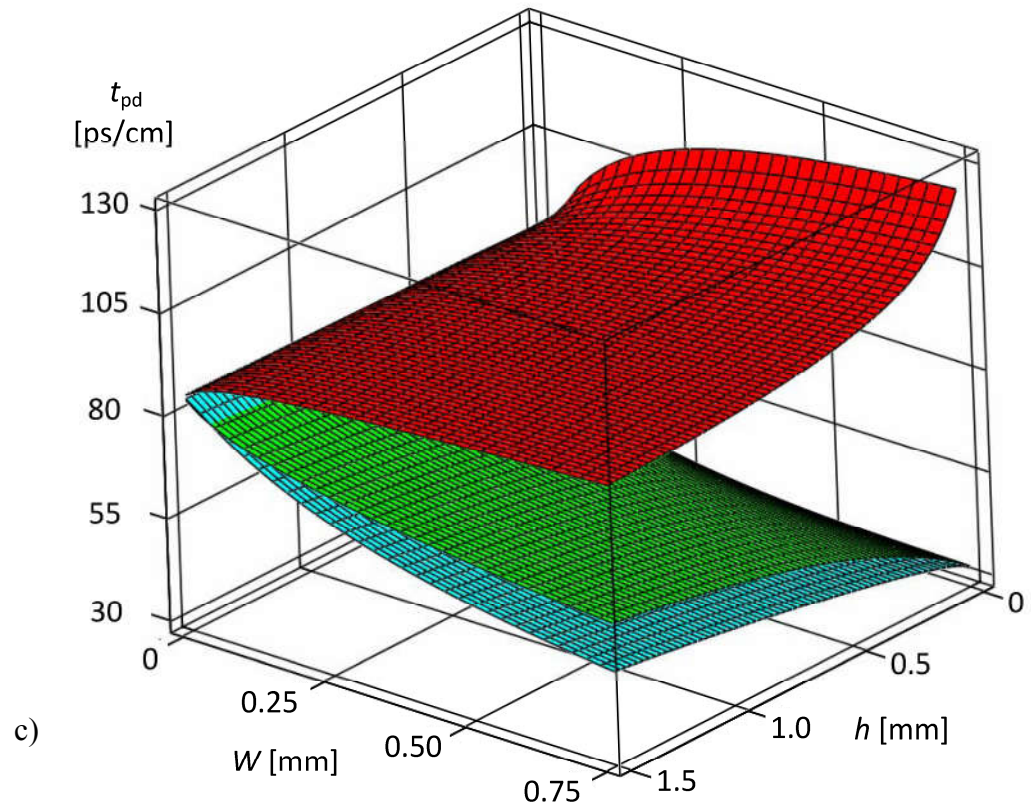
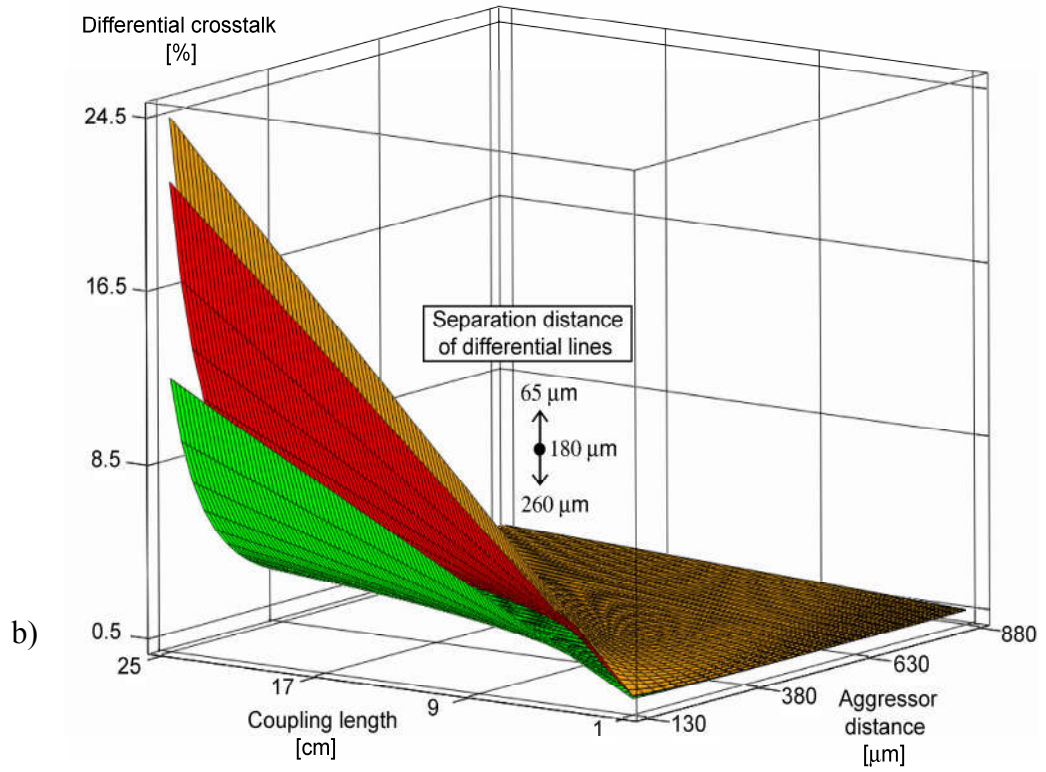


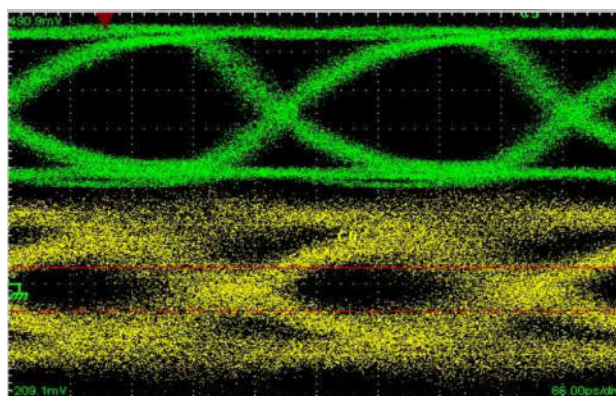
Fig. 2.6: Losses calculation: a) dielectric losses (DL) for different frequencies, even and odd mode listed, b) computational model for crosstalk estimation realized in MathCAD environment, c) propagation delay (t_{pd}) for red - isolated microstrip line, blue- even mode, green- odd mode.

Final results are presented in Fig. 2.7 in the form of eye diagrams which show parametric information about the signal. User can quickly and intuitively assessing the current digital signal quality. Eye diagram is constructed by folding of every possible parts of waveform representing simple bit sequence. Signal amplitude is analyzed on the vertical axis and signal timing on horizontal axis. Due to the repeating this construction over many samples of the simple bit sequences, the final graph will be similar to the eye. Eye opening is the one of the key parameter of digital signal quality and represents one bit period marked as Unit Interval (UI) width of the eye diagram. Measured eye diagram results for different configurations are shown in Fig. 2.7. Fig. 2.7a show differences in eye opening during signal transmission over the two analyzed backplane prototypes listed above. For longer transmission lines and cheaper PCB's the eye opening can be completely eliminated. In this case there is a possibility to improve the quality of signal at the output of the channel by using sophisticated pulse shaping techniques which allows to minimize the destructive effect of transmission channel on signal quality globally known as equalization techniques.

A conventional transmitter pre-distortion technique based on FIR filter implementation is demonstrated in Fig. 2.7b and Fig. 2.7c. It is obvious that the optimal pre-emphasis level setting is able to improve eye diagram opening. Please compare lower eye diagrams on Fig. 2.7a and Fig. 2.7b. However, other additional increase in the amount of a pre-emphasis can cause an eye diagram closure and an additional noise content in the data signal, please compare lower eye diagrams in Fig. 2.7b and Fig. 2.7c. Upper eye diagrams in Fig. 2.7b and Fig. 2.7c show that eye opening at the first glance is more suppressed in comparison with conventional signaling stream, see upper eye diagram in Fig. 2.7a. In the finals, a demonstrably better eye opening at the channel output is achieved, see again Fig. 2.7b lower eye diagram.

In this case a Xilinx Virtex IV development kit is used to generate 3.125 Gbps data rate, see Fig. 2.5b. The amount of pre-emphasis is fully programmable and is expressed in dB. This is the most common way of specifying the pre-emphasis effect at the transmitter side.

a)



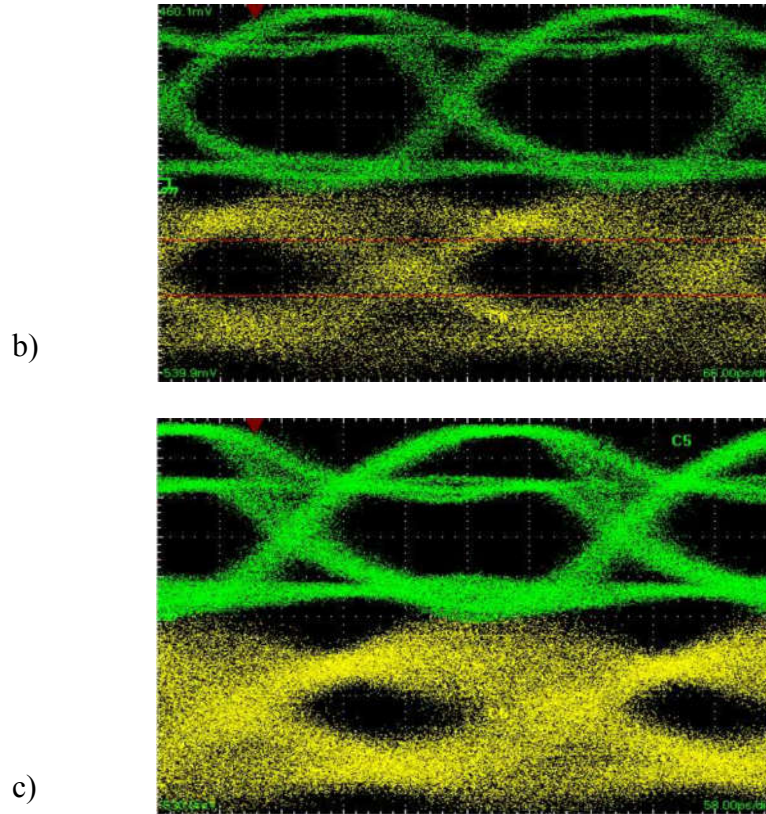


Fig. 2.7: Transmitter output eye diagram and channel output eye diagram: a) channel outputs for two analyzed backplanes prototypes upper eye: higher distance between transmission lines, lower eye - significant transmission line distance reduction, b) optimal pre-emphasis setting: upper eye - transmitter output, lower eye - channel output, c) strong pre-emphasis setting: upper eye - transmitter output, lower eye - channel output.

There are two ways to emphasis the signal. In the first case pre-emphasis can be calculated as additive to the smaller voltage. In the second case to reflect the fact that equalization can be performed as a reduction in voltage amplitude the term de-emphasis is used [14]. The resulting effect of compensation for channel loss is identical for both methods. For performance tests of variable signalling methods a professional development board DS25BR100EVK from Texas Instruments was used [63]. Thus, the performance of low-voltage differential signalling (LVDS) single channel buffers can be analyzed. Available are transmit pre-emphasis (PE) [13] and receive equalization (EQ), details see in [64], [65] where the examples of their performance testing are shown. The evaluation kit consists of three separate FR4 striplines (14 cm, 71cm and 106 cm in length). It allows the use of this board for tests of both conventional and innovative signalling techniques. Thus, signal conditioning features (pre-emphasis and equalization) can be simply compared. Based on the measured results of channels responses an appropriate communication chain in Agilent ADS development environment (hereinafter ADS) was created. The general functional diagram of proposed/modelled communication chain which will be analyzed through ADS is shown in Fig. 2.8a. Measured transfer functions of all available channels are shown in

Fig. 2.8b. The system consist of a pulse shaping part which ensures adaptive changes of the amplitude and edge shaping in order to achieve optimal eye opening and higher power efficiency. The pre-emphasis module provides precise adjustment of transmitted pulse width and its appropriate digital modulation. Thus, the signal can be precisely adapted according to the behaviour of the transmission channel due to the feedback from the monitoring of eye diagram opening at the receiver. Moreover, the real backplane channels are slowly varying and so it isn't necessary full real-time eye diagram monitoring.

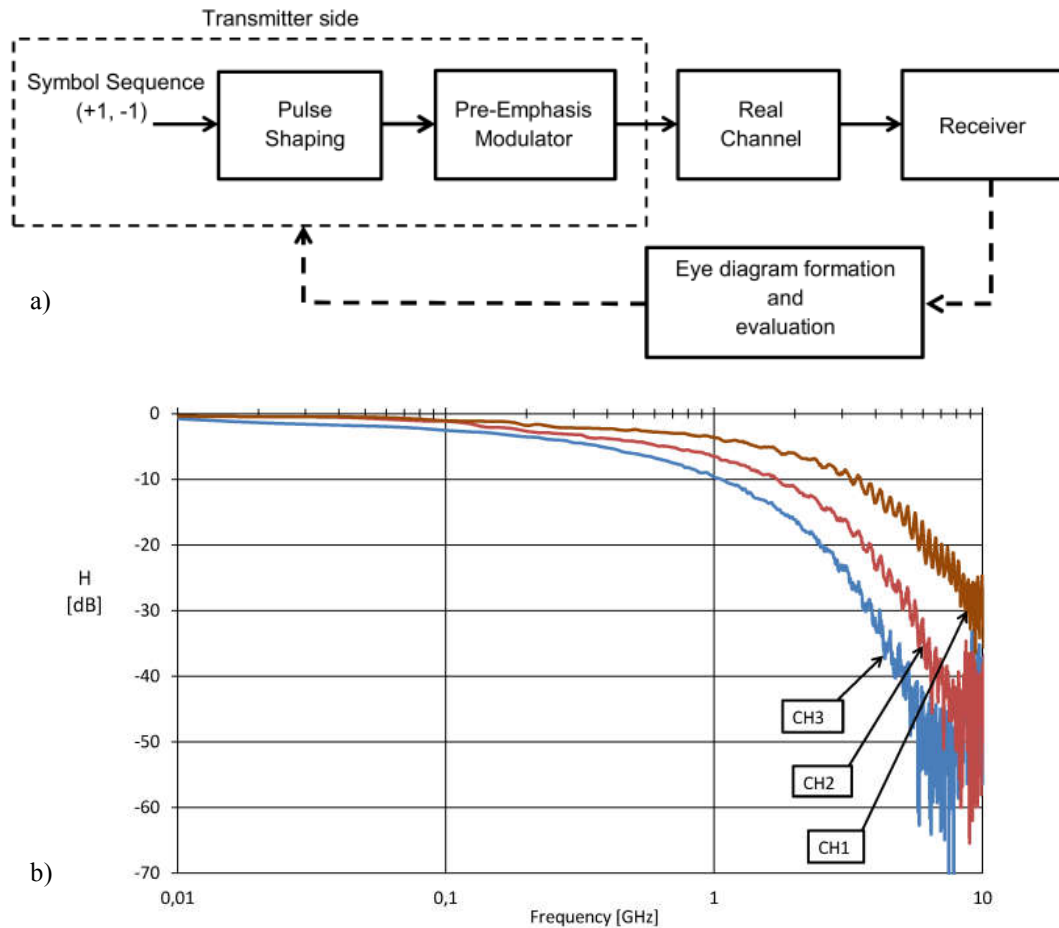


Fig. 2.8: High speed interconnection: a) simple schematic of proposed/modeled communication chain, b) measured transfer functions of real transmissions channels.

Based on the real transmission channel measurements two main impact findings are obvious from the output eye diagrams. These are pulse amplitude and pulse width. In the first case eye width and eye height are analyzed together with increasing bit rate. Fig. 2.9a shows that eye height decreases non-linearly with higher slopes and the eye width parameter has an exponential decreasing tendency with higher slopes and the eye width parameter has exponential decreasing tendency during increasing bit rate. The performance test was calculated in ADS where the real channel transfer function was used. In this case a conventional bipolar signalling with rectangular pulses was used. The pulse amplitude corresponds to the value $\pm 1V$ and pulse width corresponds with bit period T_b . The situation is somewhat different in case of increasing signal amplitude together with appropriate decreasing in pulse width to maintain the same pulse power,

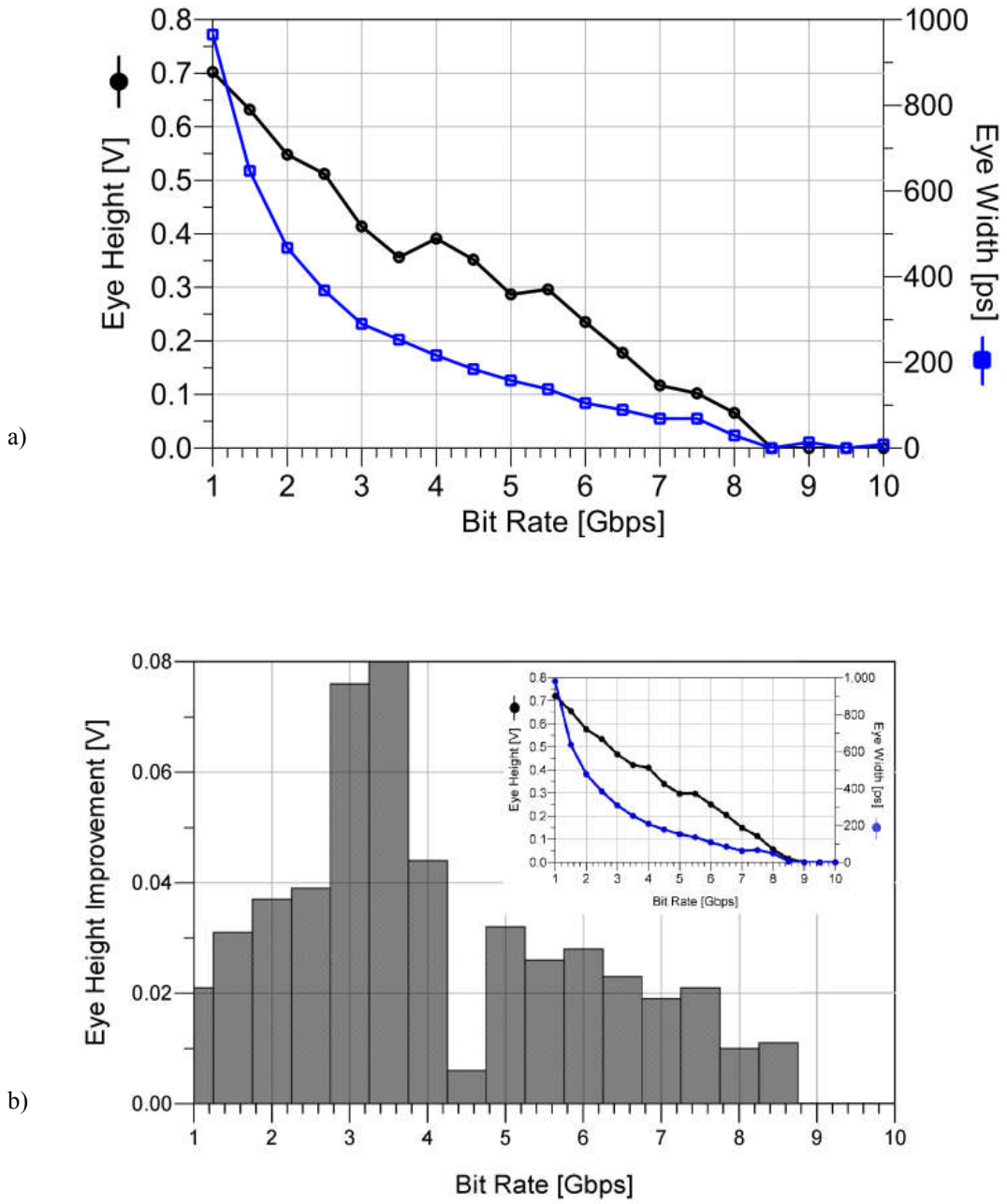


Fig. 2.9: Eye diagram performance: a) output eye diagram analysis, conventional pulse b) histogram of eye height improvement.

It is obvious that the decreasing tendency of eye width parameter remains the same as in the previous case. However, more important is the fact that eye height parameter can be improved and higher bit rates over the same channel can be achieved or the same bit rates with better signal quality. In this case, the pulse amplitude $A \neq A_{opt}$ and bit period $T_b \neq T_{bopt}$. Note that the histogram in Fig. 2.9b is unbalanced. The best values are achieved about 3 Gbps bit rate, which is nominal value of test board [63].

The communication channel is most often characterized as an idealized low-pass filter with a transfer function defined as

$$H(s) = \frac{2\pi BW}{s + 2\pi BW} \quad (2.2)$$

where BW is the typical 3 dB bandwidth parameter which controls the losses of transmission lines. It fully corresponds with low-pass RC filter transfer function.

For our analysis, we consider extended channel model where additional parameters according to real assumptions as driver impedance, load capacitance, propagation delay and source reflection coefficient are supplemented based on the findings in [1], [66] and real channel measurement. Thus, the channel transfer function is defined as

$$H_{REAL}(s) = \frac{H(s) \frac{2}{CZ_0}}{s + \frac{1}{CZ_0}} + \Gamma_1 + \Gamma_2 + \Gamma_3 + \Gamma_4 \quad (2.3)$$

where Γ represents the reflection from the load to the source and is defined as

$$\Gamma_n = \rho_s^n H(s)^{2n} e^{-s2nt_d} \left[\frac{\frac{2}{CZ_0} \left(\frac{1}{CZ_0} - s \right)^n}{\left(s + \frac{1}{CZ_0} \right)^{n+1}} \right] \quad (2.4)$$

where C is load capacitance, Z_0 is characteristic impedance of transmission line, t_d is one-way time delay, ρ_s is source reflection coefficient defined as $\rho_s = \frac{R_D - Z_0}{R_D + Z_0}$ and finally n is the number of reflections from the load to the source.

2.3 Performance of pulse-width adjusting

As the transmission line bandwidth decreases, the tendency is for the input pulses to spread or disperse in time at the output. This pulse spreading gives rise to each received output pulse interfering with the next received pulses. We consider that the input voltage pulse $v_{inp}(t)$ is defined by amplitude A and duration T_b . The output voltage impulse can be described as

$$v_{out}(t) = A \left(1 - e^{-2\pi BW_2 t} \right) (u(t) - u(t - T_b)) + v_{T_b} e^{-2\pi BW_2 (t - T_b)} u(t - T_b) \quad (2.5)$$

where $u(t)$ is the unit step function and BW_2 is a parameter forming the pulse rise time. Thus, a single pulse with exponentially shaped rising/falling edge can be obtained. Note the enormous increase in pulse width after passing through the lossy channel. The amount of ISI is defined according to last term in the previous equation as

$$ISI = \int_{T_b}^{+\infty} V_{T_b} e^{-2\pi BW_2(t-T_b)} dt = \frac{A}{2\pi BW_2} (1 - e^{-2\pi BW_2 T_b}) \quad (2.6)$$

In Fig. 2.10 two output pulses passed through the transmission channel defined by (2.3) and (2.4) are compared. It is obvious that the optimized pulse width (T_{bopt}) with appropriate increase in amplitude (A_{opt}) improve signal jitter performance and eye opening. Both optimized parameters have been calculated in ADS by using advanced parametric analysis and are shown in Table 2.1.

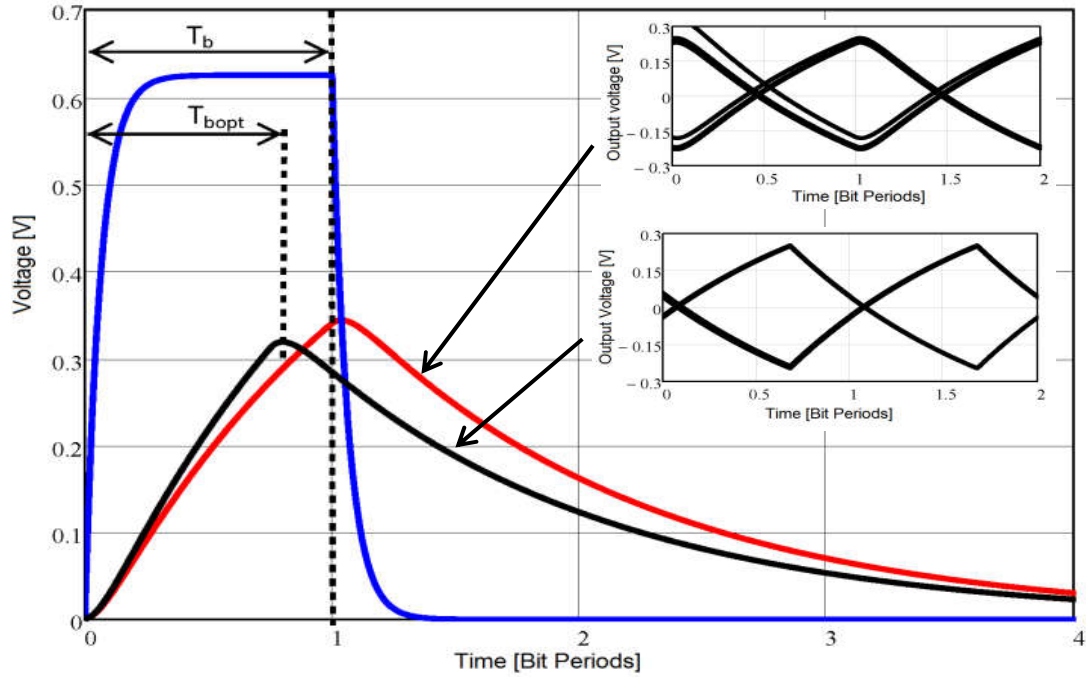


Fig. 2.10: Output eye diagram analysis, optimized pulse.

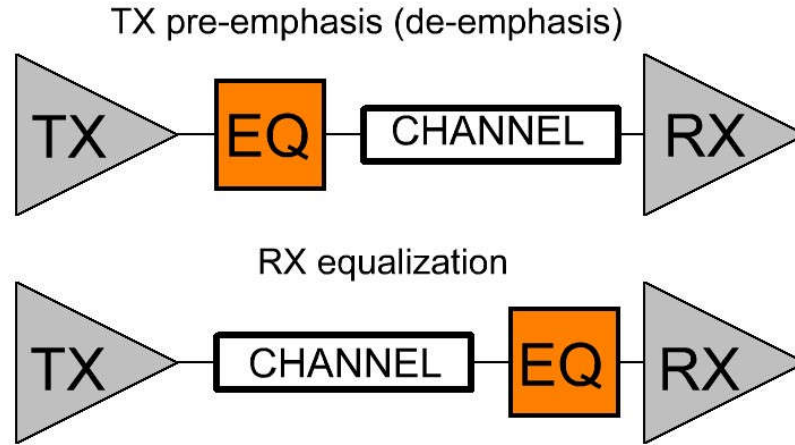
However, from Table 2.1, it is clearly seen that both optimal parameters A_{opt} and T_{bopt} for measured channel CH1 in Fig. 2.8b are not changed in the same way with increasing bit rate. The variation of A_{opt} has a linear character and the T_{bopt} is exponential. Hence the pulse shaped according to optimal parameters in Tab. 2.1 for higher bit rates is not more power efficient than conventional pulse for the same bit rate. One of the possible solutions lies in the use of non-conventional pulse shaping based on the more sophisticated pulse definition, more details in the next section.

Tab. 2.1: Optimized pulse parameters

Bit Rate	Channel Output		Optimized pulse parameters		
	Eye Height	Eye Width	A _{opt}	T _{bopt}	Percentage of T _b
[Gb/s]	[V]	[ps]	[V]	[ps]	[%]
1	0,67	1000	0,96	1000	100,0
2	0,58	465	1,02	476,2	95,2
3	0,46	310	1,05	314,5	94,4
4	0,41	218	1,05	232,6	93,0
5	0,30	163	1,08	183,5	91,8
6	0,23	114	1,10	149,3	89,6
7	0,14	79	1,12	123,5	86,5
8	0,07	6	1,15	107,3	85,8

2.4 Basic Concept of Equalization

Equalization circuits are designed to have an approximately inverse frequency response in comparison with the transmission channel transfer function across all frequencies of interest, see basic diagram in Fig. 2.11.

**Fig. 2.11:** Transmitter (TX) pre-emphasis versus receiver (RX) equalization.

The sophisticated signal equalization techniques can be implemented on both sides of the communication system. Equalization at the transmitter side is often called pre-/de-emphasis to reflect the effect of the filter operation. Equalization may also be done at the receiver where the technique is called RX equalization. In the frequency domain the equalization of channel with first-order transfer function can be simply described according to [16] where the channel first order low-pass characteristic is given by

$$H_{1st-ord}(j\omega) = \frac{1}{1 + \frac{j\omega}{\omega_{chan}}} \quad (2.7)$$

Now the equalizer is placed in series with the channel according to Fig. 2.11. The transfer function of equalizing filter is defined as

$$H_{\text{equalizer}}(j\omega) = \frac{1 + \frac{j\omega}{\omega_{\text{chan}}}}{1 + \frac{j\omega}{\omega_{p,\text{eq}}}}, \quad (2.8)$$

and the resulting complementation of both relationships shows the transfer function of equalized channel as

$$H_{\text{eq-chan}} = H_{\text{1st-ord}} \cdot H_{\text{equalizer}} = \frac{1}{1 + \frac{j\omega}{\omega_{p,\text{eq}}}}. \quad (2.9)$$

Assuming that $\omega_{p,\text{eq}}$ is larger than band-limited channel ω_{chan} , the channel bandwidth can be significantly improved by flattening the frequency response. In other words, due to the reduction in the loss variation where the difference between high-frequency bit patterns attenuation and low-frequency bit patterns attenuation is significantly reduced. This “flattening” of the magnitude of the frequency response shows the effectiveness of equalization [1]. In the time domain, the optimal equalization significantly reduces ISI as can be seen in the following Chapter in Fig. 4.1.

For more complex channel transfer function where the signal band is broken by deep notches the equalization is less effective. An equalizer for such a channel environment would need to have a very high gain near the predicted notches [16]. In this case, higher circuit complexity can be expected.

2.5 Solutions from Literature

In this section, the equalization solutions from the literature to the attenuation, dispersion and reflection problems introduced above are described. Brief overview includes a description of the basic equalization methods. These techniques can be variously modified with respect to many signaling techniques which can be examined.

2.5.1 Transmitter Equalization

Finite impulse response (FIR) filter (discrete linear equalizer) is usually implemented at the transmitter side. The most common implementation involves the use of high-speed digital-to-analog converter (DAC). Such a FIR-DAC filter has a digital input and an analog output. In [1], the basic architecture of typical FIR filter is shown. The structure of FIR filter includes delay elements known as stages of a shift register. In this case, a flip-flop is used to delay the signal with one bit time, input samples passes through these delay elements and are multiplied by the filter tap coefficients, see Fig. 3.12. The tap outputs are summed to form the output [1], [16]. In this case, the filter can be seen as de-emphasis circuit because the maximum voltage amplitude is achieved for bit stream with the most high-frequency content when there are rapid transitions in the bit stream, either from ‘0’ to ‘1’ or vice versa. When continuous bits of the same value are transmitted the output is attenuated because low-frequency content is just contained in portions of the signal. It corresponds better with leading-edge digital silicon manufacturing processes where the maximum voltage swing continues to decrease significantly below 1V [1].

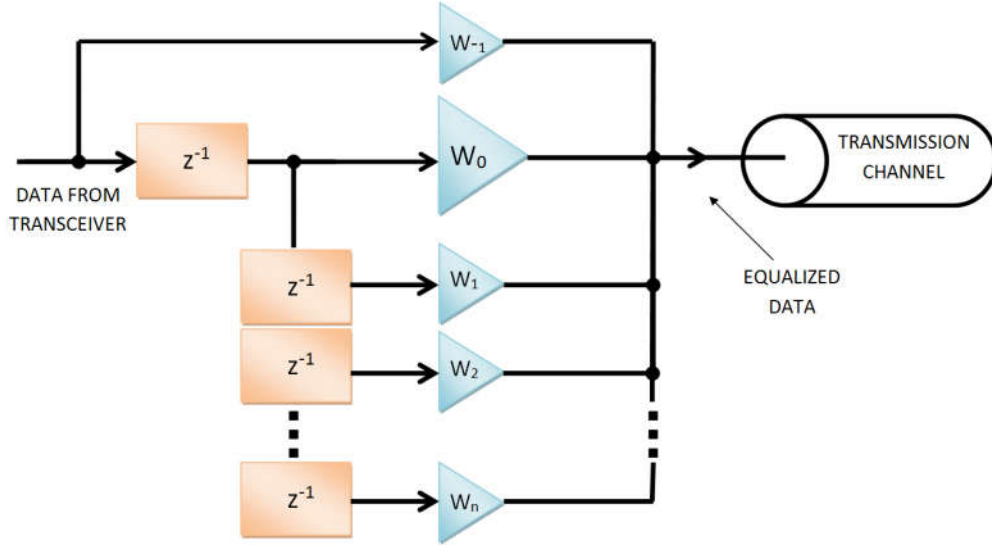


Fig. 2.12: FIR filter at the transceiver side as FFE - principle.

Simple principle of FIR filter attenuation can be demonstrated on example for z domain transfer function as below.

$$W(z) = 0.145 + 0.608z^{-1} - 0.247z^{-2} \quad (2.10)$$

From transfer function the low frequency response and Nyquist frequency response can be easily extracted. During the low frequency response the basic data patterns are assumed. It is an infinite number of 1 as [...1 1 1 1 ...]. For transfer function (2.10) it can be written as $[w_{-1} \ w_0 \ w_1] = [-0.145 \ 0.608 \ -0.247]$. At low frequency $f = 0$ and in z domain, $z = \cos(0) + j\sin(0) = 1$, the calculation of needed attenuation is expressed as

$$W(1) = -0.145 + 0.608(1^{-1}) - 0.247(1^{-2}) = 0.216 \Rightarrow -13.31 \text{ dB} \quad (2.11)$$

At the Nyquist frequency the data pattern is defined as infinite number of -1 and 1 as [...-1 1 -1 1 -1 ...]. According to Nyquist frequency definition $f = 0.5T_b$, in z domain the transfer function can be written as

$$W(1) = -0.145 + 0.608(-1^{-1}) - 0.247(-1^{-2}) = -1 \Rightarrow 0 \text{ dB} \quad (2.12)$$

In summary the FIR attenuates DC at -13.31 dB and passes Nyquist frequency at 0 dB. Figure 2.13 illustrates how FIR filter affects final transfer function of digital system. Transmission channel response shows difference between low frequency signal level and signal level at the Nyquist frequency (0.5 on the horizontal axis) almost 13 dB. After equalization the difference between low frequency and the Nyquist frequency is less than 2 dB. Thus, signal losses are equalized over the whole of observed frequency spectrum. However, the overall signal level is reduced and system can be more susceptible to additional noise content. This can be limitation for maximum equalization level which is practically usable. It depends also on receiver sensitivity. Better sensitivity allows to equalization with lower signal levels.

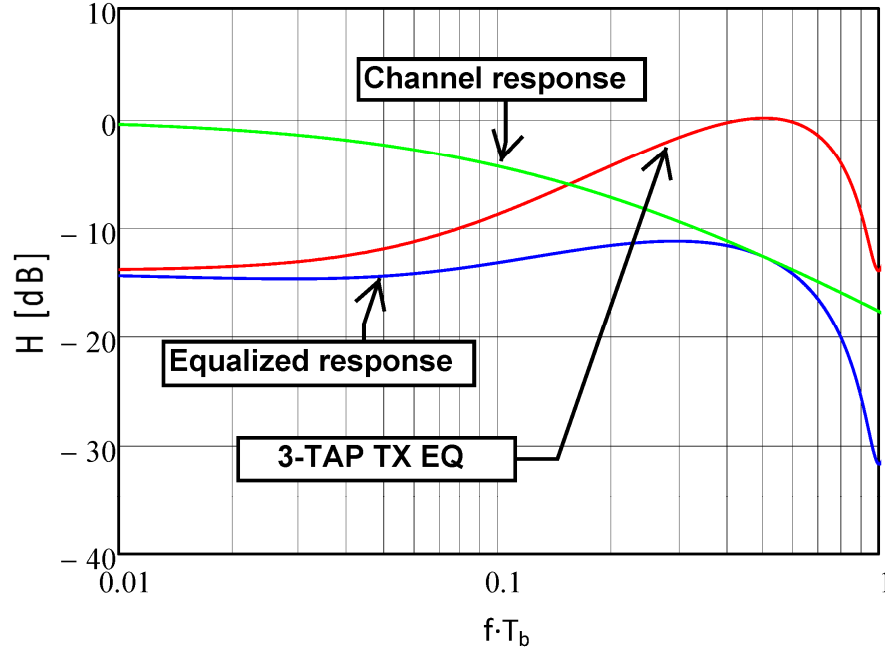


Fig. 2.13: FIR filter at the transmitter side as FFE - frequency responses

Methods described in the literature for equalization of various transmission channels such as coaxial cables, twisted pair cables and PCBs where the FIR-DAC implementation described above is used are given in [9], [10], [32], [33], [34], [35], [36]. The simplest implementation is achieved by using the 2-tap symbol-spaced FIR (SSF) filters. However, in this case loss compensation does not exceed 18 dB, e.g. [32] at 4 Gb/s (2PAM), 10 dB loss compensation and in [37] at 5 Gbps (2PAM) 18 dB loss compensation is achieved. More complex implementation in [9] where a 5-tap symbol-spaced equalizer is described can achieve 30 dB channel loss compensation at the Nyquist frequency, at 3.125 Gb/s (2PAM). In this case 5 manually tuned FIR taps are used.

From the literature introduced above it can be concluded that the simplest implementation of FIR filters with only 2-tap coefficients cannot provide more than ~20 dB of loss compensation. Further increase in loss compensation can be realized only by using more complex circuits where it is necessary to take into account more parameters that need to be tuned to match the equalizer to the channel [16].

Pulse-width modulated pre-emphasis (PWM) technique was successfully implemented and summarized in [16]. This paper describes time-domain based pre-emphasis method where pulse-width modulated scheme is used to the sophisticated pre-distortion of the input data signal. The PWM filter achieves 30 dB loss compensation to equalization of 25 m long coaxial cable. For PCB interconnect performance only FR4 backplane with simple very long single-ended trace (270 cm) is tested. However, 24 dB loss compensation is demonstrated. These values of loss compensation can be achieved with conventional pre-distortion FIR methods if more complex (multitap) filters are used. In the next chapter, the conventional PWM method is compared with proposed modified PWM-RC method which uses raised cosine (RC) signaling scheme. This provides more options to customize the filter to the transmission channel with the advantage of crosstalk reduction.

2.5.2 Receiver Equalization

Receiver equalization is often used together with transmitter pre-distortion because the information obtained at the channel output can be simply used to filter coefficients adaptation for the receiver filter as well as for transmitter filter to improve the effect of equalization. In this case, an adaptive equalization by using feedback loop can be created. The benefit of adaptive equalization is to adjust the current pre-emphasis or equalization level with respect to interconnect lengths or increase/decrease in data rates. On the other hand, additional complexity to the design and more power consumption are required. The receiver equalizers can be categorized into two main groups as continuous-time equalizers and discrete-time equalizers.

A continuous-time equalizer is based on the use of simple analog components to achieve the desired high-pass filter function. The simplest implementation is possible by using RC equalizer where the main sections of the equalizer are the termination, high-pass filter and dc power-limiting filter [1]. These types of equalizers are also designed with active components to perform the desired signal gain. More complex circuit modifications are possible by using higher-order high-pass filters. Two types of practical implementation as second-order active equalizers and equalizers using RC-degenerated stages are further discussed.

In [9] the receiver includes a second order derivative analog equalizer and implementation of multitap filter at the transmitter side is performed. The proposed equalization system is able to 30 dB loss compensation at 3.125 Gb/s. The receiver equalizer consists of three paths, DC, first-order derivative and second-order derivative [9]. The proposed concept includes several stages of variable gain amplifiers on each path. Thus, the circuit complexity and latencies through the three paths are significantly increasing. In [38] a high-speed CMOS adaptive cable equalizer is described. The circuitry of a unit equalizing filter cell is shown in Fig. 2.14. The filter has two separate paths for low-frequency and high-frequency signals. The tunable source degeneration capacitors are used to control the high-frequency boosting. The additional degeneration resistor is more complex circuit solution used to adapt low-frequency gain. Both elements are included in the impedance Z_2 which represents a larger impedance network. The impedance Z_1 is used as load resistor. By cascading multiple stages of such RC-degenerated differential pairs, in [38] 30 dB channel loss compensation was achieved in 0.18 μ m CMOS, at a speed of 3 Gbps [16]. In this case five stages were used. Each stage has a Z_2 impedance that can be switched and this allows you to precisely adjust the equalizer gain to the channel transfer function. In this case high channel loss compensation is achieved at the receiver side but both described implementations use more complex circuit solution.

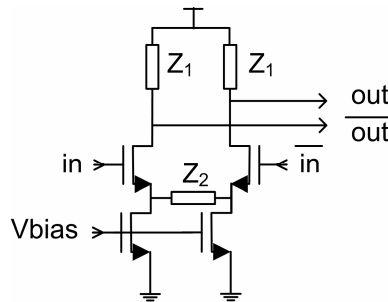


Fig. 2.14: Single RC-degenerated stage (taken from [16]).

A discrete-time receive-side equalizer architecture is the decision feedback equalizer (DFE). The concept is illustrated in [1]. In a DFE, decisions of previously detected symbols are used to remove ISI in the current symbol. The advantage of this technique is that DFE does not boost noise or crosstalk to achieve signal equalization as in the case of transmitter pre-emphasis. In situations when the transmitter pre-distortion circuit is used it is necessary to take into account an additional high-frequency noise in the signal. By using DFE equalization technique, the high-frequency noise induced in the signal can be effectively reduced. Especially for real PCBs channels of high-speed communication systems where the crosstalk at higher frequencies is dominated degradation factor, it can be an effective solution to improve the signal quality at the system output [34], [36], [41].

However, the main limitations of the DFE technique are sensitivities to error propagation because for proper functionality it is necessary to assume that the past symbol decisions are correct [1]. Incorrect value decision affects future decisions due to the feedback based decisions. In [34] it is shown that for practical implementations a 4-tap DFE can be used. A further limitation is that the DFE architecture is able only to compensate post-cursors ISI. Furthermore, at very high bit rates it can be a problem in a sufficiently feedback loop response for the first post cursor tap. Loop unrolling techniques can be used to mitigate this [36], [16], [1].

3 DISSERTATION OBJECTIVES

Signal integrity, thanks to continuous development and improvement in the field of high-speed digital design, has become a critical issue. Thus, the timing and the quality of signal to ensure reliable high-speed data transmission is still current theme. There is a still area for improvement of conventional signaling techniques to overcome transmission channel with higher order transfer function with respect to current requirements for low power chip signaling. The main goals of dissertation can be divided to the four parts.

- Modeling of the real signal integrity phenomena by using own designed computational models using the latest information in the field of high-speed digital design.
- Detailed analysis of the time-domain equalization techniques and research of the new approaches to optimize signal emphasizing for better adjustability to the transmission channels with higher order transfer function.
- Extend of conventional time-domain equalization technique to the second order realization, practical implementations and the study of performance of proposed technique during equalization of higher order transmission channels.
- Detailed analysis of the impact and influences of additional channel discontinuities on the proposed signaling method together with practical verification of achieved results during the development of advance signal integrity models.

4 TIME-DOMAIN PRE-DISTORTION TECHNIQUES

In this chapter, for the first time the PWM-RC (raised cosine) pre-distortion method is proposed to the equalization of high-speed PCBs channels. Innovative PWM method is proposed in [16] and is applied to the coaxial cable loss equalization and simple single PCB trace equalization. It provides an alternative to FIR pre-emphasis which is still commonly used in high-speed interconnect systems. The proposed time-domain pre-distortion method in [16] has the advantage for modern low-voltage CMOS devices where the maximum voltage swing is pushed markedly below 1.0 V and the implementation of the pre-distortion methods based on pulse amplitude shaping can be a problem. The first part of the chapter shows both FIR and PWM schemes, all presented simulations have been created in MathCAD and Agilent Advanced Design Studio (ADS). In the next section both conventional PWM pre-distortion methods and proposed PWM-RC are analytically compared. It is shown that PWM-RC method is able to better compensate higher-order transmission channel than conventional PWM scheme. The PWM pre-emphasis provides higher maximum loss compensation (24 dB) than the commonly used 2-tap SSF filter (18 dB), because its transfer function is able to adapt very well to the copper channel, see simulation results in Agilent ADS studio [42]. However, the crosstalk susceptibility of conventional PWM can cause additional high-frequency content in equalized data stream. Thus, the loss compensation can be significantly reduced. The proposed PWM-RC method reduces ISI, see section 4.2. Eye diagram analysis and additional high-frequency noise are analyzed in sections 4.5 and 4.6.

4.1 Pulse-Width Modulation Scheme

In Fig. 4.1, the output voltage waveforms for both 2-tap FIR signaling and the PWM signaling are shown. Transmitter output is normalized to ± 1 V. Transmission channel model has a monotonically decreasing transfer function. It corresponds approximately with PCB loss model for single trace. The current channel losses are adjusted using the typical bandwidth parameter BW_{3dB} . Actual channel losses $BW_{3dB} = 0.35$ GHz corresponds with the 70 cm long PCB trace. A similar result are shown for 25 m long coaxial cable in [16]. The optimum duty-cycle settings are strongly dependent on the channel characteristics, see Fig. 4.1. In this case the optimal coefficients are $f = 0.62$ and $dc = 56\%$ for FIR pre-distortion and PWM pre-distortion, respectively. The PWM pulse shape is similar to Manchester code for duty-cycle (dc) parameter setting to 50 %. However, the Manchester code has a fixed amplitude at 50 % without a tunable duty-cycle [16]. A duty-cycle of 100 % corresponds to transmission of a normal polar NRZ data signaling without pre-distortion. In [43] the symmetrical impulse response for the channel where dielectric losses dominated is shown. The measured results and advanced simulation model shows that this channel has nonsymmetrical pulse response, see Fig. 4.1.

The coefficients for time domain simulations are rewritten according to [16] as $c_1 = f$, $c_2 = f - 1$ with $f \in \{0.5...1\}$, resulting in one coefficient f that can be used to control the pre-distortion level. Function $p_{fir}(t)$ can be simply formulated as

$$p_{fir}(t) = \begin{cases} 0 & t < 0 \\ f & 0 \leq t < T_b \\ f-1 & T_b \leq t < 2 \cdot T_b \\ 0 & 2 \cdot T_b \leq t \end{cases}, \quad (4.1)$$

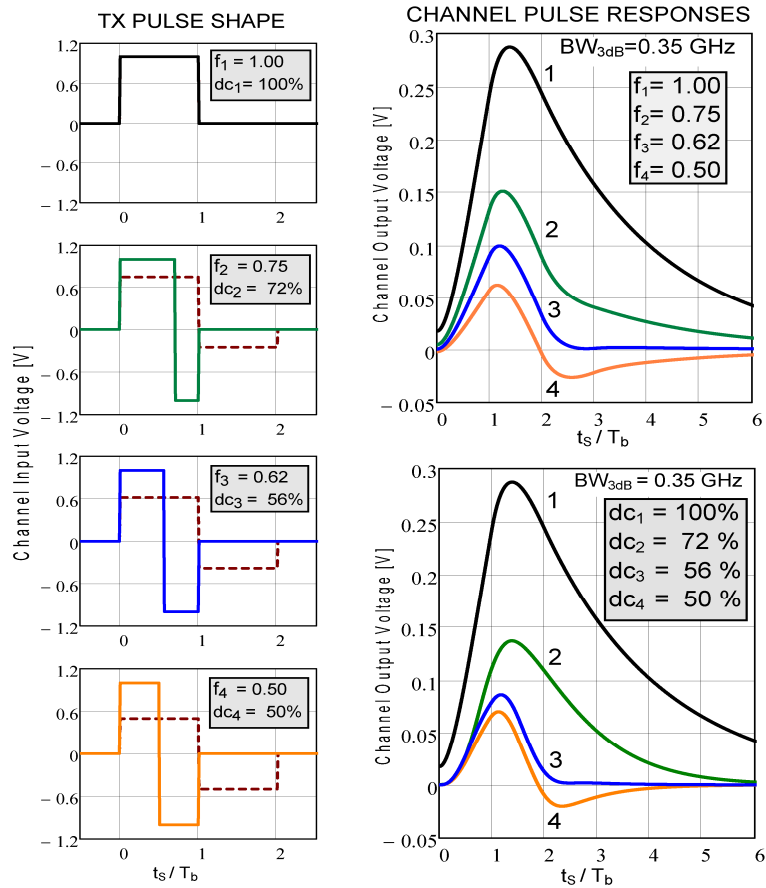
where f and $f-1$ denote the values of the first and the second FIR taps, respectively, and T_b represent the symbol period ($T_b = 200$ ps).

The PWM pulse $p_{pwm}(t)$ is defined as follows, see Fig. 4.1

$$p_{pwm}(t) = \begin{cases} 0 & t < 0 \\ 1 & 0 \leq t < dc \cdot T_b \\ -1 & dc \cdot T_b \leq t < T_b \\ 0 & T_b \leq t \end{cases}, \quad (4.2)$$

where dc denotes the duty-cycle ($0.5 < dc < 1$ fits best to PCB backplanes) and T_b again represents the symbol period ($T_b = 200$ ps).

a)



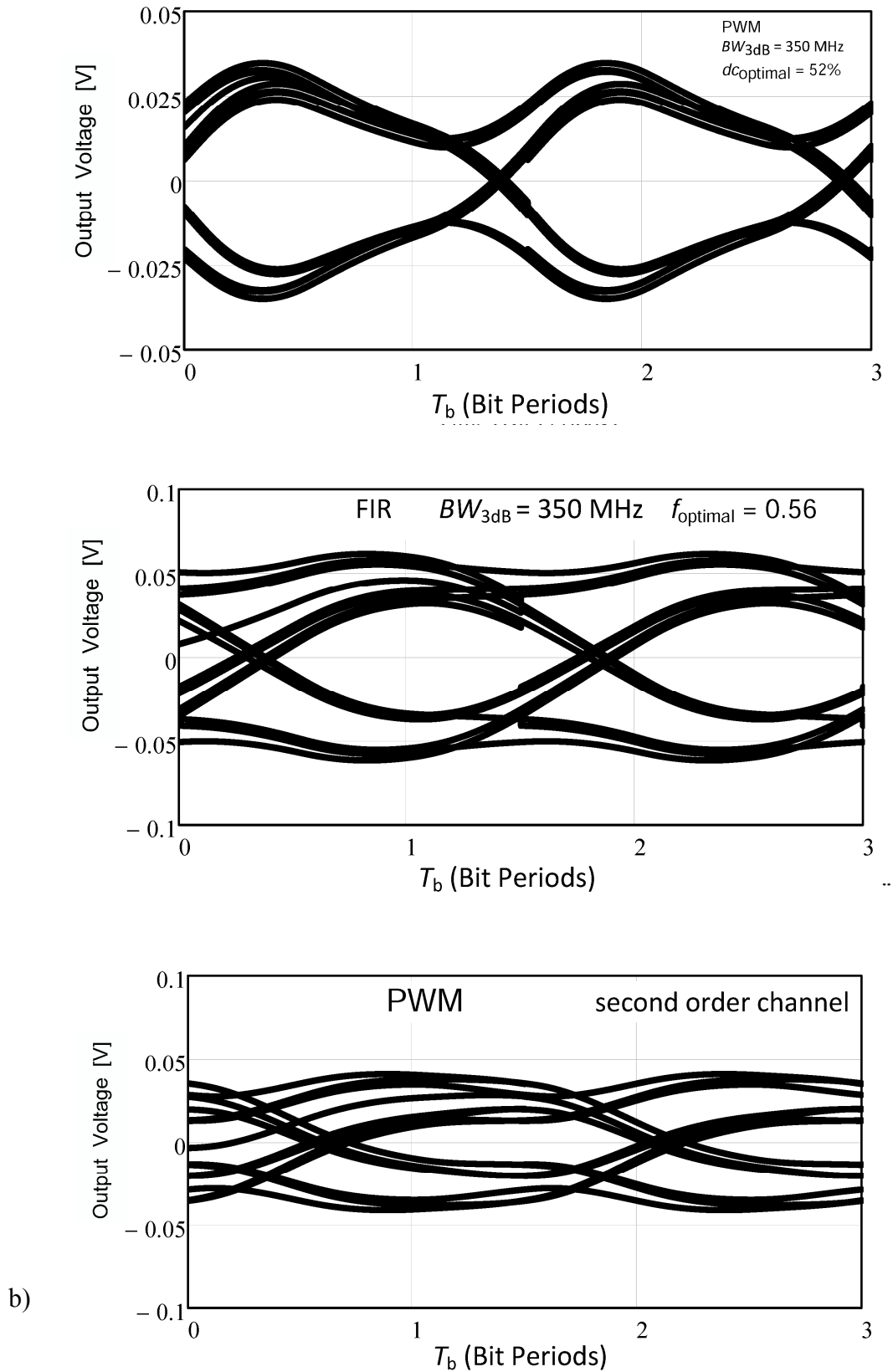


Fig. 4.1: Eye diagram outputs: a) TX pulse shapes ($T_b = 200$ ps) of FIR filter (dashed line) and PWM filter (solid line) and simulated channel pulse responses for transmission line bandwidth $BW_{3dB} = 0.35$ GHz, b) output eye diagrams for optimal coefficients setting and second order channel response for PWM.

From eye diagrams presented in Fig. 4.1b is it possible to do following conclusions. PWM method better compensate channel losses for first order channel model. Despite the overall reduction in the signal amplitude a significant jitter and ISI reduction in PWM response is visible. As a result of improvements in these parameters eye opening is greater than in the case of the FIR filter. The problem in signal integrity can occur when the channel path is affected by other disturbing elements such as vias, additional aggressor lines. Thus, signal reflection and a steeper drop in signal level at higher frequencies cause the significant degradation of leading edges shaping. In this case higher order channel modeling must be applied to the modeling of these additional signal degradations. If transfer function for second order channel defined and analyzed in section 5 is used the eye opening is significantly reduced, see last eye diagram in Fig. 4.1b. In this case pre-emphasis techniques successfully used for first order channel response fail. However, as will be shown below, it is possible to introduce into the shaping signal additional parameter to more sophisticated shaping. It allows to significantly decrease jitter and ISI effect of transmission channel in output signal. Thus, the data signal that was previously undetectable for receiver due to the significant BER growth, is detected with better BER parameters.

The time-domain pre-distortion method described above has the advantage of only one coefficient settings to achieve optimal pre-emphasis level. Thus it can be very simplified implementation process of adaptive duty-cycle settings for control algorithms which are widely used for receiver equalization. A sign-sign block least mean squares (LMS) algorithm can be used as shown in [35]. From Fig. 4.1 it is clearly seen that replacing FIR pre-distortion with PWM pre-distortion, when amplitude resolution requirements are replaced with timing resolution requirements, can be beneficial for future low voltage CMOS technologies where stringent noise margins can reduce the usable voltage amplitude for pre-distortion level settings. It is obvious that optimal pulse shaping (coefficient setting) for analyzed channel is accompanied by a reduction of signal amplitude. It should be noted that the minimum transmitted signal swing clearly depends on the receiver sensitivity and channel frequency response. This is shown in [18] where reduction in receiver sensitivity from 100 mV to 25 mV changed the minimum required transmitter signal swing from 600 mV to 200 mV while the same BER is maintained.

4.2 PWM-RC Pre-Distortion Technique

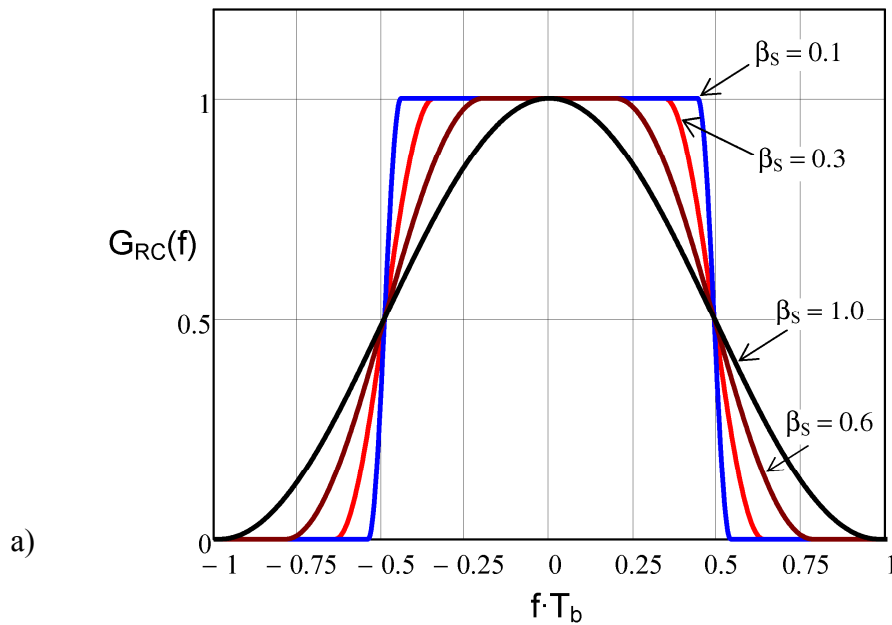
The conventional PWM scheme based on rectangular pulse shaping has many harmonic high-frequency components [16]. It can cause problems in practical implementation of this method in real communication systems, e.g. PCI Express based ones. A method proposed in this work uses a raised cosine pulse scheme to reduce crosstalk noise. The combination of PWM pre-distortion technique and appropriate pulse shaping method can provide an effective reduction of high-frequency components of the pulses. This preserves the beneficial properties of time-domain pre-distortion technique and consequently the crosstalk susceptibility as a main disadvantage of PWM scheme can be reduced. The raised cosine signaling is the process when the waveform of transmitted pulses is changed in order to achieve better signal adaptation to the band-limited channel. The raised-cosine filtering is widely used in digital modulation techniques to effectively suppress ISI. In the dissertation the PWM-RC scheme is

introduced for the first time. In the frequency domain, a function is defined in MathCAD formulation as

$$G_{RC}(f, \beta_s) = \begin{cases} 1 & \text{if } |f \cdot T_b| < \frac{1 - \beta_s}{2} \\ \frac{1}{2} \cdot \left\{ 1 - \sin \left[\frac{\pi}{\beta_s} \left(|f \cdot T_b| - \frac{1}{2} \right) \right] \right\} & \text{if } \frac{1 - \beta_s}{2} \leq |f \cdot T_b| \leq \frac{1 + \beta_s}{2} \\ 0 & \text{if } |f \cdot T_b| \geq \frac{1 + \beta_s}{2} \end{cases} \quad (4.3)$$

The raised cosine pulse transform function is shown in Fig. 4.2a. The parameter β_s (pulse roll-off parameter) is varied from 0.1 to 1.0. It controls the smoothness and the bandwidth, see β_s variation in Fig. 4.2a. The frequency on the x axis is normalized according to the current bit period T_b to easily identify bandwidth variations. For roll-off parameter values close to zero a rectangular shape in the frequency domain is obtained. Extremes are $\beta_s = 0$ and $\beta_s = 1$. In the first case for rectangular shape ($\beta_s = 0$), a significant ripples can cause that neighboring bits will interfere with the current bit. This effect becomes more pronounced for low values of the β_s parameter. It is clearly seen in the time-domain pulse analysis in Fig. 4.2b where the impulse response (inverse Fourier transform) is shown. The second case ($\beta_s = 1$) shows double bandwidth occupation but the impulse response shows more ripple reduction. The impulse response is defined as

$$h(t, \beta_s) = \text{sinc} \left(\frac{\pi \cdot t}{T_b} \right) \cdot \frac{\cos \left(\frac{\pi \cdot t \cdot \beta_s}{T_b} \right)}{1 - \left(\frac{4 \cdot \beta_s \cdot t}{T_b} \right)^2} \quad (4.4)$$



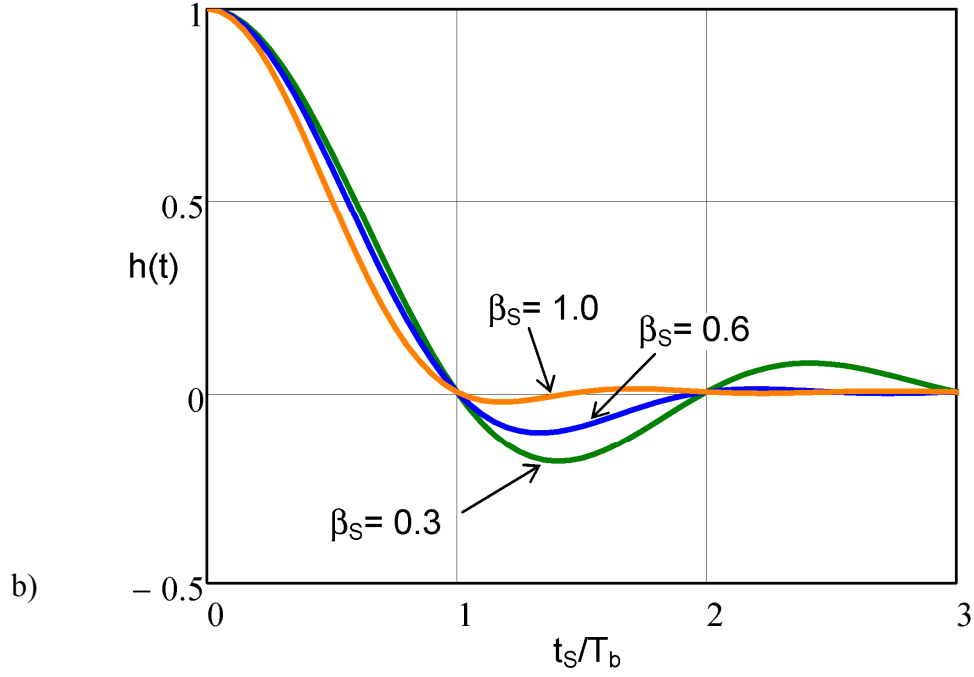


Fig. 4.2: Raised cosine pulse shaping: a) spectral analysis of raised cosine function, b) raised cosine impulse response.

The proposed PWM-RC scheme which is described below still used only one coefficient dc to achieve the required value (amount) of pre-emphasis, compare (4.2) and (4.5). Experimental pulse shaping results normalized to unity peak realized in MathCAD according to (4.5) is shown in Fig. 4.3. For the proposed PWM-RC method the pulse shaping in the time-domain is defined as

$$s_{RC}(t) = s_1(t) - s_2(t) \quad (4.5)$$

where

$$s_1(t) = \begin{cases} \frac{1}{2 \cdot dc \cdot T_b} \cdot \left(1 - \cos \frac{2 \cdot \pi \cdot t}{dc \cdot T_b} \right) & \text{if } 0 \leq t \leq dc \cdot T_b \\ 0 & \text{otherwise} \end{cases} \quad (4.6)$$

$$s_2(t) = \begin{cases} \frac{1}{2 \cdot (1 - dc) \cdot T_b} \cdot \left(1 - \cos \frac{2 \cdot \pi \cdot (t - T_b)}{(1 - dc) \cdot T_b} \right) & \text{if } dc \cdot T_b \leq t \leq T_b \\ 0 & \text{otherwise} \end{cases} \quad (4.7)$$

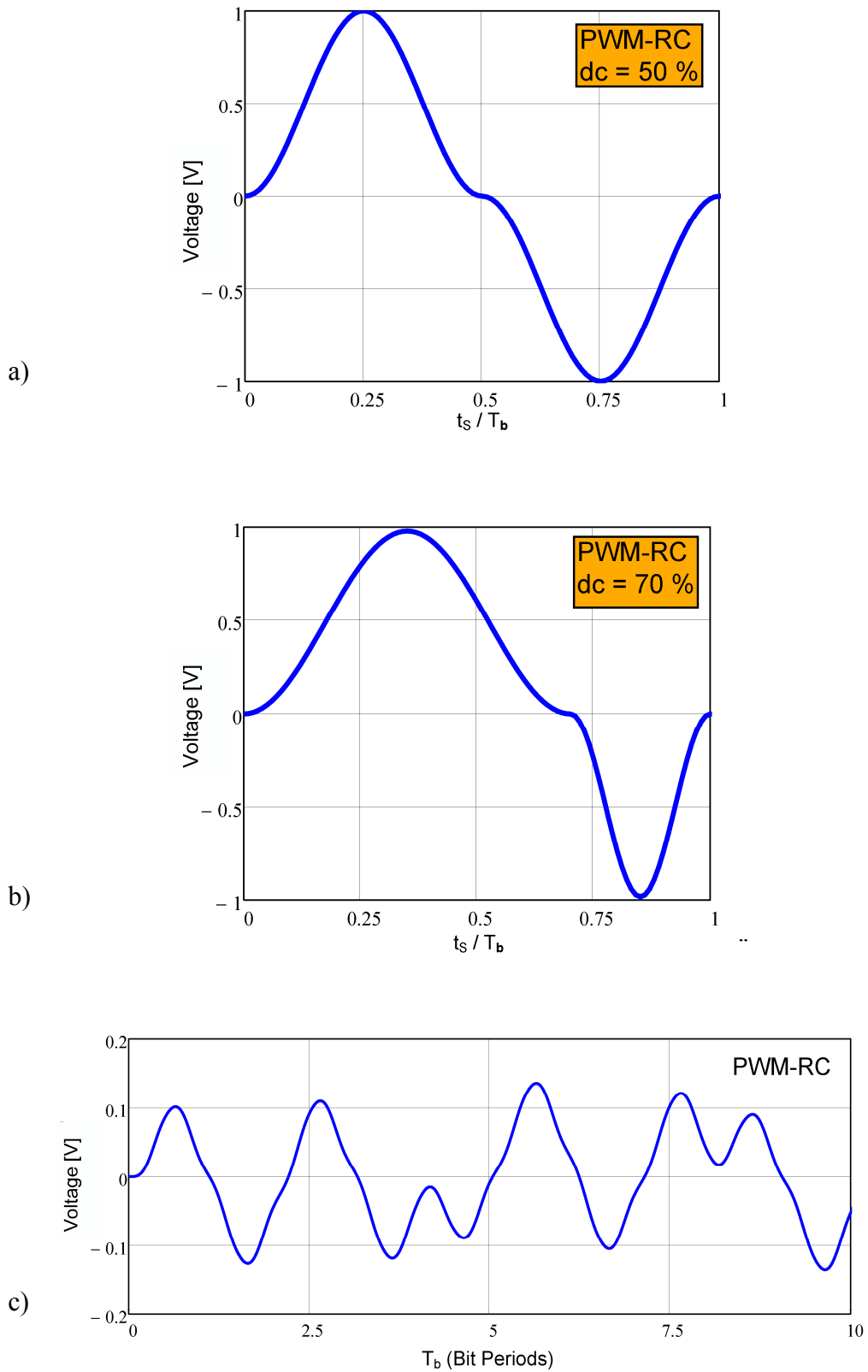


Fig. 4.3: Time-domain analysis: a) PWM-RC pulse shaping - strong pre-emphasis, b) PWM-RC pulse shaping -weak pre-emphasis, c) band-limited channel output, PWM-RC scheme enabled.

4.3 Frequency Spectrum Analysis

From the power spectral density (PSD) analysis for both FIR and PWM pre-distortion methods described in detail in [16], it is clearly seen that the spectrum of PWM pulse is shaped and moved to higher frequencies. In Fig. 4.4a the PSD analysis for both FIR and PWM signal pulses is shown. The coefficients settings are chosen according to the analysis in Fig. 4.1 where, for analyzed band-limited channel, optimal coefficients to minimize ISI are given. Finally, the spectrum of a conventional NRZ pulse is shown. The power spectral density of the stochastic signal $PSD(\omega)$ for the PWM filter is calculated according to a formula in [43]

$$PSD(\omega) = \frac{|P(\omega)|^2}{T_b} \sum_{k=-\infty}^{\infty} R(k) \cdot e^{j\omega k T_b} \quad (4.8)$$

where $P(\omega)$ is the Fourier transform of $p(t)$ (in this case it is $p_{pwm}(t)$ and $p_{fir}(t)$) and $R(k)$ is the autocorrelation function for a polar NRZ signaling ($R(k)$ is the same for PWM as for polar NRZ) and is completely calculated in [44], [16].

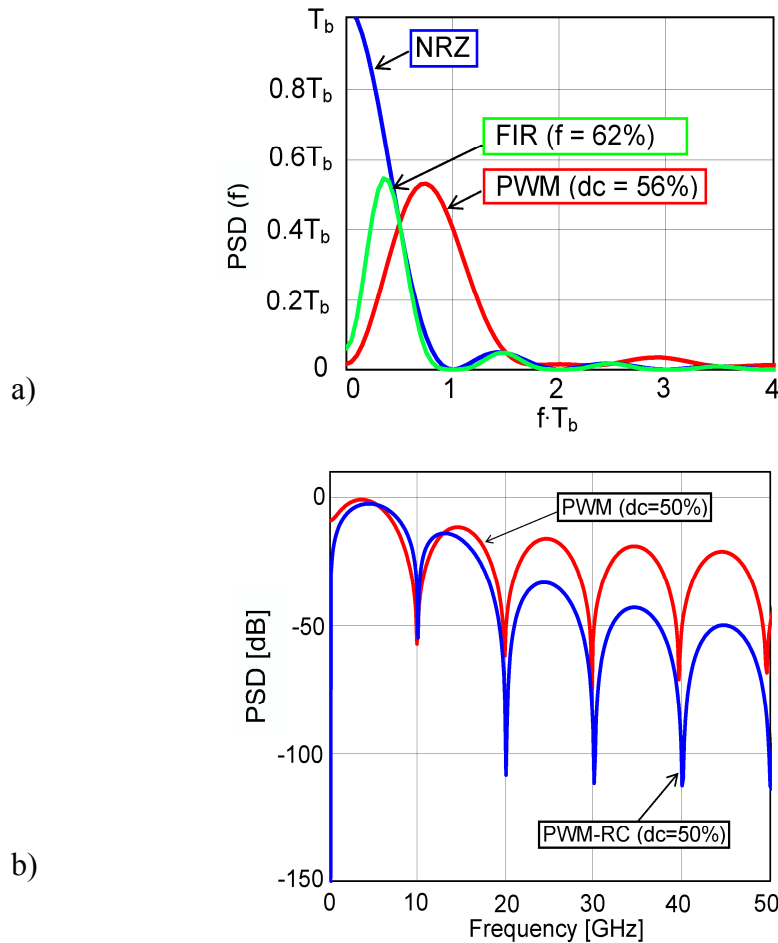


Fig. 4.4: Spectrum analysis: a) analysis of PSD for different signal types, b) frequency spectrum analysis of conventional PWM pulse vs. PWM-RC pulse.

The spectrum of PWM pulse is more boosted at higher frequencies above Nyquist frequency (0.5 on the x axis) approximately for d values from 65 % or less. It can be important factor for higher performance to compensate more lossy channels. The main disadvantage of the PWM method proposed in [16] is that the output pre-distorted signal has many harmonic high frequency components, especially if low-frequency pattern is transmitted. This situation is critical with increasing level (amount) of pre-emphasis. Furthermore, it is necessary to take into consideration that for practical implementations optimal duty cycle coefficients for more lossy channel are just located about strong pre-emphasis level between 50 % and 60 %. In Fig. 4.4b the frequency spectrum analysis for both conventional PWM and proposed PWM-RC pre-distortion methods is shown. In this case a strong pre-emphasis level ($dc = 50\%$) is chosen. It is clearly demonstrated that for proposed PWM-RC pulse the high-frequency harmonic components are more attenuated. It can be an important factor to suppress high-frequency harmonic content in a conventional PWM scheme and also a potential crosstalk noise. Both signal pulses have $T_b = 200$ ps.

The PWM pulse $p_{pwm}(t)$ definition is used to calculate the spectrum of the PWM filter by taking the Fourier transform, similarly in [16] as

$$P_{pwm}(\omega) = \int_{-\infty}^{+\infty} p_{pwm}(t) \cdot e^{-j\omega t} dt = \int_{-T_s/2}^{(d-0.5)T_s} e^{-j\omega t} dt - \int_{(d-0.5)T_s}^{T_s} e^{-j\omega t} dt. \quad (4.9)$$

Now for proposed PWM-RC pre-emphasis the frequency domain transfer functions can be calculated according to (4.5) by taking (4.6) and (4.7) into account. The frequency transfer function response for PWM-RC filter can be calculated as follows

$$H_{PWM-RC}(\omega) = \frac{P_{pwm}(\omega)}{G_{RC}(\omega)}. \quad (4.10)$$

In Fig. 4.5a the PWM-RC filter transfer function for various duty cycle coefficients settings is shown. In this case, the pulse roll-off parameter β_s is set to 0.4. The proposed PWM-RC scheme is capable of higher loss compensation around Nyquist frequency (0.5 on the x axis). For example, the gain 10 dB of PWM-RC equalizer corresponds with value 0.6 on the x axis, see Fig. 4.5a. The conventional PWM filter shows the same gain value but for the value 0.8 on the x axis. The proposed method allows not only to set the optimal pre-emphasis level by changing the duty cycle but the β_s parameter can be used to adjust the optimal equalization characteristic according to current channel losses. It is obvious that the Nyquist frequency varies according to the actual data transmission rate. For lower data rates the β_s parameter can be set to a higher value. In this case high frequency noise and crosstalk, which can degrade performance in real systems, are effectively reduced because high frequency boost is tempered. For higher data rates it is possible to achieve higher channel loss compensation because the amount of equalization around the Nyquist frequency can be effectively adjusted depending on where current high slopes in channel frequency response occur. For completeness, compare channel losses at Nyquist frequencies for 4 Gbps data rate and for 8 Gbps data rate, where the parasitic notch significantly increases the channel losses, see Fig. 2.4a.

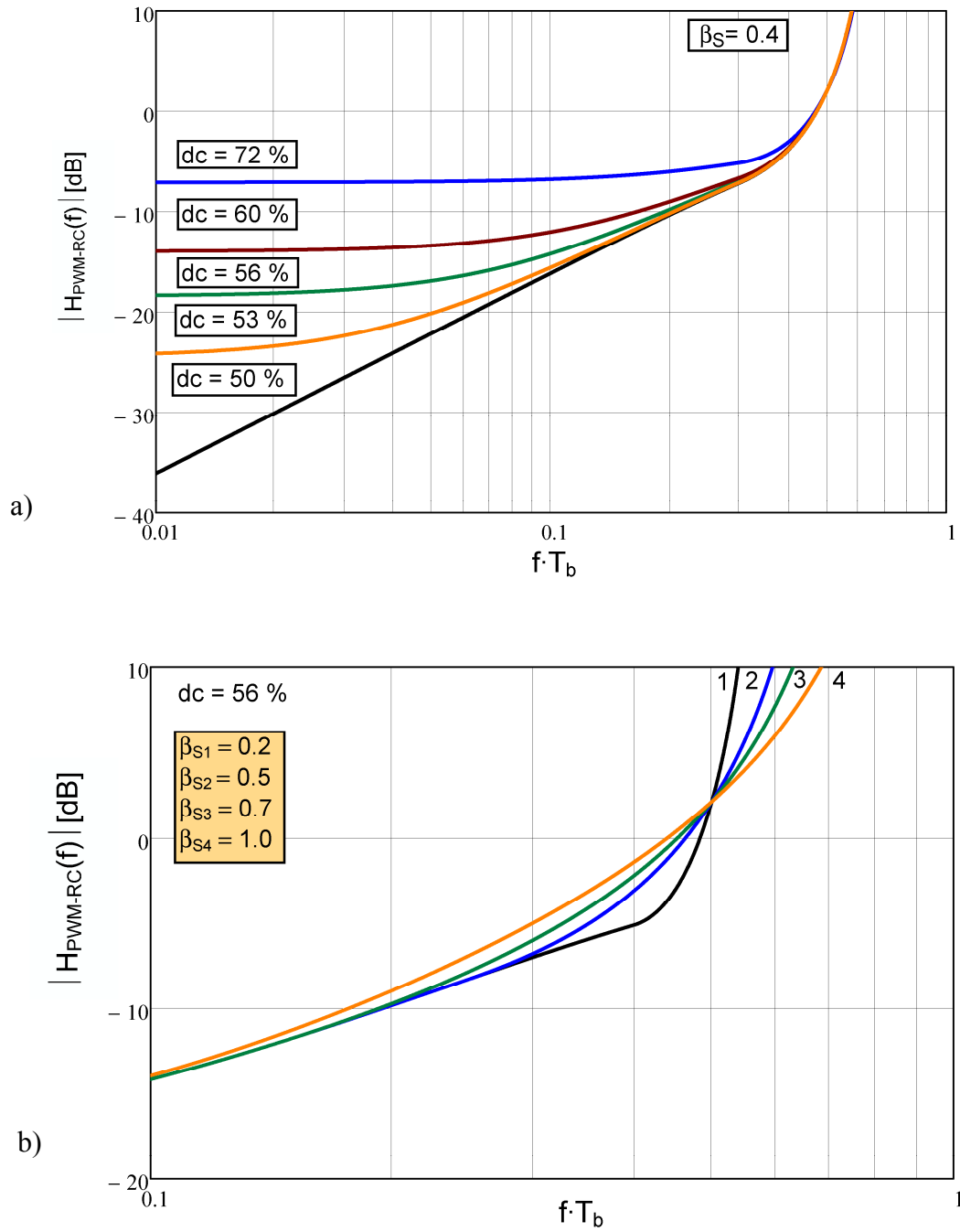


Fig. 4.5: PWM-RC frequency domain analysis: a) Calculated magnitude of PWM-RC filter transfer function ($\beta_S = 0.4$) b) high-frequency compensation settings for different values of β_S parameter.

The main advantage of the proposed PWM-RC pre-distortion method lies in its adjustable variability. Comparing the conventional PWM pre-emphasis and FIR pre-emphasis transfer functions is shown in [16]. In this case the proposed PWM-RC method retains the same behavior for low-frequencies as the FIR filter and conventional PWM filter. The PWM scheme due to the time-varying has high-order transfer function and so effective gain of the PWM filter increases to infinity [16]. It can cause also additional high-frequency noise in output pre-distorted signal even if weak pre-emphasis is applied. The PWM-RC pre-emphasis technique is capable to find optimal settings for both low-frequency and high-frequency signal content and additional high frequency content can be minimized due to the adjustability at higher frequency compensation, see Fig. 4.5b.

4.4 Equalized Channel Transfer Functions

The verification of proposed PWM-RC method is performed by using two type channel models. In the first case, the band-limited channel ($BW_{3dB} = 0.35$ GHz) with first order transfer function is used. This channel has a monotonously increasing attenuation with frequency. The maximum loss compensation (strong pre-emphasis, $dc = 50$ %) is selected. The decisive factor for the performance of the proposed equalizer is how the overall swing is reduced in order to achieve the reduction in minimum-to-maximum loss for the system. In other words, how the equalizer is able to reduced difference between attenuation of low-frequency signal content and high-frequency signal content. This is usually called “flattening” of the magnitude of the frequency response [1]. In [43] better performance of the PWM filter for equalization of the 1st order cable channel transfer function (approximately corresponds to channel transfer function of theoretical channel [49], [50]) is shown. The performance of all analyzed pre-emphasis methods for maximum loss compensation is shown in Fig. 4.6a. In Fig. 4.6b the overall loss compensation of all equalizers for various BW_{3dB} setting is shown.

It is obvious that the reduction in the loss variation for FIR filter (note that f_N is at 0.5 on the x-axis) is only approximately 7 dB improved compared with a transmission channel loss at the same $BW_{3dB} = 100$ MHz. The conventional PWM method reduces overall losses to 14 dB. The proposed PWM-RC method due to the possibility of high frequency loss compensation adjustment, see Fig. 4.5b is able to decrease the overall losses to 12 dB. For $BW_{3dB} = 350$ MHz setting this reduction approximately triples the frequency at which the eye closes completely from 0.8 GHz to 2.5 GHz, see chapter 2 where 6 dB limitation is described. In the case of conventional PWM filter the reduction in the loss variation allows only shifting the frequency at which the eye closes completely from 0.8 GHz to 1.8 GHz.

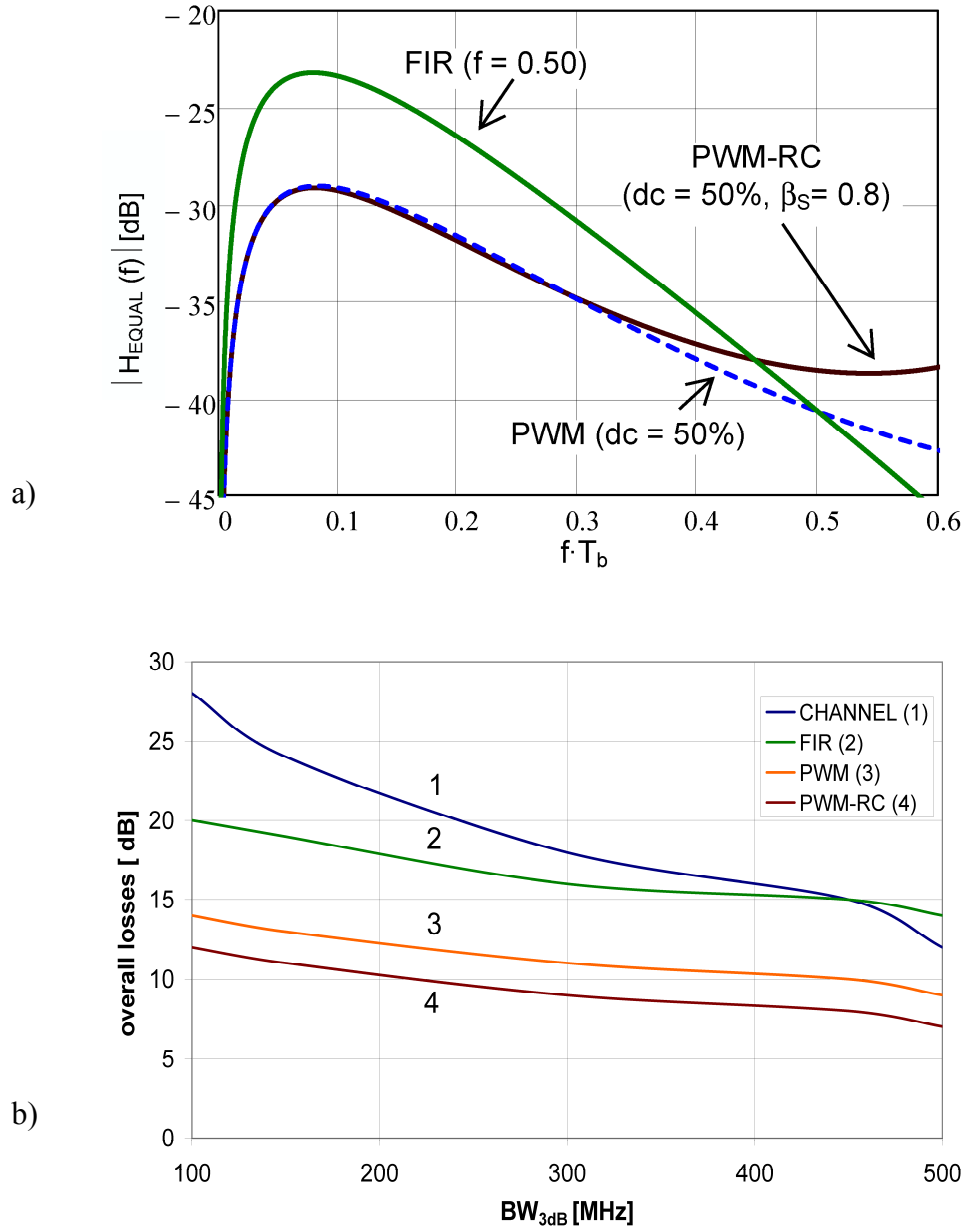


Fig. 4.6: Equalization performance: a) equalized first order channel transfer function (strong pre-emphasis), b) pre-emphasis techniques overall losses compensation performance analysis.

Similarly, the equalized transfer function of PCB channel with higher-order transfer function was performed. For the analysis of higher-order transfer function a simplified model of transmission path is described in [46]. The analyzed model depicts this situation in which the propagating signal currently jumps from signal layer 1 to signal layer 2 through the use of an electrical via, an impedance discontinuity arises at the location of the electrical via [46]. The MathCAD model of higher-order transmission channel for analysis is created by using source code from [46], [47]. The value of parasitic via capacitances C_{VIA} is varied from 2 pF to 4 pF and the performance of all equalizers to overall loss compensation is calculated in Fig. 4.7b. In this case the overall loss compensation is calculated as the difference between attenuation of parasitic peak

and attenuation at Nyquist frequency (0.5 on the x axis). It is clearly seen that conventional PWM method is not able to achieve the same performance as conventional FIR method, see Fig. 4.7a. The proposed PWM-RC method significantly improves the equalized transfer function by increasing high-frequency loss compensation. For more complex channel transfer function it is necessary to consider filters with multitap coefficients. However, the proposed equalization method due to its adjustability is able to better equalize real PCB channel discontinuities that come from the vias, connectors and packages used in the design of PCB transmission channel.

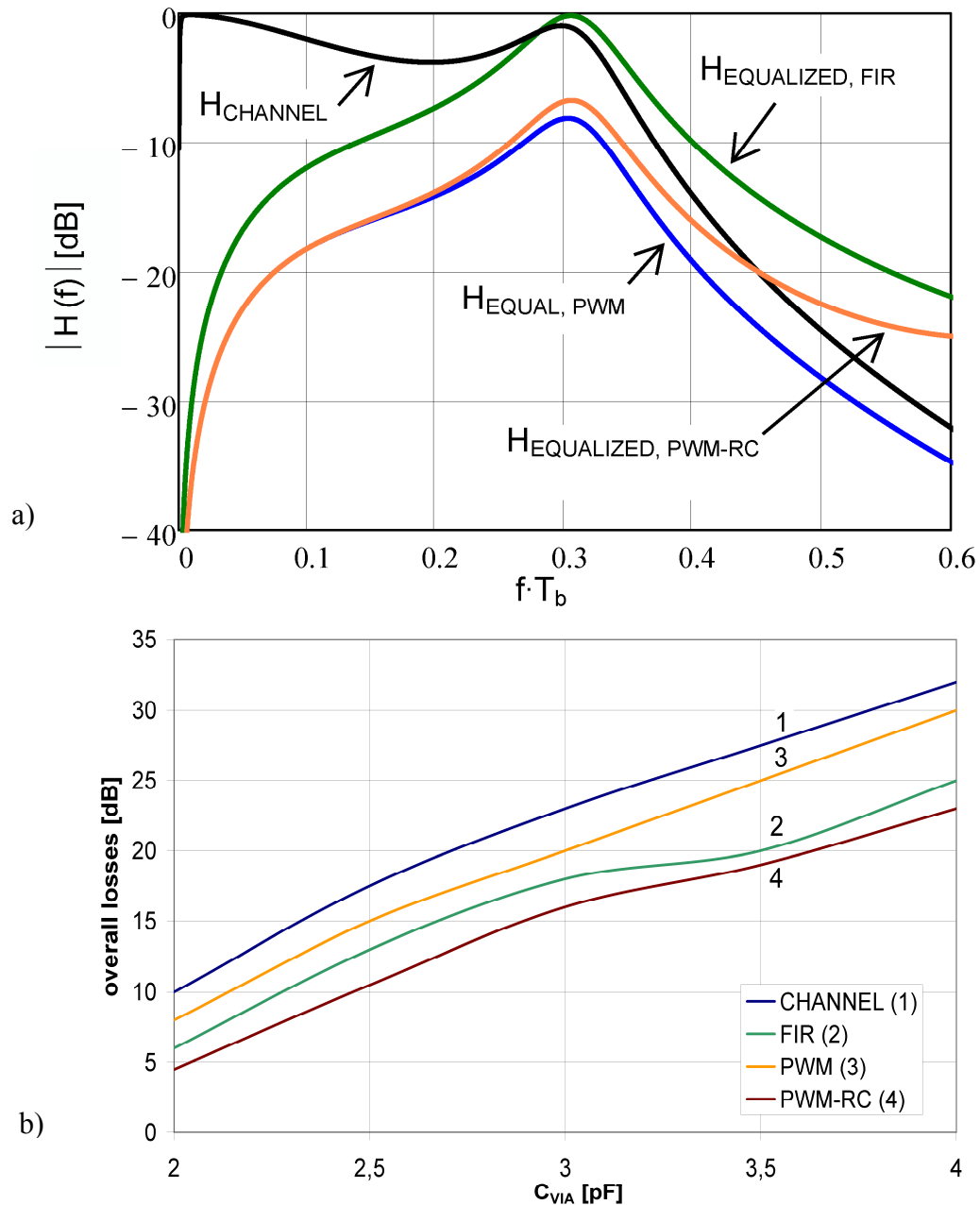
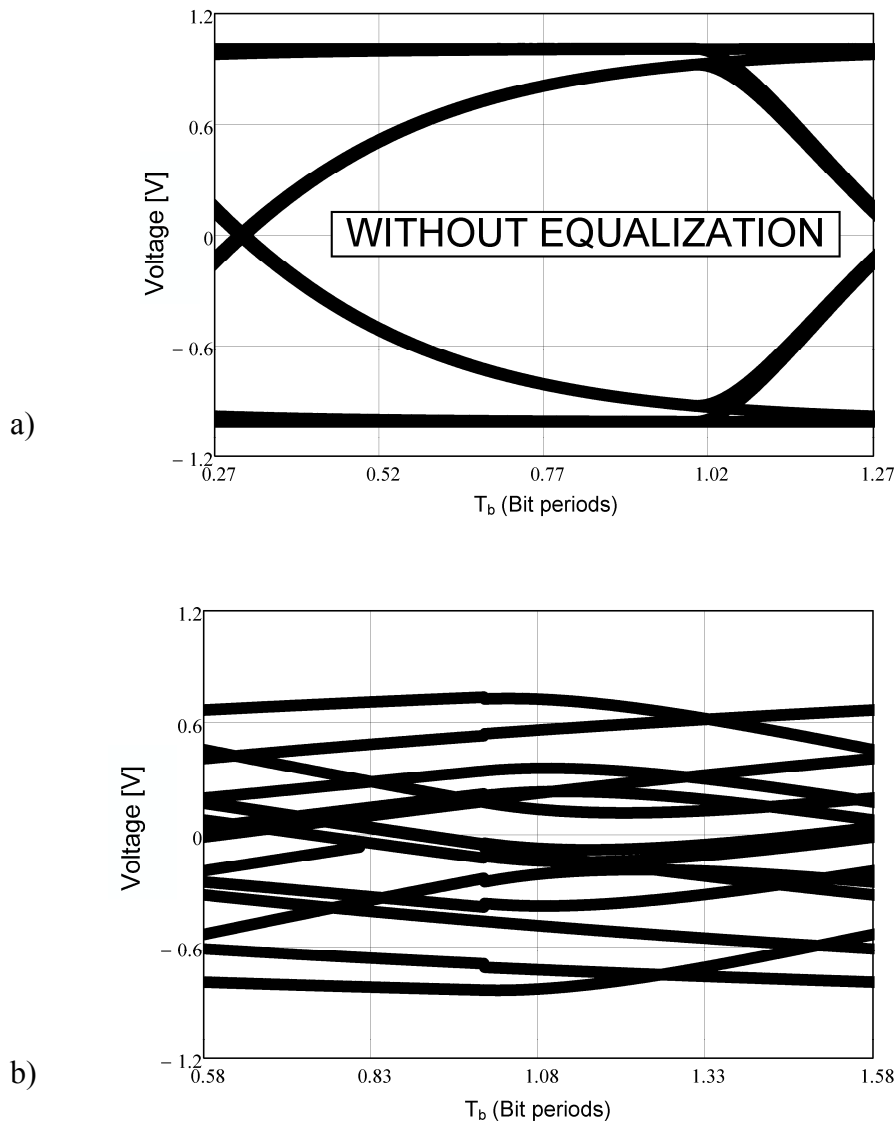


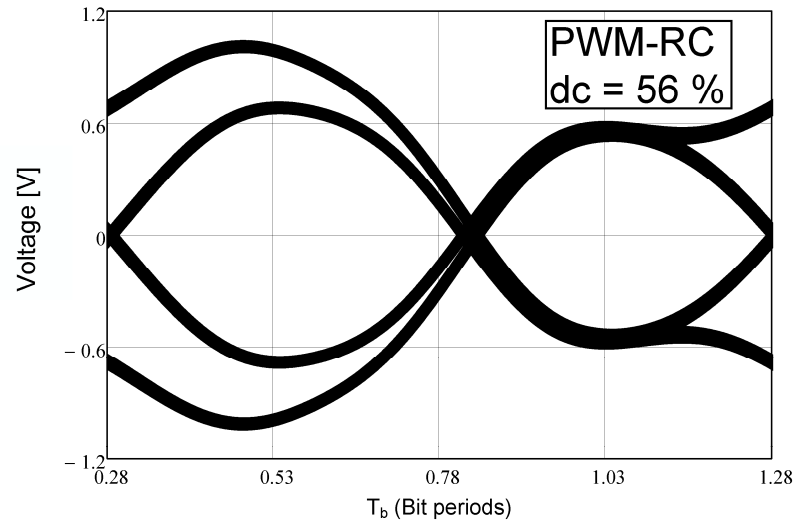
Fig. 4.7: Performance of higher order equalization: a) equalized higher order channel transfer function (strong pre-emphasis) b) pre-emphasis techniques overall losses compensation for higher-order channel.

4.5 Eye Diagram Analysis

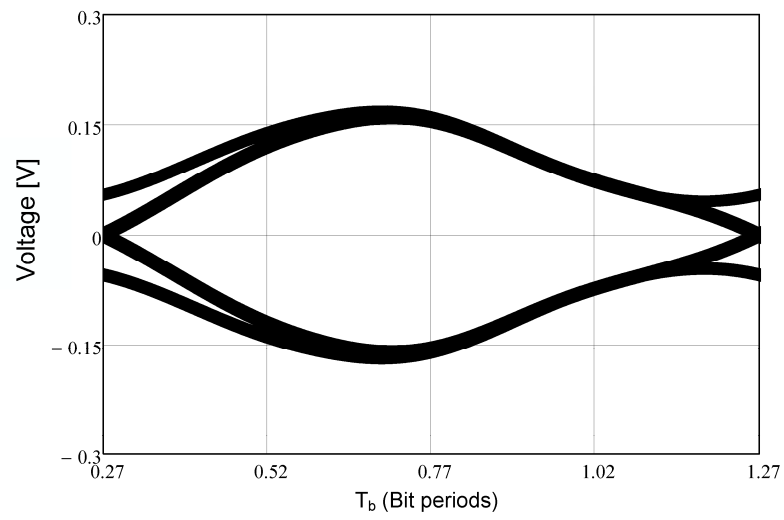
The effect of adjusting the dc parameter of the PWM filter and f parameter of the FIR filter is shown in Fig 4.8 where all described pre-emphasis methods are compared. The model of the communication system for PWM and PWM-RC pre-emphasis methods was created in MathCAD and has not been published in any paper yet. The simulated pulse shaping for PWM method corresponds very well with the measured results [16]. The left and right edges in the eye diagrams correspond to the symbol edges. For all analyzed methods an optimal coefficient settings were selected according to the analysis in Fig. 4.1. The optimal value of pre-emphasis is strongly dependent on current channel losses, see eye diagrams, where over-emphasis is shown [42], [48]. The channel response without any pre-emphasis technique is also shown. Note that the time scale is the same for all eyes and one bit period is intercepted. Note how the proposed PWM-RC method minimizes ISI while the maximum eye opening is maintained, compare PWM and PWM-RC channel output eye diagrams.



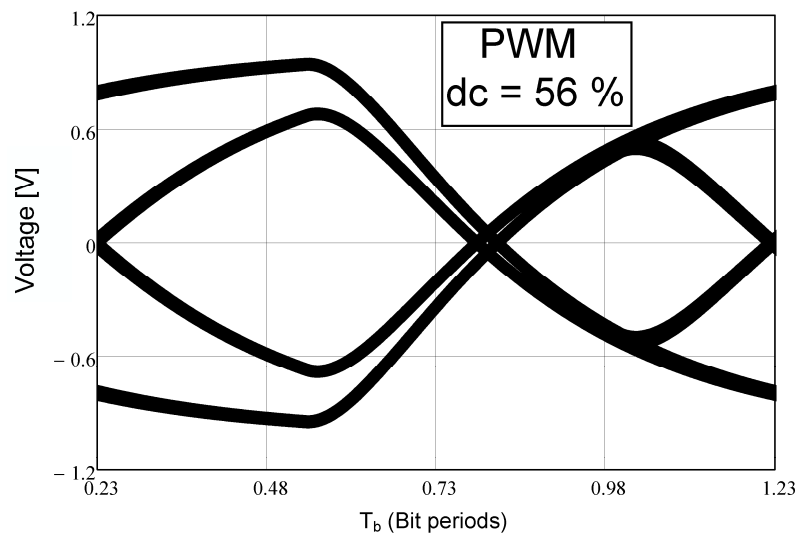
c)



d)



e)



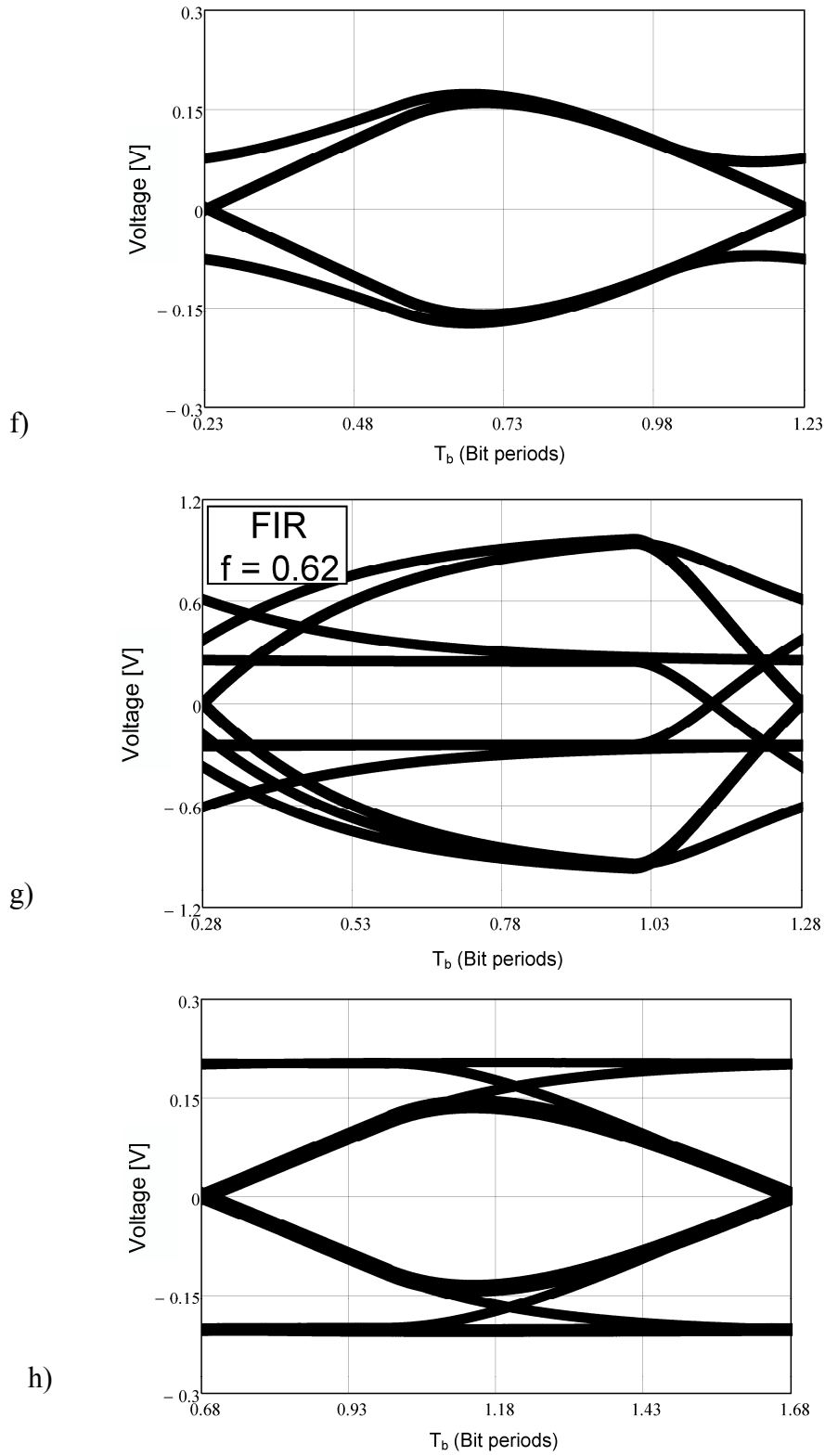


Fig. 4.8: Eye diagram analysis ($BW_{3dB} = 350$ MHz): a) transmitter output at 5 Gbps, b) channel output, c) transmitter output for PWM-RC signalling, d) channel output for PWM-RC signalling, e) transmitter output for PWM signalling, f) channel output for PWM signalling, g) transmitter output for FIR signalling, h) channel output for FIR signalling.

4.6 Signal spectrum analysis

The main disadvantage of conventional pre-emphasis methods as previously described above is a strong susceptibility to crosstalk [15], [16]. In [16] by using a simple Fourier series calculation it is shown that the output spectrum of conventional filter exhibits more high frequency components if low-frequency (LF) pattern (transmitting many 1s in succession) is transmitted. It can cause complications if channel which has been equalized is predisposed to crosstalk formation. In Fig. 4.9 and Fig. 4.10 the frequency spectrum analysis at the band-limited channel output for both PWM methods is shown. In the first case the strong pre-emphasis setting is selected. The real random high-speed 5 Gbps data stream is formed. The proposed PWM-RC method significantly reduces high frequency harmonic components.

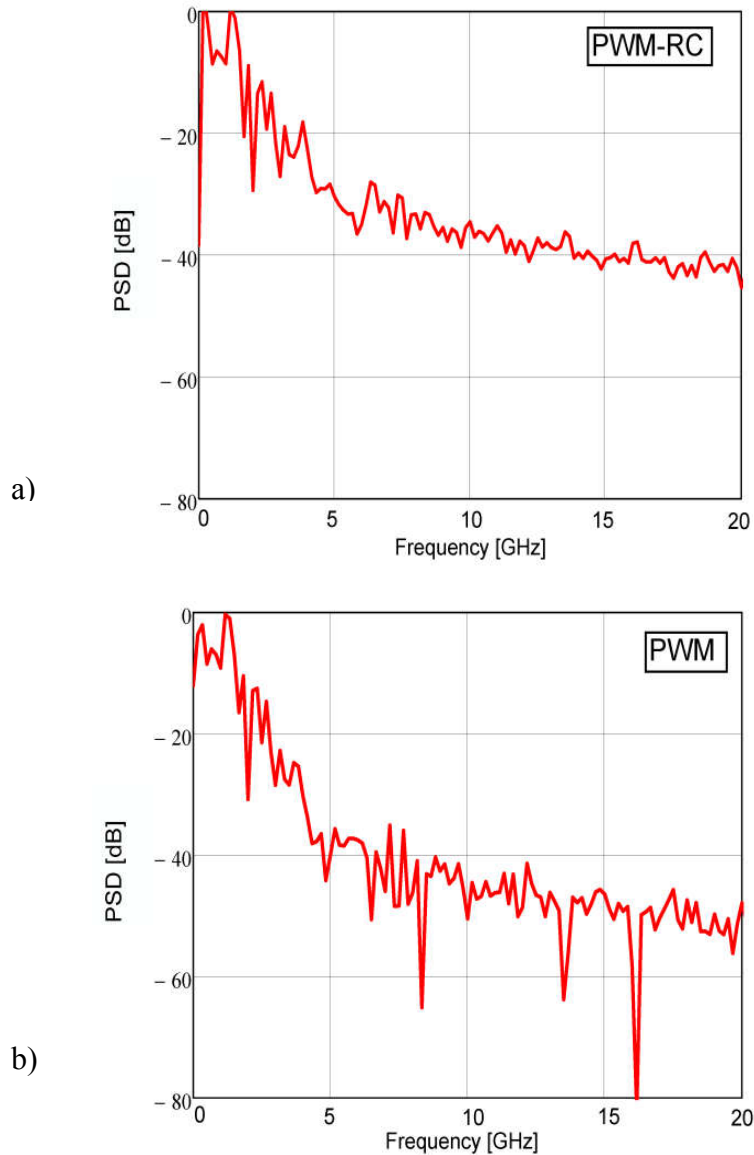


Fig. 4.9: Channel output frequency spectrum analysis if random data pattern is transmitted at 5 Gbps ($BW_{3dB} = 150$ MHz, strong pre-emphasis enabled $dc = 50\%$): a) PWM-RC scheme b) PWM scheme.

In the second case the frequency spectrum analysis is focused on the problem described above. The optimal pre-emphasis level is enabled. Now, the LF pattern is transmitted over the band-limited channel. We can see again the significant reduction in high-frequency components. It can be concluded that the proposed PWM-RC scheme is able to sufficiently compensate the additional high-frequency components for lower switching frequency. This behavior is close to conventional FIR filter where the filter exhibits less power for lower switching frequency. For the HF pattern the difference between FIR and PWM scheme is only in phase (time-shift) [16]. However, in Fig. 4.9 it is clearly seen additional high frequency harmonic content compensation if proposed PWM-RC scheme is used.

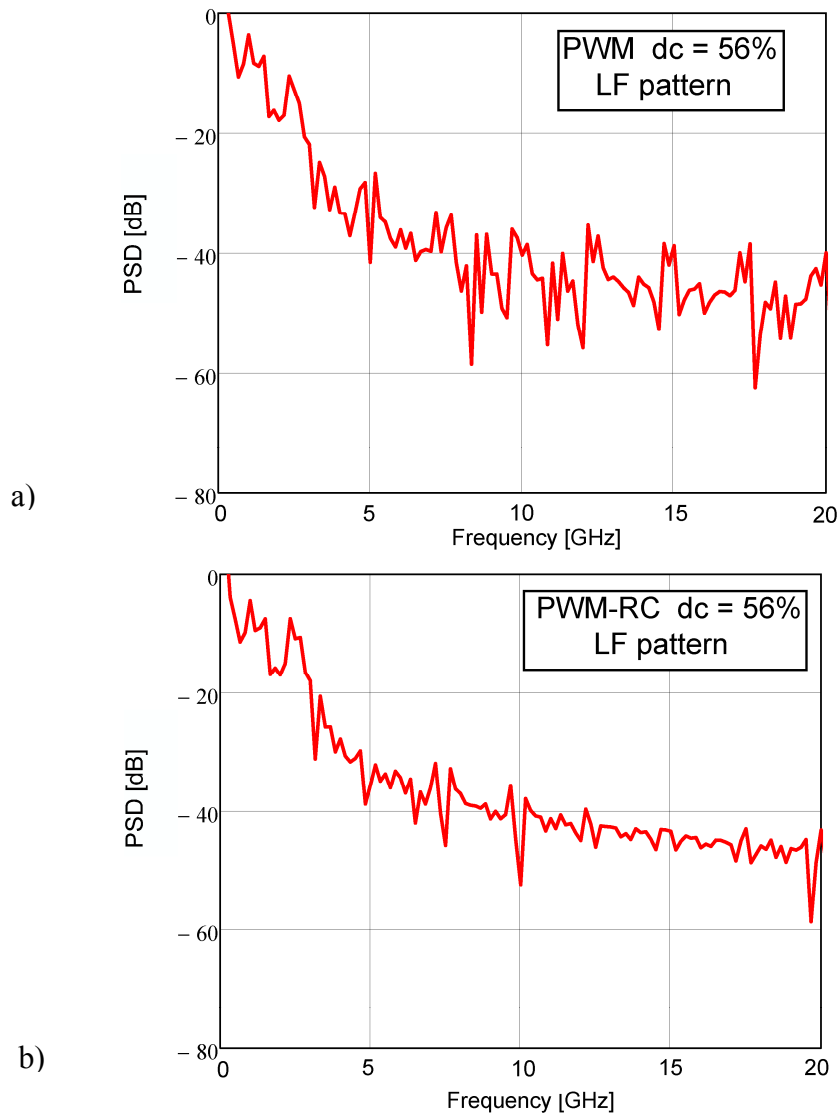


Fig. 4.10: Channel output frequency spectrum analysis if LF data pattern is transmitted at 5 Gbps ($BW_{3dB} = 350$ MHz, optimal pre-emphasis enabled): a) PWM-RC scheme b) PWM scheme.

4.7 Optimization of raised-cosine pulse

Based on the results discussed in section 4.6 and the results presented in [82], [83] a modified pulse is proposed. The most commonly used Nyquist pulse is the raised-cosine pulse [84]. In [82], [83] pulse shaping based on cosine functions is successfully applied in high-speed signaling communication through real lossy transmission channels. Thus, more variants of signal conditioning are applicable to improve signal integrity through the lossy channels. As can be shown in Fig. 2.10 pulses at the output of the transmission channel are spread over several symbol periods with exponential character.

The proposed signal pulse uses a flipped-exponential function, firstly published in [85]. The invention lies in adaptation of this function to the pulse shaping filter which uses time-domain and amplitude pre-emphasis. Thus, a novel pulse shaping is achieved. The assumptions are based on the similar functionality as in the case of equalizers used in high-speed communication signaling where equalizer transfer function is ideally inverse to transmission channel response. Thus, the conventional raised-cosine pulse shaping is replaced. As will be shown below, this causes better pulse adaptation to pass through the lossy transmission channel. Together with optimized adaptive pulse shaping a better performance is achieved compared to the conventional pulse [85], [86], [87]. The modified pulse is defined in time-domain as

$$s_{\text{exp}}(t) = A_{OPT} \text{sinc}\left(\frac{\pi t}{T_b}\right) \left[\frac{4\beta_x t \pi z_1 + 2\beta_x^2 z_2 - \beta_x^2}{4\pi^2 t^2 + \beta_x^2} \right] \quad (4.11)$$

where

$$z_1(t) = \sin\left(\pi\alpha_x \frac{t}{T_b}\right) \quad \text{and} \quad z_2(t) = \cos\left(\pi\alpha_x \frac{t}{T_b}\right) \quad (4.12)$$

The key pulse parameter which establishes an inverse exponential function is β_x . The modification of the proposed pulse shaping lies in two parameters. The first parameter A_{OPT} is adaptively changed together with parameter β_x which is defined as

$$\beta_x = \frac{\ln 2}{\alpha_x B_x} \quad (4.13)$$

where B_x variable is set similarly according to analysis described above in section 4.2 where pulse-width raised cosine pre-emphasis is described. The maximum value $B_x = 1/(2T_b)$ but optimal value will be lower, $B_{xopt} = 1/T_{bopt}$. The variable α_x is represented as in the case of raised cosine pulse roll-off factor.

4.8 Simulation Results

In Fig. 4.11 all the analyzed pulses are shown. It is obvious that the magnitudes of the two largest side lobes of the pulses based on the flipped-exponential function are smaller than the magnitudes of the two largest side lobes of the conventional raised-cosine pulse. If we compare both pulses based on the flipped-exponential function, we can see additional better performance for optimized exponential pulse where magnitudes of two largest side lobes have still decreasing tendency. Moreover, notice the difference in pulse shaping of optimized exponential pulse where steeper transition is evident. This reduces pulse width and minimizes the pulse spreading due to the channel ISI effect.

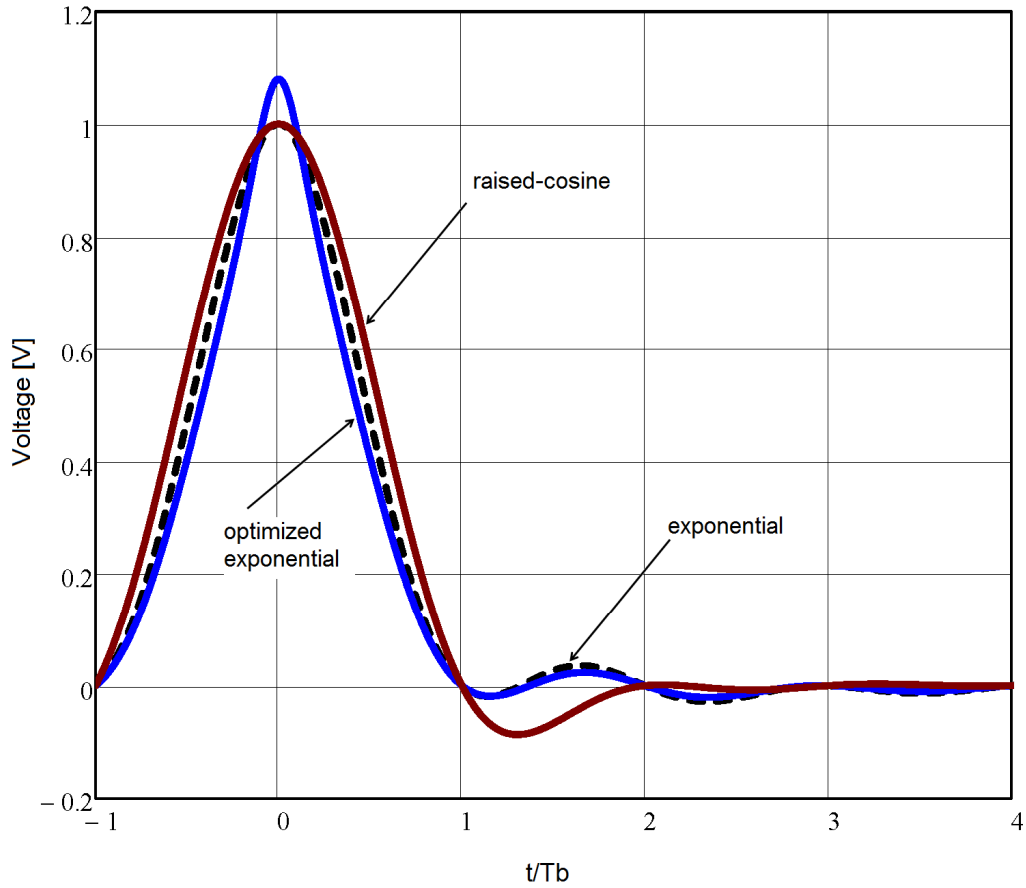


Fig. 4.11: Impulse responses of all compared pulses.

The parameter β_x can be adjusted by changing two variables. Both of the parameters are swept linearly. However the response of β_x is different for each of them. Increasing value of the first variable α_x causes an exponential decreasing of β_x . Increasing value of the second variable T_b shows linear increasing of β_x . This situation is clearly shown in Fig. 4.12.

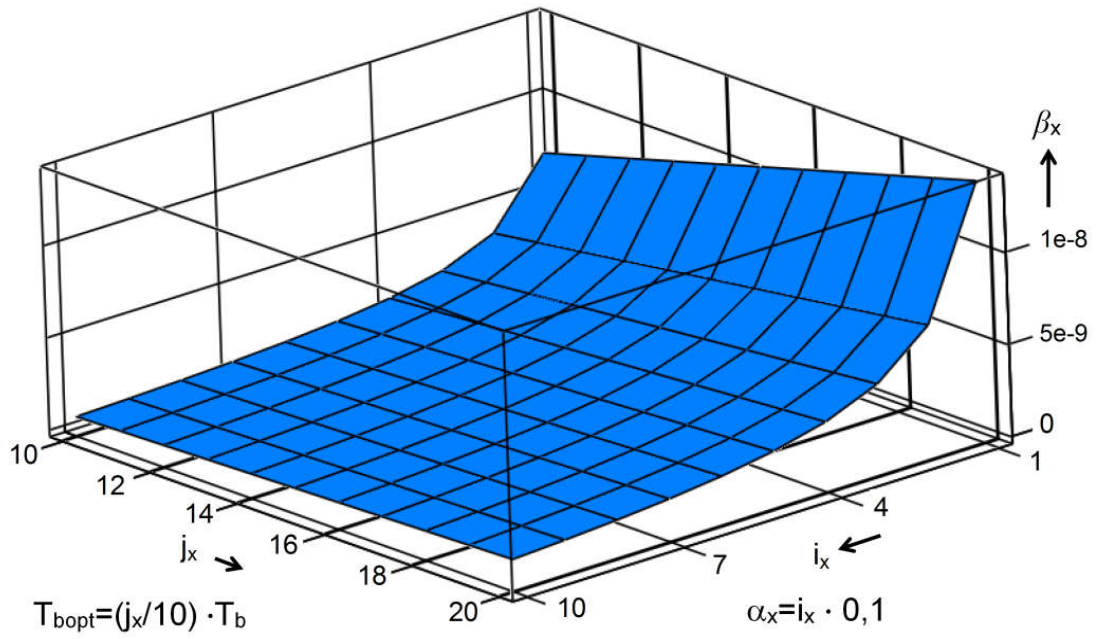


Fig. 4.12: Dependence of β_x when variables α_x and T_{bopt} are linearly swept.

For optimal setting of both parameters, it is necessary to analyze their impact on output signal. In Fig. 4.13 it is shown the impulse response and output eye diagram of proposed pulse during the α_x variation.

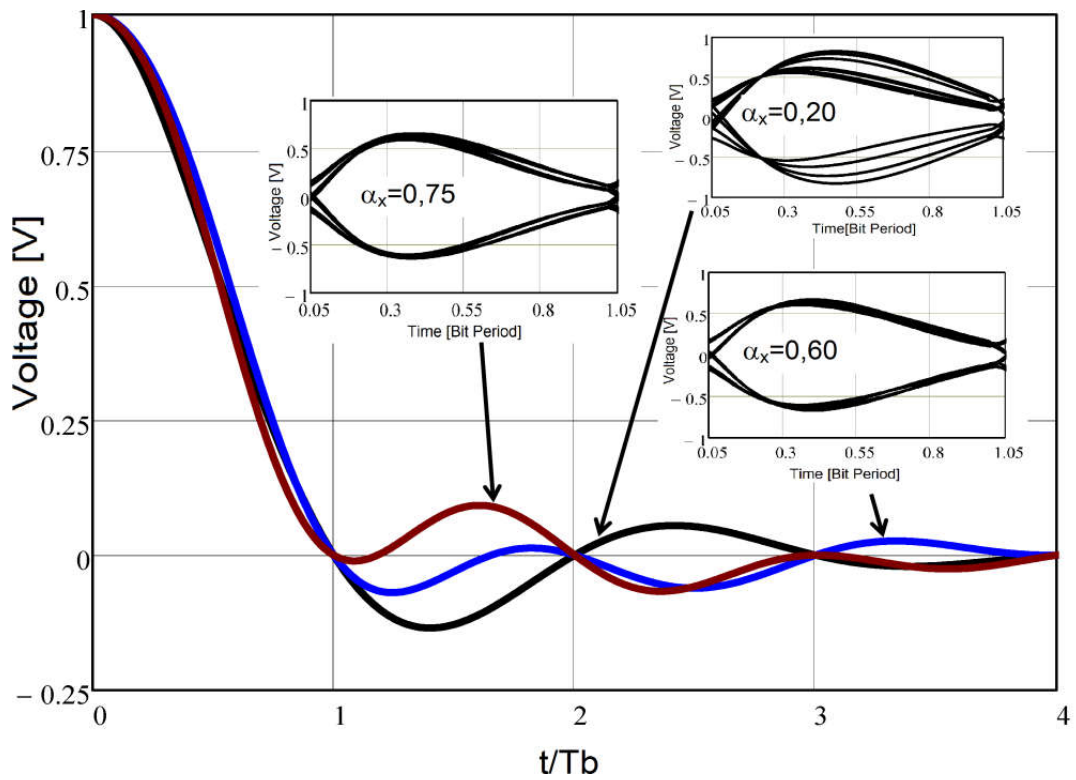


Fig. 4.13: Impulse response and eye diagram performance for various α_x .

It is obvious that appropriate α_x setting can improve jitter and eye opening. In this case transmission channel with small losses was used. Optimal α_x value lies approximately in the middle of range ($\alpha_x = 0.60$). Two possible extremes of α_x are 0 and 1 but in this case eye diagram shows strong ISI. Very low value of α_x can cause significant ISI between symbols and additional signal jitter as well higher α_x values. The second variable T_b shows additional jitter during variation. The situation is clearly shown in Fig. 4.14. As in the previous case, an optimal eye opening is strongly dependent on accurate setting of variables. Both variables complement each other due to the different response of β_x parameter on variation of each of them, see Fig. 4.14. The optimal setting process for β_x parameter includes two main steps. Firstly, the optimal value of α_x variable is found with a set of maximum value of B_x . The next step involves adjusting of variables T_b to achieve jitter reduction.

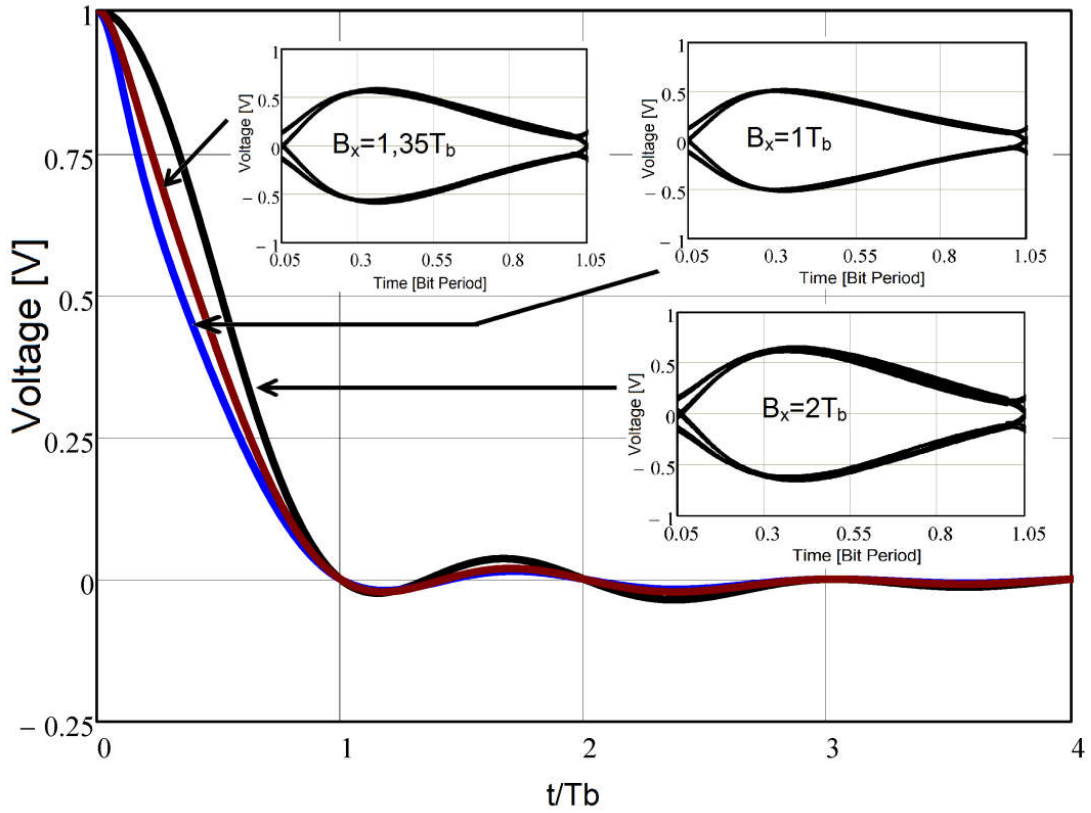


Fig. 4.14: Impulse response and eye diagram performance for various T_b .

Very important is the analysis of pulses susceptibility to system errors. In this case a BER analysis is performed for several values of variable α_x . The BER was analyzed for SNR = 15 dB. Below are shown results of error probabilities for all analyzed pulses in Tab. 4.1, Tab. 4.2 and Tab. 4.3. Note that the error rates are better (smaller) for all α_x variations and timing offsets of the proposed exponential-optimized pulse.

Tab. 4.1 BER analysis, raised cosine pulse.

α_x	t/T_b	$t/T_b \pm 0.05$	$t/T_b \pm 0.1$	$t/T_b \pm 0.2$	$t/T_b \pm 0.25$
0.25	3.33E-07	5.51E-07	1.48E-06	2.37E-05	9.71E-05
0.55	4.93E-08	1.07E-07	2.29E-07	2.45E-06	1.64E-05
0.65	4.99E-08	5.03E-08	9.94E-08	1.40E-06	6.94E-06

Tab. 4.2 BER analysis, exponential pulse.

α_x	t/T_b	$t/T_b \pm 0.05$	$t/T_b \pm 0.1$	$t/T_b \pm 0.2$	$t/T_b \pm 0.25$
0.25	2.55E-07	3.82E-07	1.03E-06	1.55E-05	6.50E-05
0.55	6.05E-08	6.63E-08	9.10E-08	1.62E-06	7.70E-06
0.65	2.09E-08	2.65E-08	4.98E-08	1.16E-06	6.66E-06

Tab. 4.3 BER analysis, exponential-optimized pulse.

α_x	t/T_b	$t/T_b \pm 0.05$	$t/T_b \pm 0.1$	$t/T_b \pm 0.2$	$t/T_b \pm 0.25$
0.25	2.35E-07	3.70E-07	9.92E-07	1.41E-05	5.79E-05
0.55	2.08E-08	2.34E-08	5.79E-08	1.09E-06	6.02E-06
0.65	1.32E-08	1.53E-08	2.89E-08	4.00E-07	5.99E-06

Eye diagram outputs of all analyzed pulses are shown in Fig. 4.15. The conventional raised-cosine pulse shows more ISI predisposition than pulses based on the flipped-exponential function. This may cause former eye closing during the increasing channel losses. Better immunity to ISI shows flipped-exponential variants of pulses. This confirms our consideration that pulses based on flipped-exponential functions can be less degraded by the channel itself. However residual signal jitter is reduced if exponential-optimized pulse is used.

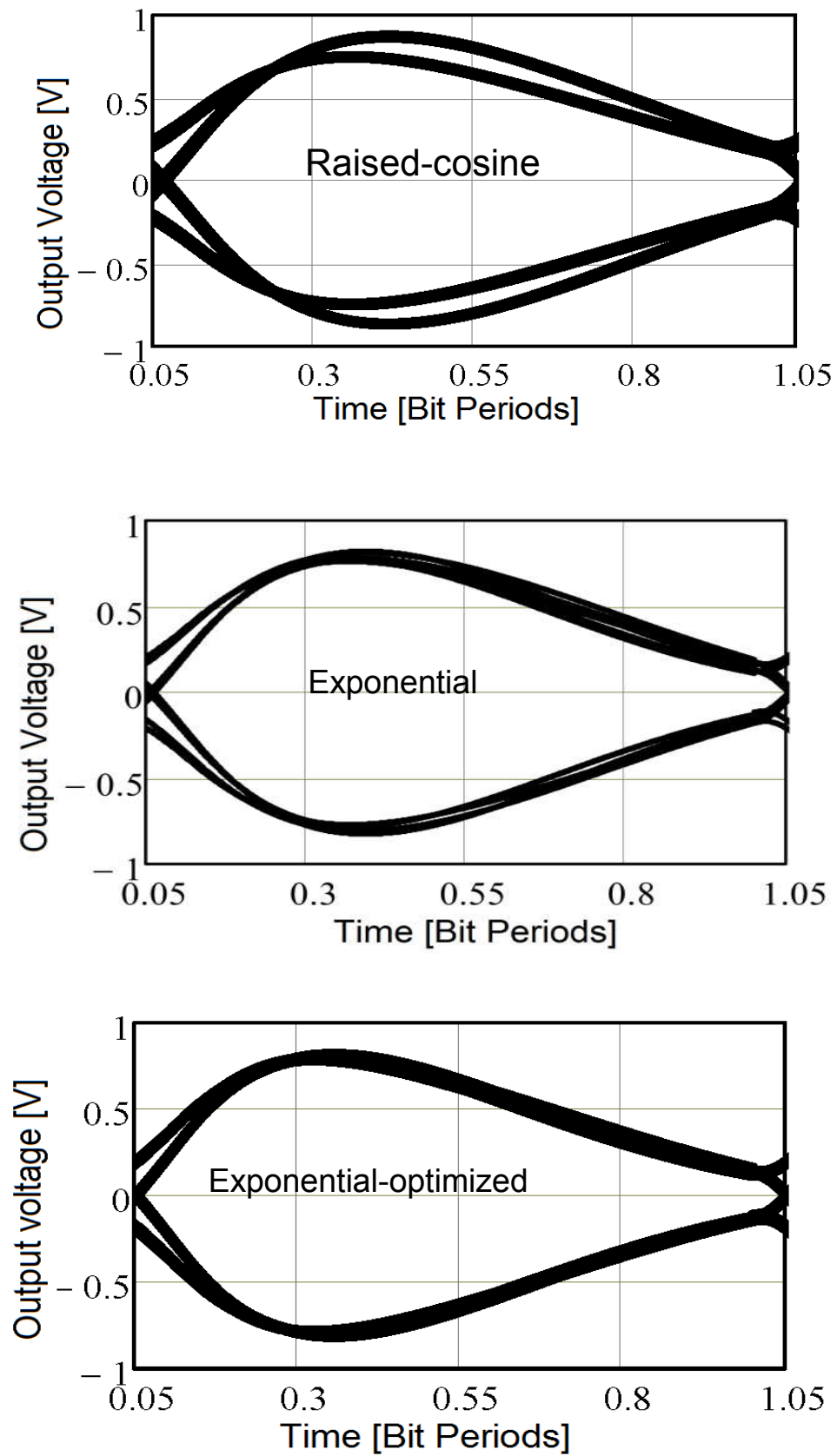


Fig. 4.15: Eye diagram performance of all analyzed pulses.

The BER results for the last set values of $\alpha_x = 0.65$ are plotted in Fig. 4.16. The optimal values of both variables for exponential-optimized pulse are determined as $\alpha_x = 0.65$ and $T_{bopt} = 1.75T_b$.

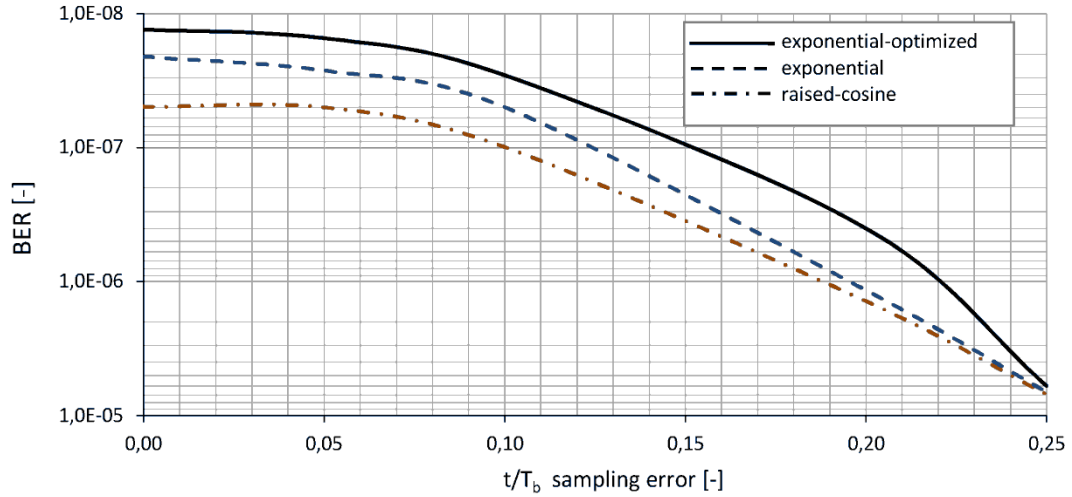


Fig. 4.16: ISI error probability

We can see that raised cosine pulse and exponential pulse have tendency to increase BER during increasing of sampling error. Higher values of sampling errors show almost identical BER results for both pulses. Note also steep increase of BER if sampling error exceeds value ± 0.10 . On the other hand, exponential-optimized pulse shows a different behavior during sampling error variation. In this case the increase of the BER is gradual. As a critical value of sampling error can be designated ± 0.25 . Above this value the BER results are similar for all pulses.

4.9 Summary

In this chapter the effect of raised cosine pulse shaping applied in time-domain PWM signalling techniques was clearly demonstrated. Due to the better ability to overcome higher channel losses which occur in the vicinity of Nyquist frequency, the raised cosine shaping can be effectively deployed for equalization of transmission channels with higher order transfer function. Typically the higher order channels are represented by longer low cost coaxial cables or PCB traces which are affected by some of the signal discontinuities as vias, stubs discussed in section 6. As can be shown in section 5, the raised cosine shaping has considerable impact on the overall performance of higher order signalization techniques because if the pulse shaping is arranged at the transmitter output in such way that the raised cosine pulse shaping similarity is achieved at the channel output the ability to achieve better eye opening for higher transmission rate is significantly supported.

5 EXTENSION OF PWM-RC TECHNIQUE FOR SECOND ORDER CHANNELS

In previous chapter it was shown great potential of PWM equalization technique to improve signal quality at the output of channel with high losses. But the first order channel must be replaced by more complex transfer function because of more disturbing factors which can occur in advanced multi-chip communications systems. Other effects as crosstalk predisposition, via stubs needed for multilayer PCB's can cause that transfer channel function has character of a higher order functions. Thus, the effect of PWM modulation for the first order channel can be easily suppressed and in some extreme situation may be insufficient for proper equalization of channel losses. In this chapter the concept of the first order equalization to higher order equalization will be extended. This is the innovative core of the dissertation and shows the great potential of PWM modulation for higher order equalization.

5.1 Second Order Pulse-Width Modulation Scheme

The coefficients for time domain simulations are defined as dc_1 with $dc_1 \in \{0...0.5\}$ and dc_2 with $dc_2 \in \{0.5...1\}$. In this case it is not possible to use one coefficient as above because optimal results of signal shaping require different coefficients setting. Function $p_{pwm-2}(t)$ in the time domain can be simply formulated as

$$p_{pwm-2}(t) = \left\{ \begin{array}{ll} 0 & t < 0 \\ 1 & 0 \leq t < dc_1 \cdot T_b \\ -1 & dc_1 \cdot T_b < t \leq \frac{1}{2} \cdot T_b \\ -1 & \frac{1}{2} \cdot T_b < t \leq dc_2 \cdot T_b \\ 1 & dc_2 \cdot T_b < t \leq T_b \\ 0 & t > T_b \end{array} \right\}, \quad (5.1)$$

Optimal coefficient setting for the second order pulse-width modulated scheme (PWM-2) is strictly dependent on overall channel impulse response. Due to the more variability in PWM-2 pulse shaping the better adaption to different types of transmission channels may be achieved. As can be seen in Fig. 5.1 the optimal setting of both duty cycle coefficients can result in significant intersymbol interferences reduction. This effect can be achieved for transmission channels with higher losses in relation to the considered transmission rate, see example of transmission channel with significant reduced bandwidth parameter on $BW_{3dB} = 250$ MHz, where the optimal duty cycle coefficients are $dc_1 = 79\%$ and $dc_2 = 29\%$. Significant jitter reduction for PWM-2 signalling is obvious, compare all eye diagrams in Fig. 5.1b. However, the significant amplitude reduction in the case of PWM-2 is obvious. It can be a problem if the noise margin is higher than the residual signal amplitude.

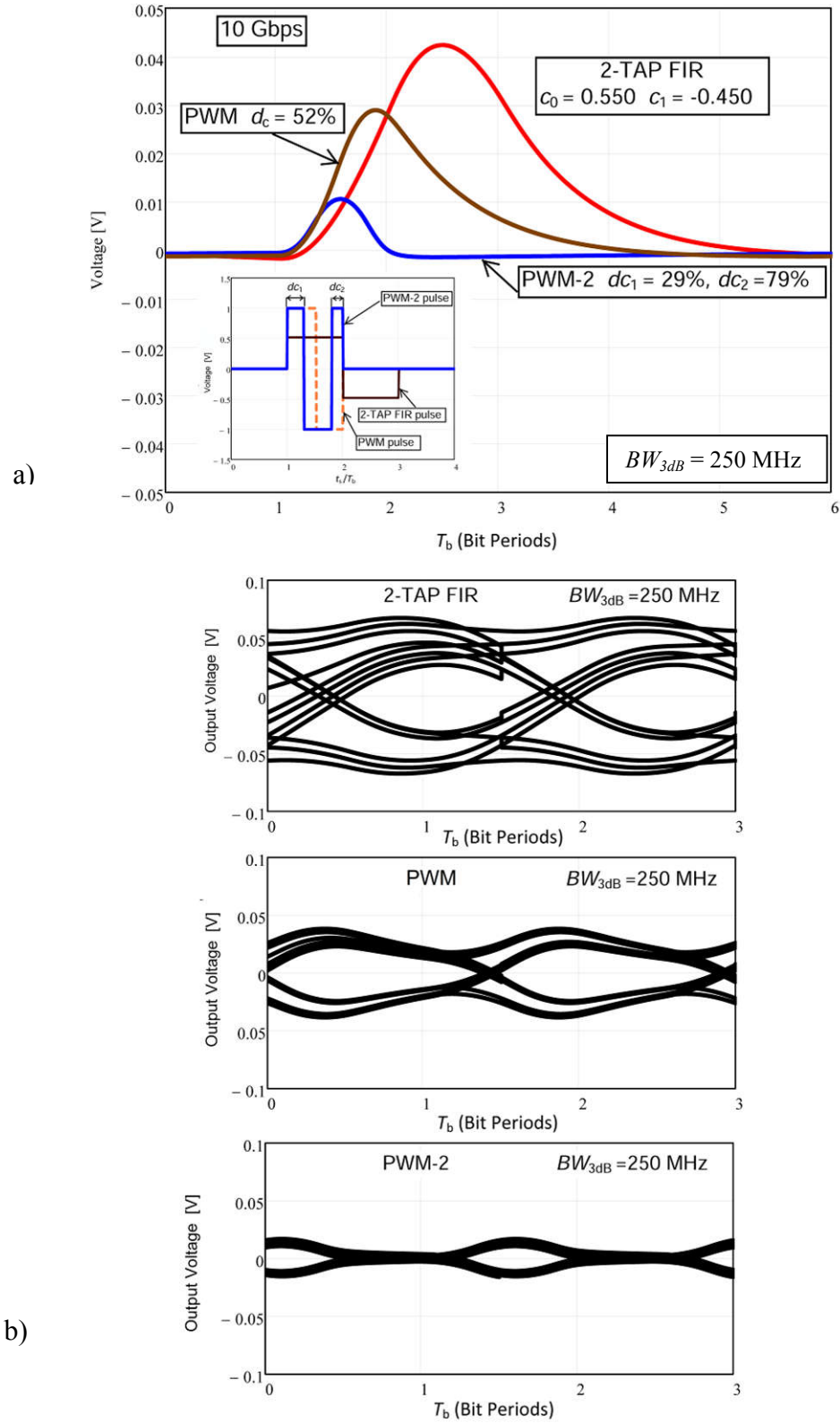


Fig. 5.1: Time-domain analysis: a) impulse responses for FIR, PWM and PWM-2 pulse shaping, b) eye diagrams to evaluate signalling performance after passing through the channel with significant bandwidth restriction.

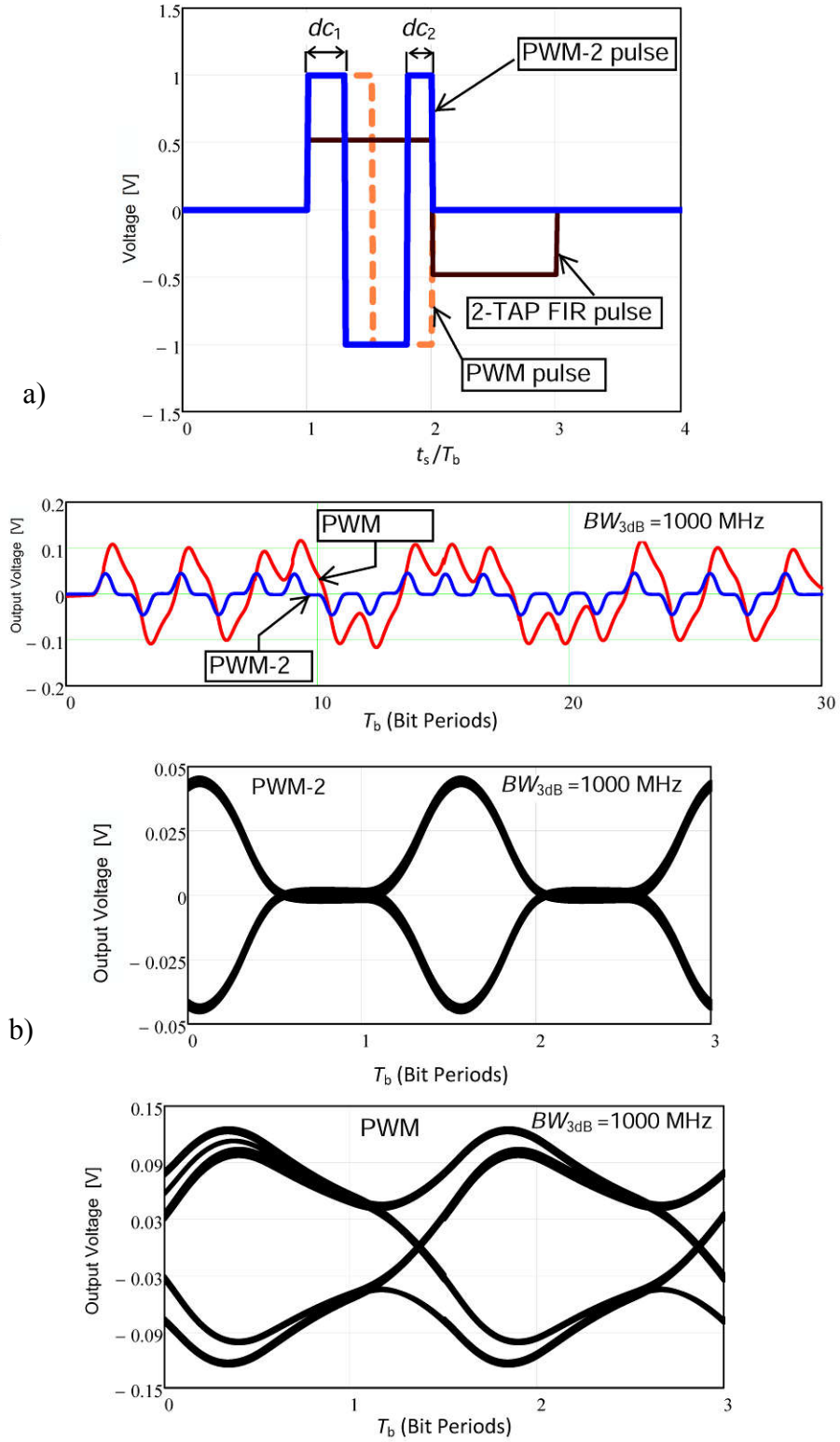


Fig. 5.2: Time-domain analysis: a) PWM-2 pulse shaping with channel output bit stream demonstration, b) the relevant eye diagrams for both PWM and PWM-2 signalling technique.

Figure 5.2 illustrates both PWM and PMW-2 pulse configuration. It is obvious that output 8 Gbps data stream which passes through the channel with bandwidth restriction parameter $BW_{3dB} = 1000$ MHz has pulse shaping similar to raised cosine PWM shaping for PWM-2 signal at the channel input, compare pulse shaping in Fig. 4.3 with output data stream in Fig. 5.2a. The original idea of using raised cosine shaping for time-domain pre-emphasis techniques was for the first time published in research paper [82].

One of the important parameter of equalization technique is own power consumption during the signaling. Thus, calculation of the signal amplitudes during variation of duty-cycles coefficient should be done. For the simplicity during the calculation only basic signaling $V_+ = 1$ V and $V_- = 0$ V is considered. As mentioned above, the duty cycle can be presented either as a percentage or as number ranging from 0 to 1. Basically any electrical signal such as PWM can be considered to be the sum of an infinite amount of sine and cosine waves of varying amplitude and frequency. So the PWM waveform can be expressed as

$$p_{pwm}(t) = \frac{a_0}{2} + \sum_{n=1}^{\infty} a_n \cos\left(\frac{2n\pi t}{dc}\right) + \sum_{n=1}^{\infty} b_n \sin\left(\frac{2n\pi t}{dc}\right) \quad (5.2)$$

where dc represent duty cycle coefficient, the signal pulse width is defined by setting of dc coefficient due to basic signaling consideration.

In (5.2) the coefficients a_n and b_n are obtained as

$$a_0 = \frac{2}{dc} \int_{-\frac{dc}{2}}^{\frac{dc}{2}} p_{pwm}(t) dt, \quad (5.3)$$

$$a_n = \frac{2}{dc} \int_{-\frac{dc}{2}}^{\frac{dc}{2}} p_{pwm}(t) \cos\left(\frac{2n\pi t}{dc}\right) dt, n = 1, 2, \dots \quad (5.4)$$

$$b_n = \frac{2}{dc} \int_{-\frac{dc}{2}}^{\frac{dc}{2}} p_{pwm}(t) \sin\left(\frac{2n\pi t}{dc}\right) dt, n = 1, 2, \dots \quad (5.5)$$

where the coefficient a_0 represents the DC offset component of the signal. The a_1 and b_1 describe the amplitudes of the fundamental frequency sine and cosine waves, while coefficients with higher indices correspond with n harmonics of the fundamental frequency. The pulse definition for calculation can be simply formulated as

$$p_{pwm}(t) = \begin{cases} 0 & -\frac{T_b}{2} < t < -\frac{dc}{2} \\ V_+ & -\frac{dc}{2} < t < \frac{dc}{2} \\ 0 & \frac{dc}{2} < t < \frac{T_b}{2} \end{cases} \quad (5.6)$$

Using simplifications for border conditions $T_b = 1$, because only one period is analyzed, the equations (5.3) - (5.5) can be simplified to

$$a_0 = \int_{-\frac{1}{2}}^{\frac{1}{2}} p_{pwm}(t) dt = \int_{-\frac{dc}{2}}^{\frac{dc}{2}} V_+ = V_+ \cdot dc \quad (5.7)$$

$$\begin{aligned} a_n &= \int_{-\frac{1}{2}}^{\frac{1}{2}} p_{pwm}(t) \cos(n\pi t) dt = \int_{-\frac{dc}{2}}^{\frac{dc}{2}} V_+ \cos(n\pi t) dt \\ &= \frac{V_+}{n\pi} \left[\sin\left(n\pi \cdot \frac{dc}{2}\right) - \sin\left(-n\pi \cdot \frac{dc}{2}\right) \right] = \frac{2}{n} \cdot \frac{V_+}{\pi} \sin\left(n\pi \cdot \frac{dc}{2}\right) \end{aligned} \quad (5.8)$$

Now the amplitude variations during dc changes for both PWM and PWM-2 signals at the fundamental frequency can be calculated. Figure 5.3 illustrates how the signal amplitude varies if it is considered the optimal dc coefficient setting for transmission channel with higher losses, see zones marked by circle. The amplitudes are normalized according to use of bipolar signaling. It is obvious that for optimal equalization settings the PWM-2 scheme requires less power than conventional PWM scheme. This observation is then verified in section 7 where practical implementation was performed.

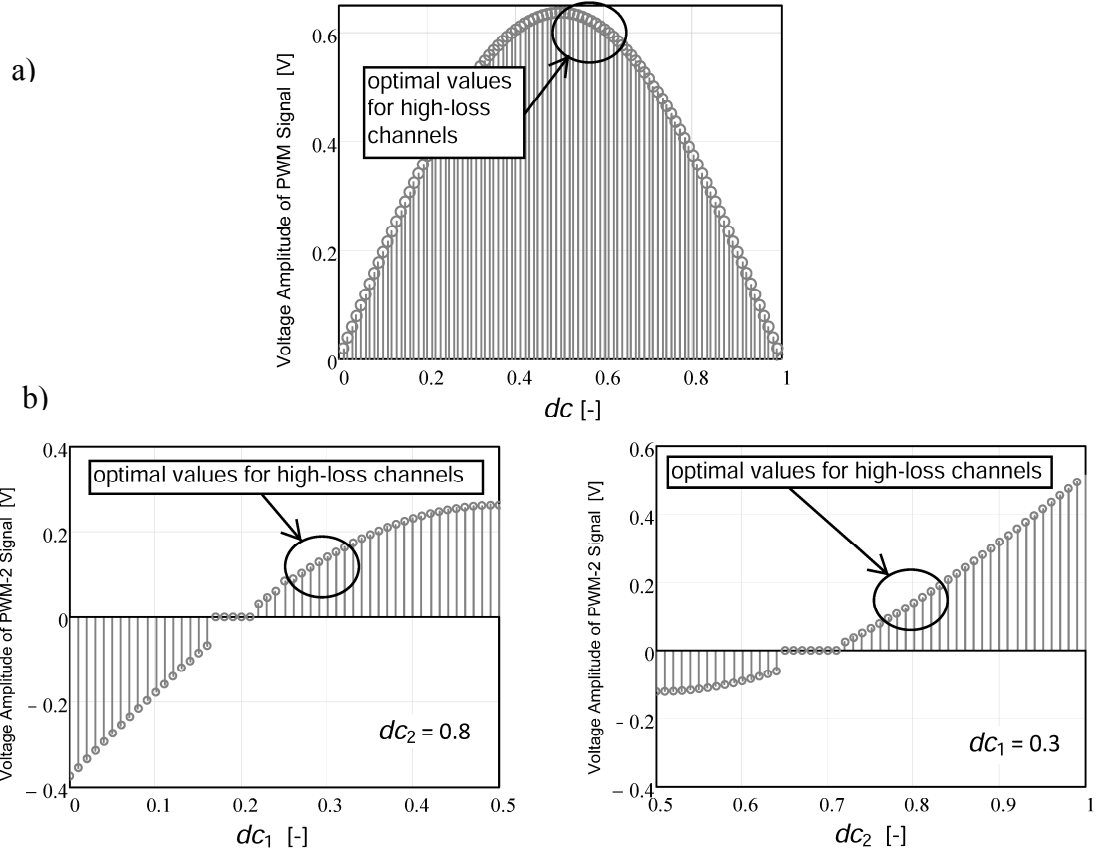


Fig. 5.3: Duty cycle variations: a) amplitude variations of PWM signal during duty-cycle changing, b) amplitude variations of PWM-2 signal during duty-cycle changing.

5.2 Frequency Domain Behavior

For meaningful comparisons previously presented signalling techniques with newly proposed signalling method the PSD is calculated. The voltage scheme is normalized again to ± 1 V. The spectrum $P_{pwm-2}(f)$ of the PWM-2 pulse is calculated through Fourier transform of $p_{pwm-2}(t)$ as

$$P_{pwm-2}(\omega) = \int_{-\infty}^{\infty} p_{pwm-2}(t) \cdot e^{-j\omega t} dt = \int_{-\frac{T_b}{2}}^{-dc_1 \cdot T_b} e^{-j\omega t} dt - \int_{-dc_1 \cdot T_b}^{(dc_2 - 0.5) \cdot T_b} e^{-j\omega t} dt + \int_{(dc_2 - 0.5) \cdot T_b}^{\frac{T_b}{2}} e^{-j\omega t} dt. \quad (5.9)$$

After simplification:

$$P_{pwm-2}(j\omega) = \frac{2 \cdot e^{-j\omega \cdot (dc_2 - 0.5) \cdot T_b} + e^{j\omega \cdot T_b} - 2 \cdot e^{j\omega \cdot dc_1 \cdot T_b} - e^{-j\omega \cdot 0.5 \cdot T_b}}{j\omega} \quad (5.10)$$

Now we can calculate the power spectral density PSD_{pwm} for the PWM-2 filter:

$$PSD(\omega) = \frac{|P(\omega)|^2}{T_b} \sum_{k=-\infty}^{k=\infty} R(k) \cdot e^{j\omega k T_b} \quad (5.11)$$

$$\begin{aligned} PSD(\omega) &= \frac{\left| -2j \cdot e^{-j\omega(dc_2-0.5)T_b} - j \cdot e^{j\omega T_b} + 2j \cdot e^{j\omega dc_1 T_b} + j \cdot e^{-j\omega 0.5 T_b} \right|^2}{\omega^2 \cdot T_b} = \\ &= \frac{\left| -2 \cdot e^{-j\omega(dc_2-0.5)T_b} - e^{j\omega T_b} + 2 \cdot e^{j\omega dc_1 T_b} + e^{-j\omega 0.5 T_b} \right|^2}{\omega^2 \cdot T_b} = \\ &= \frac{1}{\omega^2 T_b} \left\{ \left[2 \cos \omega dc_1 T_b - 2 \cos(\omega(dc_2 - 0.5)T_b) + \cos \omega 0.5 T_b - \cos \omega T_b \right]^2 + \right. \\ &\quad \left. + \left[2 \sin \omega dc_1 T_b + 2 \sin(\omega(dc_2 - 0.5)T_b) - \sin \omega 0.5 T_b - \sin \omega T_b \right]^2 \right\} \end{aligned} \quad (5.12)$$

where $P(\omega)$ is the Fourier transform of $p(t)$ (in this case it is $p_{pwm-2}(t)$ and $R(k)$ is the autocorrelation function for a polar NRZ signaling ($R(k)$ is the same for PWM as for polar NRZ) and is completely calculated in [44], [16].

If (5.12) is taken into the account for calculation of PSD_{pwm-2} following graphical outputs in Fig. 5.4 are obtained. Note that the normalization for bit periods on x-axis and y-axis is for better understanding of the performance of the new proposed pulse. The dc coefficients are set for equalization of transmission channel with higher losses. The spectrum of PWM-2 pulse is even more boosted at higher frequencies than conventional PWM pulse above Nyquist frequency (0.5 on the x axis). It can be important factor for higher performance to compensate more lossy channels. The main disadvantage of the PWM method proposed in [16] is that the output pre-distorted signal has many harmonic high frequency components. In the case of PWM-2 pulse it can be expected also a significant high frequency content but due to the ability to higher loss compensation the final signal level where equalization will be done is lower than for the conventional PWM filter. Thus, a stronger low pass effect of the transmission channel will be expected. Finally, this effect may contribute to the higher loss compensation of PWM -2 filter with possibility of sustainable eye opening.

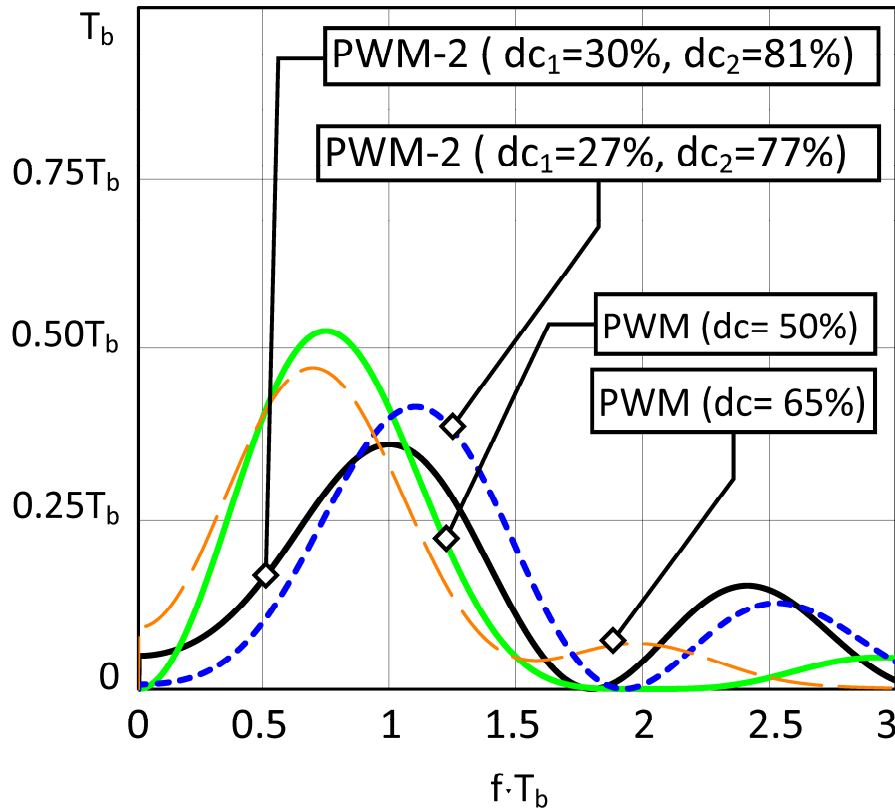


Fig. 5.4: PSD calculation for PWM-2 pulse

In Fig. 5.5 it can be found PSD calculation normalized in dB. It can be clearly seen that during strong pre-emphasis the PWM-2 signal is able theoretically compensate higher channel losses up to almost 40 dB. Note that we need to achieve the flattest equalizer response if we compare signal attenuation on low frequency side versus the side of Nyquist frequency. The harmonic content is comparable for both type of PWM and PWM-2 filters. On the other hand PWM-RC filter shows significant reduction of harmonic content but at the cost of signal level reduction over the frequency spectrum. In Fig. 5.6 in detail the possibility of better loss compensation in the case of PWM-2 filter can be seen. Conventional PWM scheme shows maximum low frequency content suppression about 23 dB. Modified PWM-RC scheme shows 30 dB but with 4 dB reduction of signal level around the Nyquist frequency (in this case the $f_N = 5$ GHz). However, the flattening of signal spectrum above Nyquist frequency shows better performance for loss equalization of higher frequency component in data signal. Finally, the PWM-2 filter shows maximum theoretically low frequency content suppression almost 40 dB together with boosted spectrum above Nyquist frequency. The flattening of signal spectrum above Nyquist frequency is the best with respect to other compared pulses.

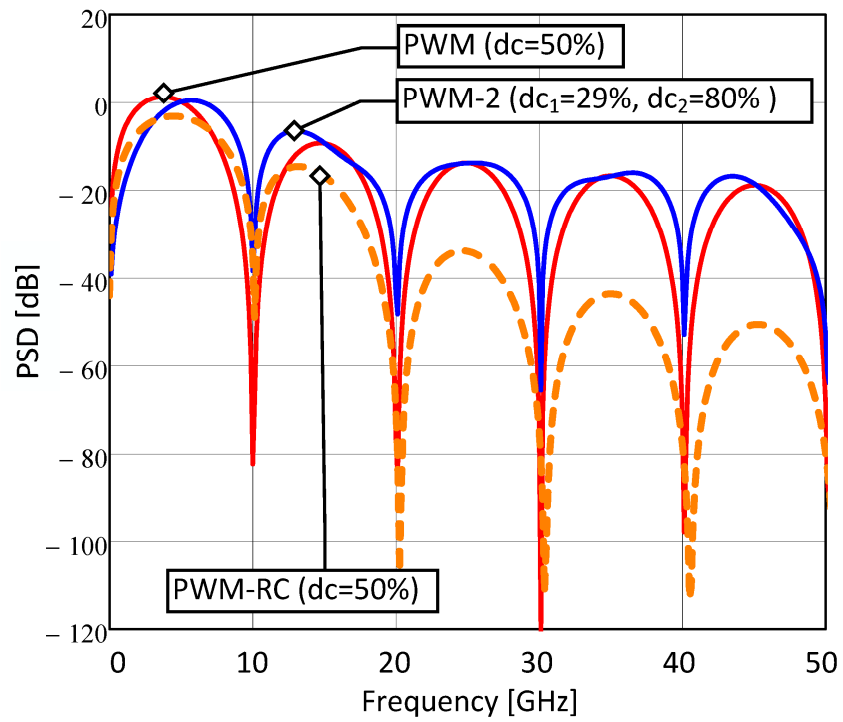


Fig. 5.5: PSD calculations normalized in dB.

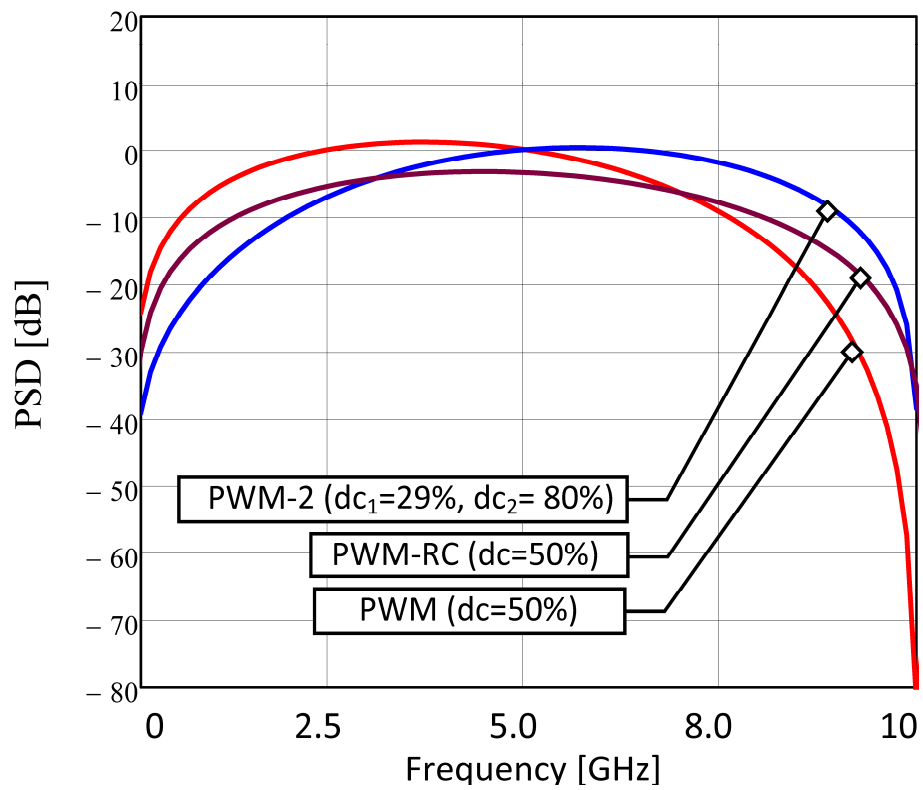


Fig. 5.6: Detailed view of the signal spectrum.

5.3 Transfer function analysis

The transfer function for new presented PWM-2 filter can be calculated similarly as in the case of PWM filter [16]. For relevant comparison of both types of filters the spectrum of normal polar NRZ pulse of width T_b and height 1 is used for normalization of both functions and the final expression is defined as (5.13) below.

$$H_{PWM-2}(\omega) = \frac{P_{pwm-2}(\omega)}{P_{NRZ}(\omega)} \quad (5.13)$$

The equation for transfer function can be rewritten as :

$$H_{PWM-2}(j\omega) = \frac{P_{pwm-2}(j\omega)}{P_{NRZ}(j\omega)} = \frac{2 \cdot e^{-j\omega(dc_2-0.5)T_b} + e^{j\omega T_b} - 2 \cdot e^{j\omega dc_1 T_b} - e^{-j\omega 0.5 T_b}}{e^{j\omega 0.5 T_b} - e^{-j\omega 0.5 T_b}} \quad (5.14)$$

Taking the modulus yields:

$$|H_{PWM-2}(\omega)| = \frac{\sqrt{\left[2 \cos \omega(dc_2 - 0.5)T_b + \cos \omega T_b - 2 \cos \omega dc_1 T_b - \cos \omega 0.5 T_b\right]^2 + \left[-2 \sin \omega(dc_2 - 0.5)T_b + \sin \omega T_b - 2 \sin \omega dc_1 T_b + \sin \omega 0.5 T_b\right]^2}}{2 \cdot |\sin \omega 0.5 T_b|} \quad (5.15)$$

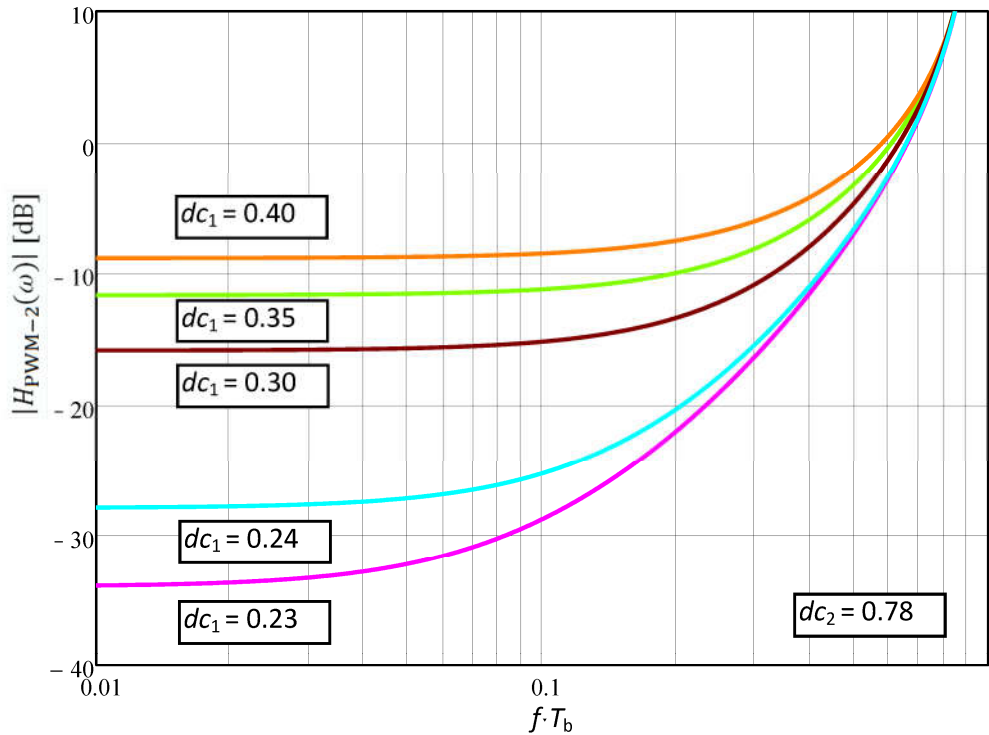


Fig. 5.7: Calculated magnitude of PWM-2 filter transfer. Note that f_N is at 0.5 on the x-axis.

This function is illustrated in Fig. 5.7 for several values of dc_1 . The second coefficient dc_2 is set to the value which corresponds with the necessity to higher intersymbol interference compensation. A precondition therefore is that the pulse response of the channel is formed by long tail which does affect more bit periods. One of the evaluated parameters is above discussed low-frequency compensation, compare Tab. 5.1 and Tab 5.2. It is obvious that PWM-2 filter achieve worse performance during compensation of less lossy channels. On the other hand the ability to achieve better loss compensation results for more channels with significant bandwidth restriction is better almost by 26%.

Tab. 5.1: PWM filter loss compensation

Channel BW_{3dB} [MHz]	dc [%]	LF compensation [dB]
2000	61	13
1000	57	17
500	54	22
250	52	27
The maximum theoretical compensation is 36 dB, $dc = 50$ %		

Tab. 5.2: PWM-2 filter loss compensation

Channel BW_{3dB} [MHz]	dc_1 [%]	dc_2 [%]	LF compensation [dB]
2000	36	83	9
1000	29	79	16
500	23	79	28
250	23	78	34
The maximum theoretical compensation is 54 dB, $dc_1 = 22$ %, $dc_2 = 78$ %			

5.4 Equalized channel transfer function

Last section of the chapter 5 is focused on the practical using of proposed PWM-2 scheme for equalization of second order channel transfer function. If it is considered that during practical implementation and testing low cost coaxial cable will be used we need to simulate appropriate channel pulse response which corresponds with long tail asymmetrical pulse.

The second order system (impulse) response can be similarly, as in the case of the first order function (2.2), defined by using of two bandwidth coefficients BW_1 and BW_2 as

$$h_{2nd}(t) = \frac{1}{\frac{1}{2\pi \cdot BW_2} - \frac{1}{2\pi \cdot BW_1}} (e^{-2\pi t \cdot BW_2} - e^{-2\pi t \cdot BW_1}) \quad (5.16)$$

where the ratio between the both coefficients determine the final pulse shaping.

Thus, pulse with long tail which represents transmission channel prone to intersymbol interferences can be effectively modeled, see pulse shaping variation with different BW coefficients settings in Fig. 5.9. Note that the pulse response with more symmetry is typical for PCB channels with strong RMS roughness effect, more in chapter 6. On the other hand more asymmetry pulse shaping is typical for channels where skin-effect loss is dominated factor.

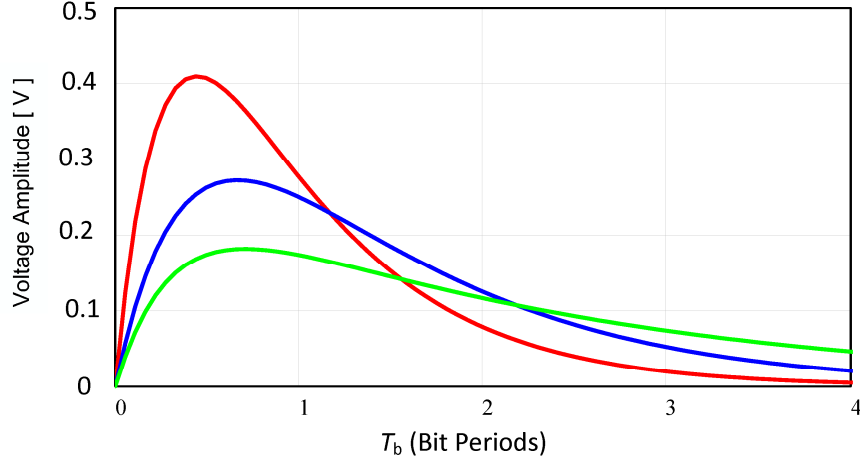


Fig. 5.8: Second order pulse responses.

Finally, the equalized channel transfer function can be calculated for FIR filter and both PWM and PWM-2 filters. As can be analyzed in section 5.1 a theoretical first-order channel with significant bandwidth restriction is sufficiently equalized by using of all three equalization techniques. However, a real cable or PCB trace, especially with additional signal discontinuities, does not have a first order transfer function. From analysis depicted in chapter 4 is obvious that the higher order transfer functions, typically for multilayer boards where vias occurs, still can be equalized with PWM and PWM-RC pre-emphasis with better results than by using of conventional 2-Tap FIR filter. The equalized transfer function is calculated by taking into the account the measured results presented in Fig. 2.18, concretely channel 3 response which exhibits more losses on the considered Nyquist frequency for 10 Gbps transmission rate $f_N = 5$ GHz. In this case the channel losses exceed more than 35 dB. This is the limitation of conventional PWM scheme where was achieved a maximum loss compensation about 30 dB [16]. Now it can be clearly determined the flatness in the frequency interval $[0, f_N]$. The channel response for FIR filter is only flat to within 12 dB. It is obvious that FIR filter is not reliable to equalize such high losses. The channel response for PWM filter shows flatness only 7 dB. In the case of the new proposed signaling scheme PWM-2 the flatness is achieved with less than 3 dB differences between low frequency signal level and high frequency signal level. It can be clearly seen from Fig. 5.9c that the PWM-2 filter is able to “almost eliminate” or better said equalize higher channel losses. Thus, the bandwidth where the signal reduction is 3 dB is extended over the all analyzed range of filtration from 0 to f_N . Note that the better equalization is achieved on the lower signal level. Thus, the decisive factor for effective using of the PWM-2 equalization lies also in the current receiver sensitivity and in the current noise content which occurs during the equalization.

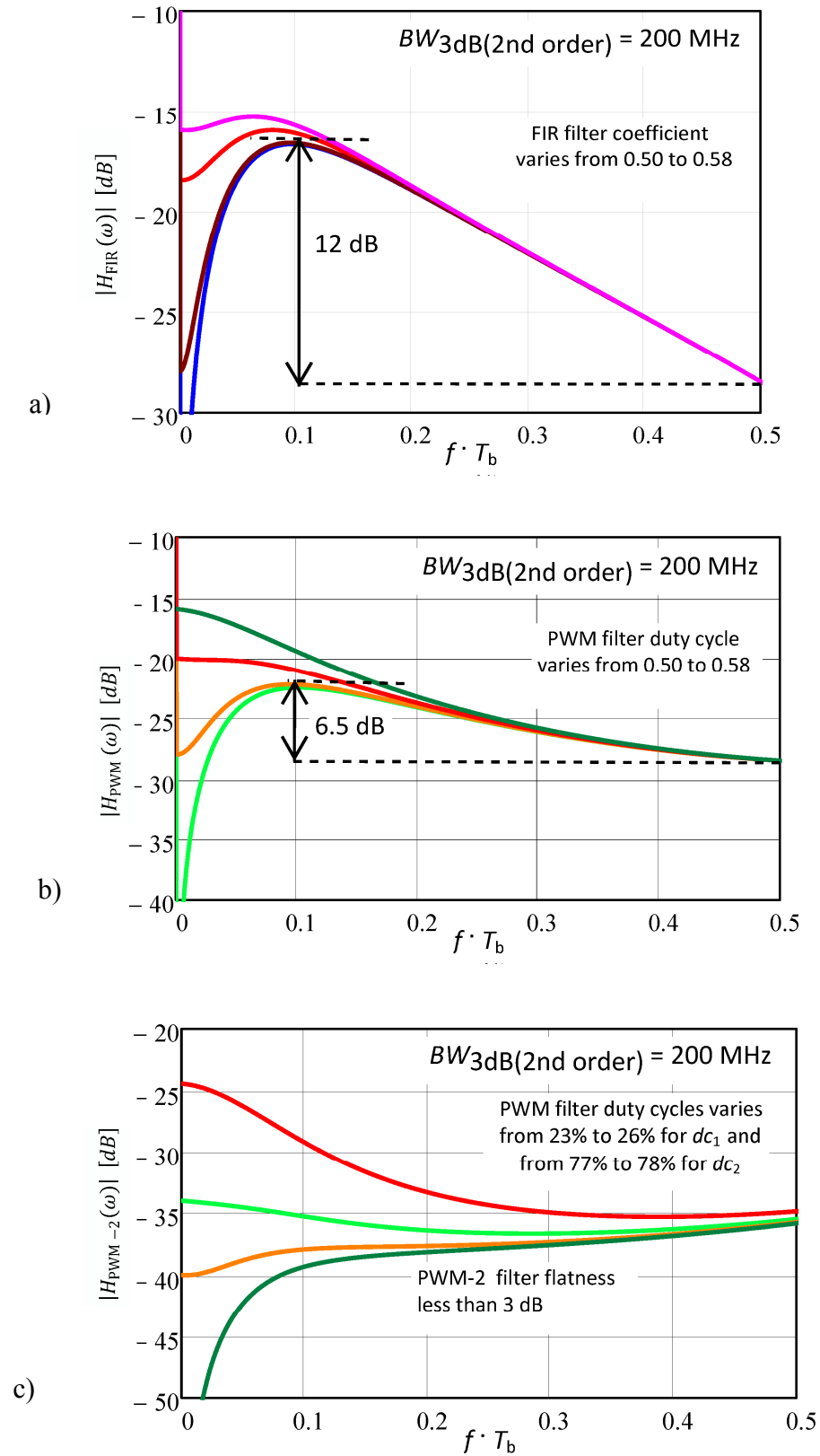


Fig. 5.9: Equalized transfer function, second order channel used: a) FIR filter, b) PWM filter, c) PWM-2 filter.

5.5 Summary

In this chapter the conventional PWM filter scheme with the new proposed second order scheme of the PWM-2 filter was clearly compared in detail. The performance of both filters during loss compensation is clearly illustrated in Fig. 5.10. It is obvious that PWM-2 scheme has great potential to equalize higher order channels with significant losses which occur around the Nyquist frequency for selected transmission rates, in our case 8 Gbps and 10 Gbps. Thus, the higher transmission rate can be successfully passed through the low cost cable or PCB channel. If we summarize the characteristics of both compared PWM filters, it can be expected comfortable performance of PWM filter during equalization of channels with the first or second order transfer function. On the other hand, PWM-2 filter shows great potential to equalize channel pulse responses with more long tails and due to the both side variability of pulse shaping can be setting of filter better adapted to the current transmission channel characteristic.

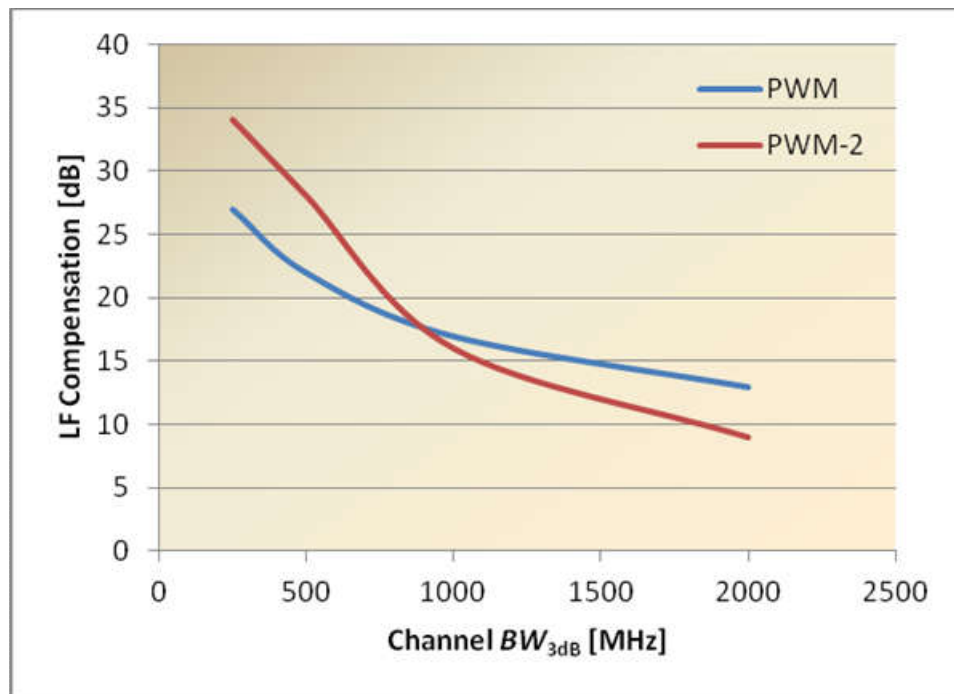


Fig. 5.10: LF compensation comparison for PWM and PWM-2 filter

6 SIGNAL INTEGRITY PROBLEMS IN DIGITAL SYSTEMS

Signal integrity problems include a wide range of problems. In this chapter some of them are modelled and performance of analyzed signalling techniques is monitored. A good understanding of this issue can avoid the errors creation during interconnect analysis and design of communication systems.

6.1 RMS Surface Roughness

Some of this problematic was briefly discussed in section 2. In this part the advanced modelling is used to reveal potential problems of analysed signalling techniques during specific configuration of channel parameters. A transmission line as a integral part of interconnect system are typically made of copper. Typically low cost dielectric is FR4. The copper foils in very frequently used configuration are roughened for better adhesion of signal traces to the substrate. The problem of roughness is negligible for system working with smaller data transmission speed. At high-speed systems which operate at multi-GHz frequencies this effect significantly affect the overall losses. The skin effect as a main parameter to determine impulse response for channel modelling can be boosted by additional conductor loss mechanism caused by current travelling over the non-smooth surfaces. Thus, the shaping of pulse response which is used for modelling of channel losses can be diametrically different and does not correspond with real measurements. Ultimately, this affects overall equalization technique performance during the assessment of maximum signal loss compensation. There are several studies on surface roughness effect and frequency dependent dielectric behaviours listed in [67] -[71]. Some of the modelling techniques ignore additional high frequency effects and skin effect loss is the dominant factor during the conductor loss mechanism calculation [72]. The frequency domain analysis listed in Fig. 2.2 shows additional loss and a steeper channel transfer characteristics. In general for smaller W (conductor width) and smaller h_c (conductor height) parameters, which are used during advance miniaturization on PCB's, the conductive losses are becoming the dominate factor in overall channel losses calculation. An Accurate simulation and modelling of channel discontinuities for multi gigabits systems is still current issue in modern communication systems and during the interconnect analysis as can be found in [73] - [75]. For calculation and modelling of surface roughness effect following empirical formula extracted from microstrip line measurements listed for example in [76] is used.

$$K_{SR} = 1 + \frac{2}{\pi} \arctan[1.4(\frac{\Delta}{\delta})^2] \quad (6.1)$$

where Δ is the surface roughness RMS value and δ is the skin depth. Notice that the value of K_{SR} equals to 1 at DC and asymptotically approaches 2 at very high frequencies.

Thus, the overall losses for transmission channel can be defined as a sum of following components, where conductive losses are multiplied by K_{SR} coefficient

$$\alpha_{total} = \alpha_{conductive} \cdot K_{SR} + \alpha_{dielectric} \quad (6.2)$$

where α_{total} represents overall channel losses, $\alpha_{conductive}$ represents conductive channel losses and $\alpha_{dielectric}$ represents dielectric channel losses.

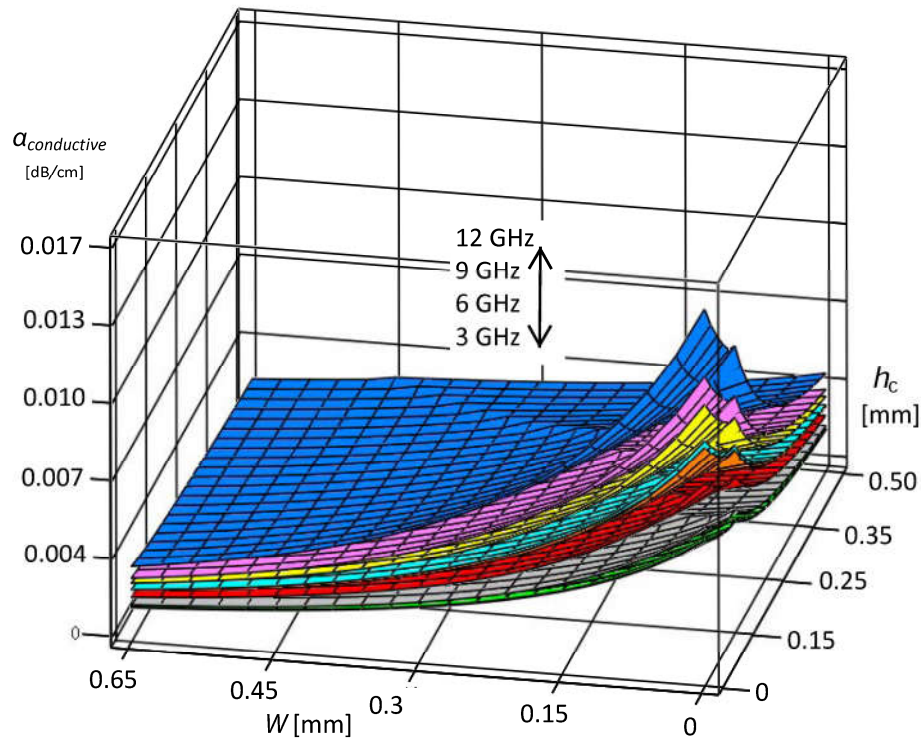


Fig. 6.1: Conductive losses, without RMS surface roughness - green (3 GHz), red (6 GHz), light blue (9 GHz), yellow (12GHz), with RMS surface roughness - gray (3 GHz), orange (6 GHz), purple (9 GHz), blue (12 GHz).

Fig. 6.1 illustrates critical growth of channel losses during variations of both parameters W and h to lower values. If the effect of RMS surface roughness is taken into the account the difference between mode with and without this effect show growing divergence during increasing frequency. This is just confirmation that channel which is designed for 10 Gbps can be inappropriate for further increasing the transmission speed because many of equalization techniques generate during strong pre-emphasis additional noise content which can be ultimately amplified and mixed into the useful signal. Now the pulse response can be calculated for different configuration settings in computational model, see Fig. 6.2. It is interesting to compare pulse response number 3 and pulse response number 4. The overall pulse spreading over the bit periods (intersymbol interference) is the same for both compared pulses. However, the drop in signal amplitude for channel with RMS surface roughness is significant. In practice it may happen that due to the small total amplitude the overall equalization effect of conventional amplitude pre-emphasis technique will be insufficient. On the other side

due to the relatively symmetrical pulse shaping the PWM-2 second order technique can be successfully applied. In this case it is possible to minimize the overall intersymbol interference by appropriate setting of both dc_1 and dc_2 coefficients from both sides of the pulse.

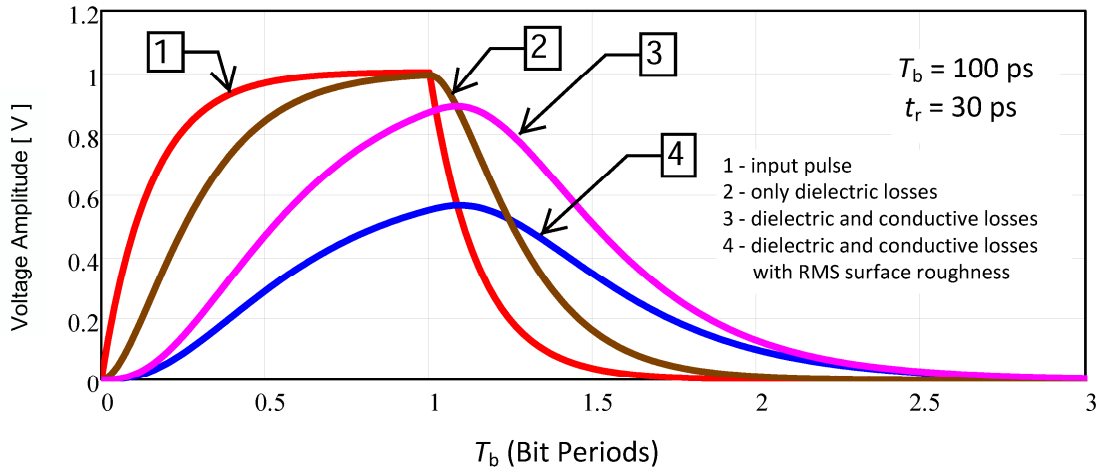


Fig. 6.2: Channel pulse responses comparison for various channel losses effects.

The considerations listed above can be practically verified by advanced modelling through the transmission channel which includes all these losses. In this case the $BW_{3dB} = 350$ MHz. The situation for conventional FIR signalling is shown in Fig. 6.3 where eye diagrams for channel output are listed. Due to the RMS surface roughness eye opening is significantly reduced. Even though the overall amplitude of the signal is also reduced intersymbol interference is stronger and jitter effect is increasing. This is the reason why the FIR filtering seems like the better than PWM filtering for less lossy channels. In the moment when the less lossy channel is used a conventional FIR filter exhibit better eye height and eye width parameters and also jitter is significantly reduced. On the other hand the PWM filter exhibit a greater reduction in signal amplitude and worse parameters for eye opening due to the additional signal transitions which are added to the data signal. However, this disadvantages are paradoxically eliminated during signal transitions over the channel with higher losses where the high frequency content is significantly reduced. PWM signaling scheme shown in Fig. 6.4 has still relatively high jitter. On the other hand after comparing of both PWM signalling methods with FIR filtering the following findings can be included in our research. The PWM signaling exhibit more improvement in jitter. The eye shaping is more symmetric and obviously better adaptable to the higher order channel characteristics. Performance comparison for all equalization techniques is listed in Tab. 6.1.

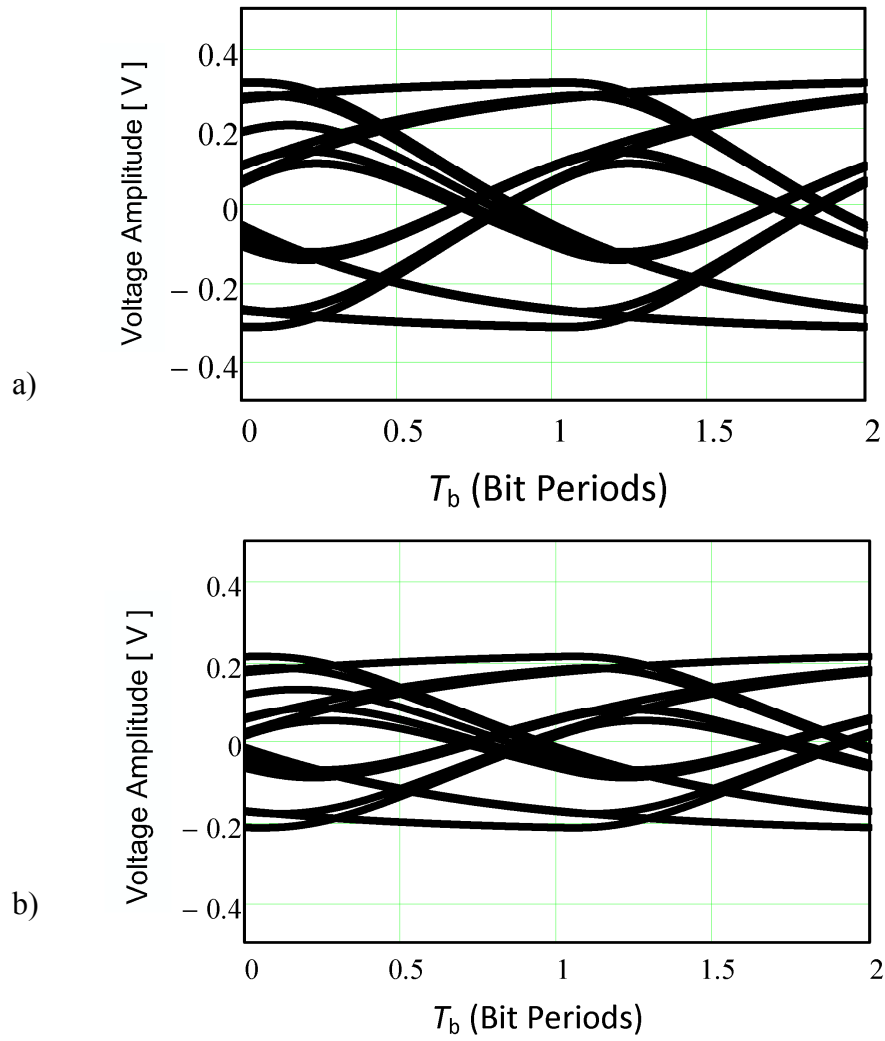
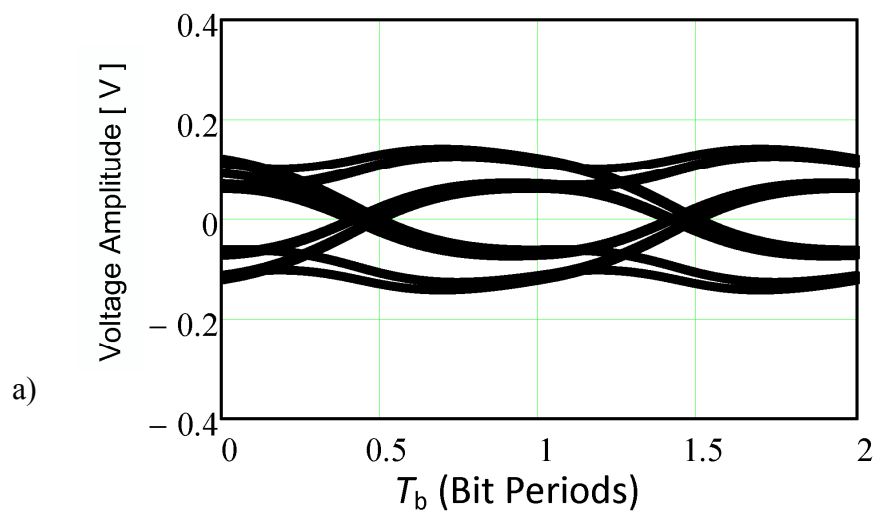


Fig. 6.3: Output eye diagram for conventional FIR filtering: a) transmission channel without RMS surface roughness, b) channel with RMS surface roughness.



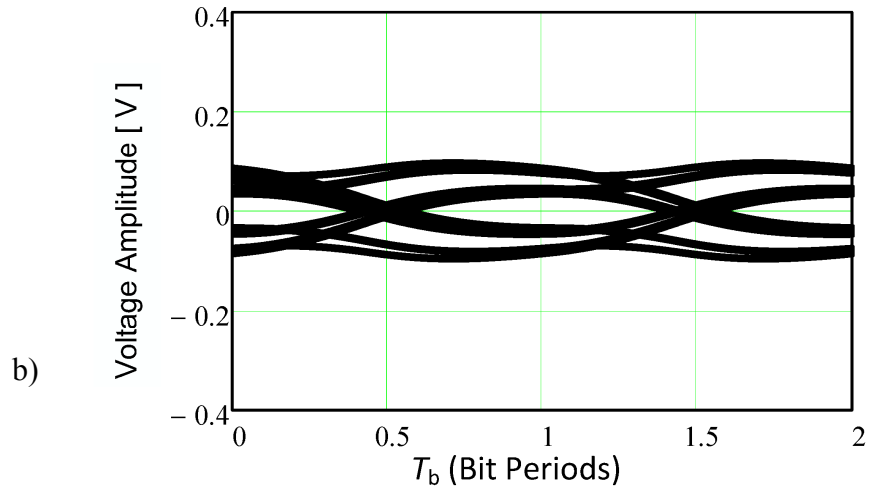


Fig. 6.4: Output eye diagram for PWM filtering: a) transmission channel without RMS surface roughness, b) channel with RMS surface roughness

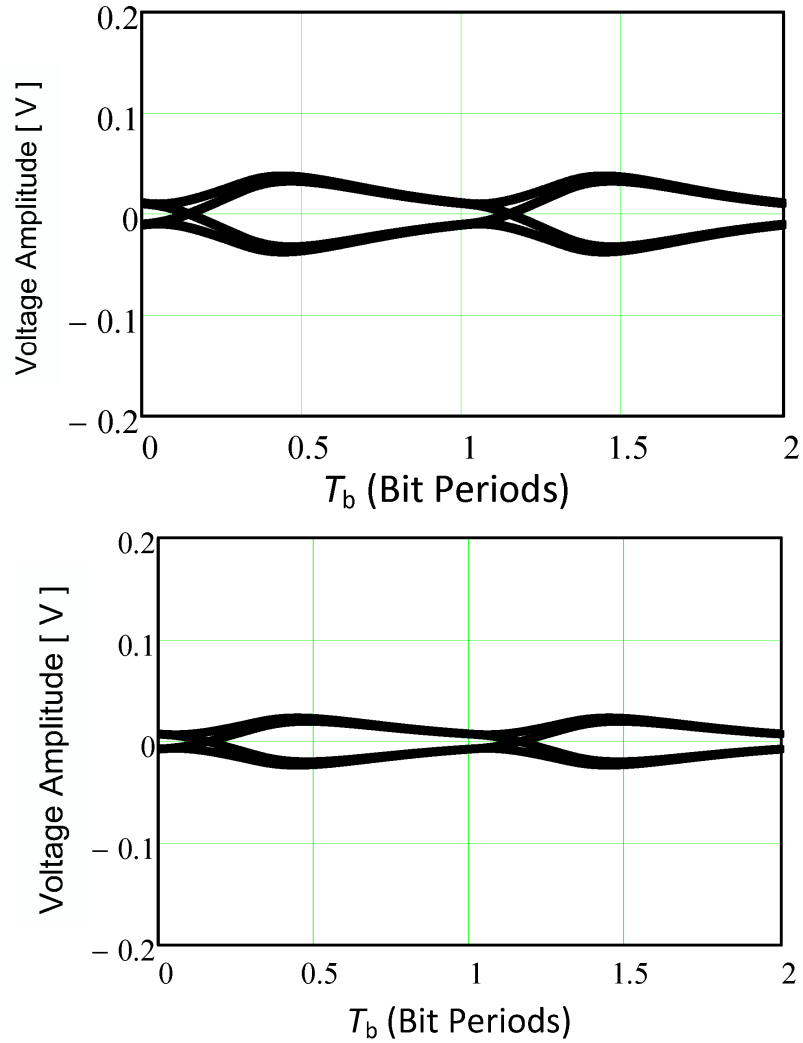


Fig. 6.5: Output eye diagram for PWM-2 filtering: a) transmission channel without RMS surface roughness, b) channel with RMS surface roughness.

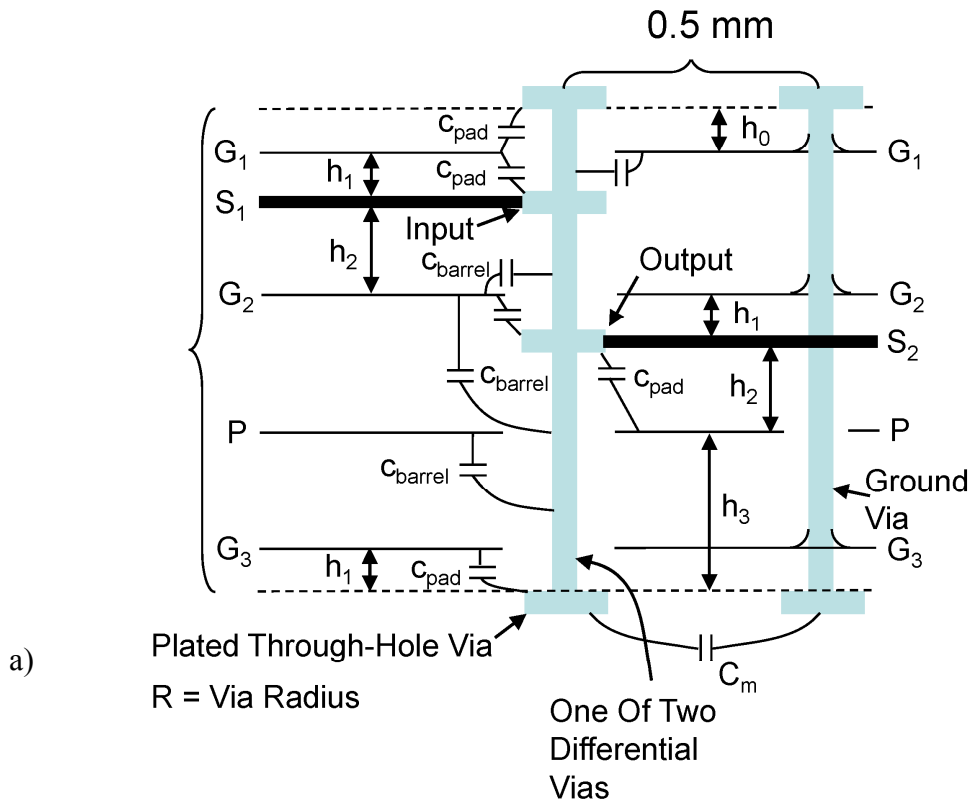
Tab. 6.1: Performance of equalization techniques, surface roughness.

	PWM		
10 Gbps	without surface roughness	with surface roughness	Deterioration
Eye height [mV]	34.3	21.7	36.7 %
Jitter RMS [ps]	12.2	16.6	36.1 %
	PWM-2		
10 Gbps	without surface roughness	with surface roughness	Deterioration
Eye height [mV]	32.2	19.4	39.8 %
Jitter RMS [ps]	4.2	5.5	31.1 %
	FIR		
10 Gbps	without surface roughness	with surface roughness	Deterioration
Eye height [mV]	56.6	26.5	53.2 %
Jitter RMS [ps]	18.6	26.4	41.9%

6.2 Impact of Vias and Open Stubs on Signal Integrity

In practice it is necessary to route differential signal between two different signal layers. In this case the vias together with open stubs are analyzed as a part of transmission channel discontinuities. A via presents a short section of change trace geometry and can be modeled as a capacitive and/or an inductive discontinuity [77]. Usually vias are configured to have no stubs or long stubs after that the measurements are made with a Network analyzer, on stripline structures of various length and various via configuration [78], [79]. Frequencies 1 MHz to 20 GHz are used to generate S-parameters. Another structure measured is a full Z-interconnect board, which has zero via stubs on all signal layers and has controlled via structures to maximize high frequency performance [80], [81]. The configuration of analyzed circuit with marked parasitic capacitances is shown in Fig. 6.6. Due to the cost limitations, vias are often extended throughout the entire thickness of the board and are typically very short compared with the overall length of the channel traces. Thus, a conductive portion of the via which is not connected represents an unterminated transmission line with significant signal degradation dependent on its resonant frequency. The longer the stub, the larger the impedance discontinuity and consequent additional losses are added to the transmission channel path. In general, a stub can be considered for more dangerous factor of signal degradation than the via itself. It is important to include these effects into the signal modeling during the design of high-speed communication system. Usually the impact of commonly used open stubs can be neglected for rise times $t_r > 500$ ps but for multi gigabits systems the values of t_r drop significantly below this value. Indwelling stubs are generally removed by back-drilling, in our modelling circuit will be shown both of this configuration with/without back drilling of stubs. Figure 6.6 shows situations in which differential signal jumps between two different signal layers due to the use of differential vias. The portions of the vias that extend beyond the signal layers to the bottom and top of the board form open-stubs. In our analyzed system, the length of the open stubs are equal to $h_2 + h_3$ at the output side and the input side has the same

stubs length consisting of lengths $h_0 + h_1$. The values for h_1 and h_2 are 0.1 mm and 0.3 mm, respectively, and should not be modified in order to maintain the desired $100\ \Omega$ differential impedances on signal layers S1 and S2. Parasitic capacitances C_{pad} and C_{barrel} exist between the open stubs of the vias and reference planes. These shunting paths can cause signal fades to occur in the multi-gigahertz frequency range. If the rise time of the propagating signal corresponds to a frequency that lies within the fade, then signal distortion will occur along the rise time. Typically, the risetime of the propagating signal corresponds to a frequency of about $1/(2t_r)$. In addition to these parasitic capacitances, there exist mutual capacitances (C_m), between the pads of the differential vias at the end of each stub. The first case addresses the situation in the differential signal jumps across a reference ground plane. The second case addresses the situation in which the differential signal jumps across a reference power plane. It is assumed that a ground via exists physically close to the differential vias when signal jumping occurs across a reference ground plane. It is also assumed that this ground via is much closer to the differential vias than the nearest decoupling capacitor. On the other hand, it is assumed that a decoupling capacitor exists physically close to the differential vias when signal jumping occurs across a reference power plane, and that this capacitor is much closer to the differential vias than the nearest ground via. In this simulation, the ground via or the decoupling capacitor are either 0.5 mm or 1 mm from the nearest differential via. In addition, it is assumed that via pads only exist on the two outer layers, as well as on the two signal layers. This situation implies that the via parasitic capacitances are mostly significant where the via pads exist on the PCB, and are mostly negligible where only the via barrel capacitance exists on the PCB.



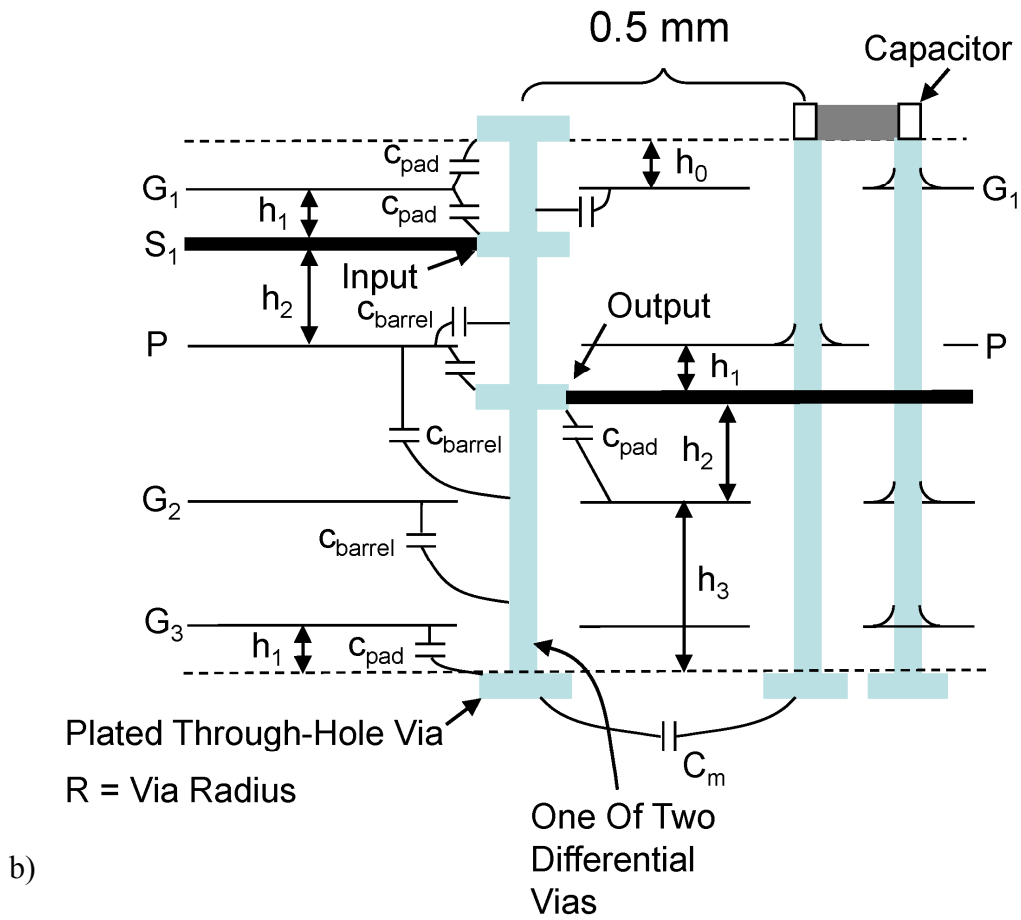


Fig. 6.6: Two configurations of simulated model: a) differential signal jumps across a reference ground plane, b) differential signal jumps across a reference power plane.

The first input dynamic impedance can be calculated, see Fig. 6.7. It is very important factor of impedance discontinuities along the transmission channel, because the impedance "seen" by the rise time and fall time of the propagating signal can be highlighted. The rise time and fall time typically characterize the highest frequency components of the generated data signal. The input dynamic impedances are characterized with peak impedances that occur at different resonant frequencies. Our target is to operate the digital system with rise times that avoid exciting these resonances. In general, the peak impedance for jumping across a reference ground plane is significantly higher than the peak impedance when jumping across a power plane. In simulation there was considered $t_r = 40$ ps as 40 % of the bit period and $T_b = 100$ ps (equivalent to the 10 Gbps transmission rate). Thus, the frequency associated with the input rise time is 12.5 GHz.

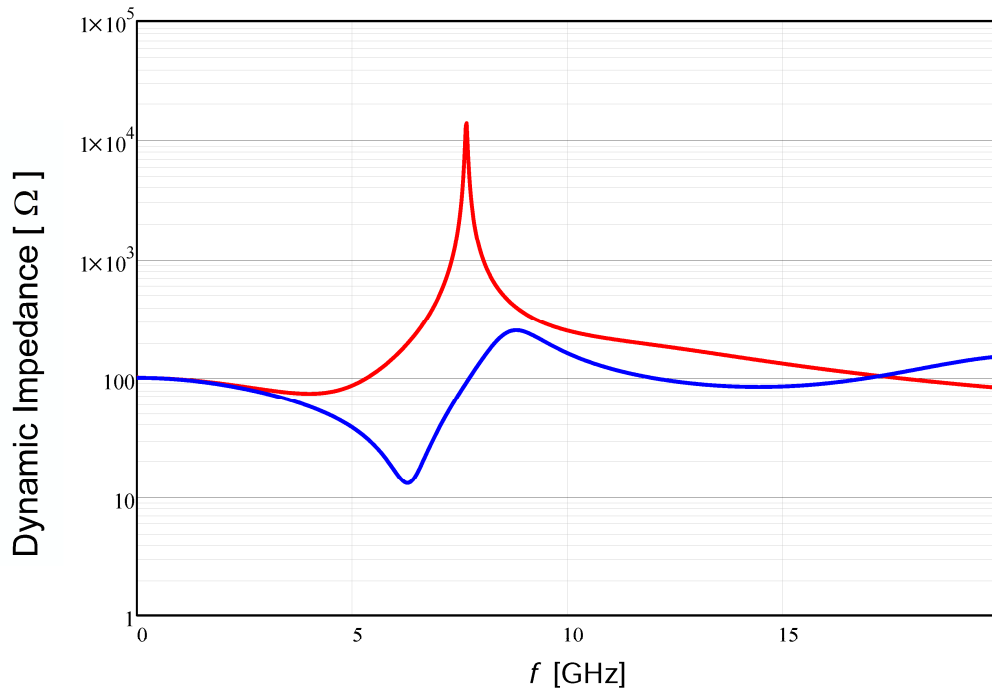
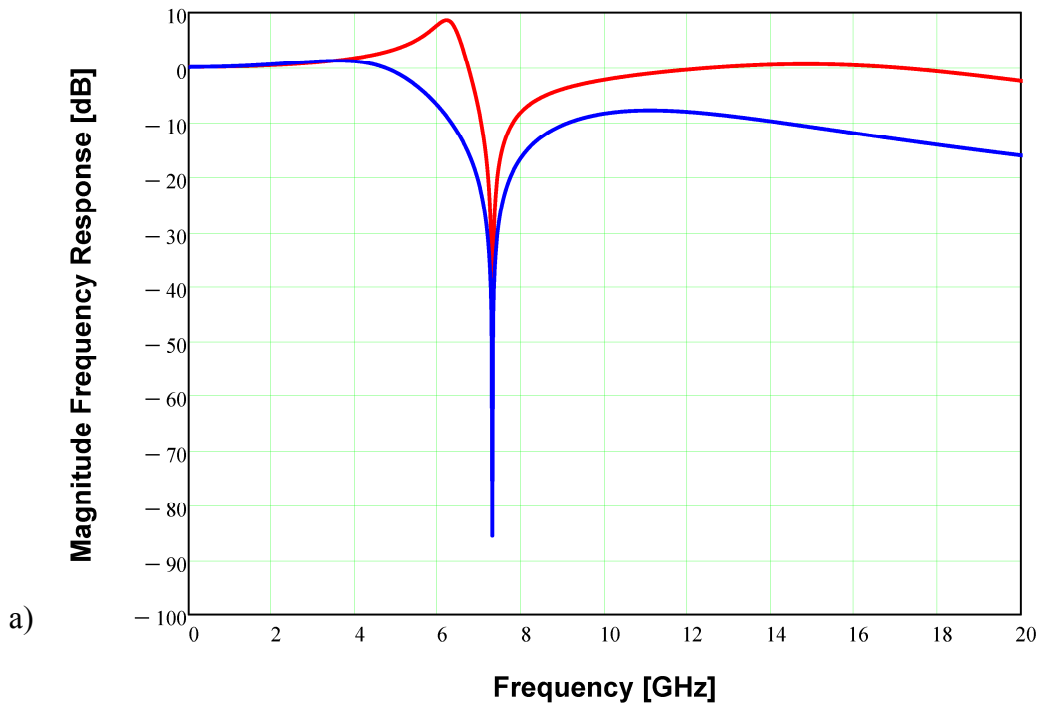


Fig. 6.7: Input dynamic impedances: red - jumping across a power plane, blue jumping across a ground plane.

Channel transfer responses for above listed discontinuities are shown in Fig. 6.8a. It is obvious that significant notch occurs near the 7 GHz frequency. Finally this can significantly affect the high frequency signal content, especially pulse edge shaping. In Fig. 6.8b is shown pulse frequency content for both affected output pulses in comparison with input pulse. Thus, the place where should be expected significant signal level reduction is clearly detected.



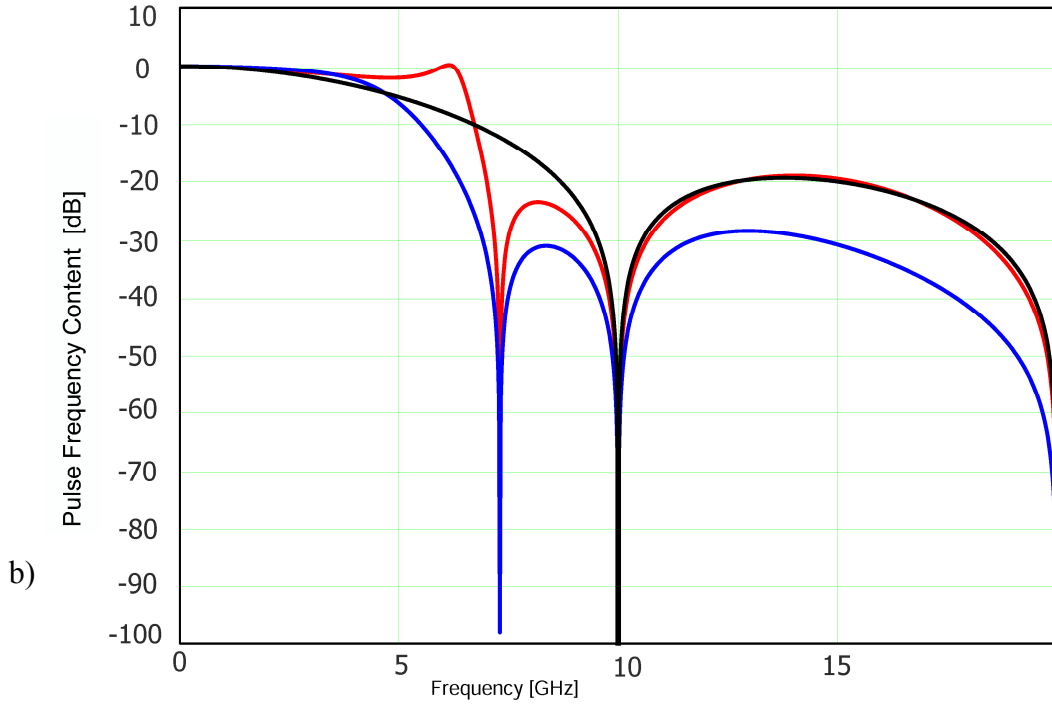


Fig. 6.8: Frequency domain analysis: a) channel response, b) pulse frequency content. Note that the black colour represents input pulse, red colour show pulse affected by jumping across a power plane, blue colour pulse represent effect of jumping across a ground plane.

Fig. 6.9 illustrate the pulse responses of the simulated system extracted directly from the frequency responses listed in Fig. 6.8. As can be shown in section 5 the PWM-2 pulse scheme is able to significantly close pulse spreading during the strong intersymbol interferences. Appropriate setting of dc_2 coefficient should reduce signal overshoots. The situation at the output of the analyzed transmission channel is clearly seen on final eye diagram for both of the signal integrity issue. In Fig. 6.10a is shown distortion which is typical for channels equalized by using signal de-emphasis. The second output eye diagram show the signal integrity issue during the signal jumping across a power plane. As can be seen from the extracted pulse response in Fig. 6.9 the pulse is more symmetrical than the other two pulses and show significant spreading over the other bit periods. In this case the appropriate setting of the second duty cycle coefficient dc_1 can be successfully applied. It is obvious that proposed second order PWM-2 scheme brings more options for pre-emphasis of the data signal according to the current characteristic of the transmission channel.

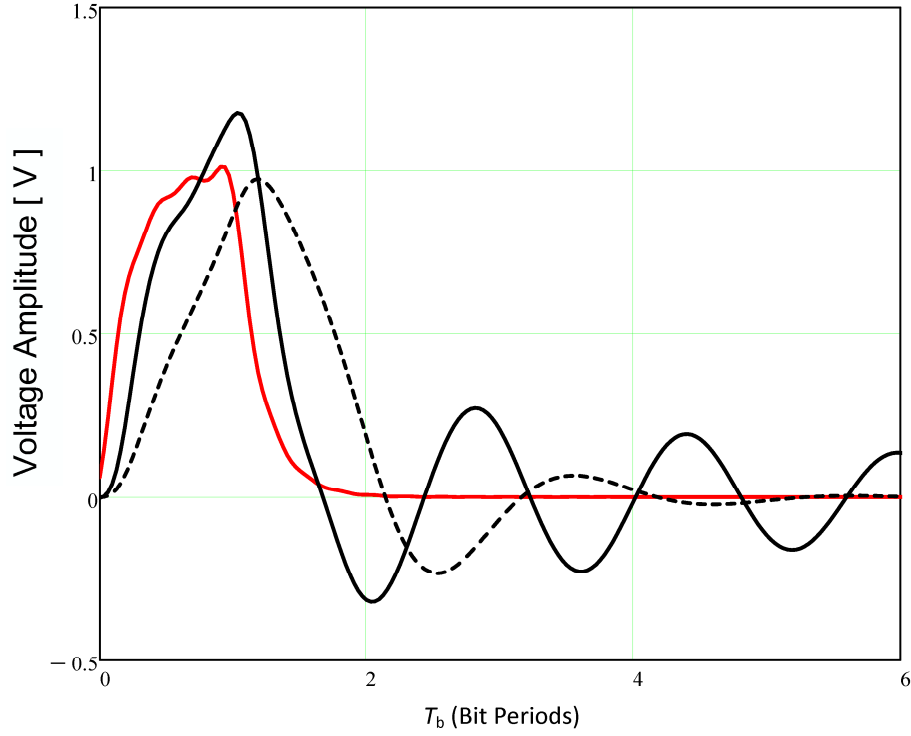


Fig. 6.9: Pulse responses extracted directly from the frequency responses, red pulse represent input pulse, black pulse represent the pulse affected by jumping across a power plane, pulse marked by dashed line represent effect of jumping across ground plane.

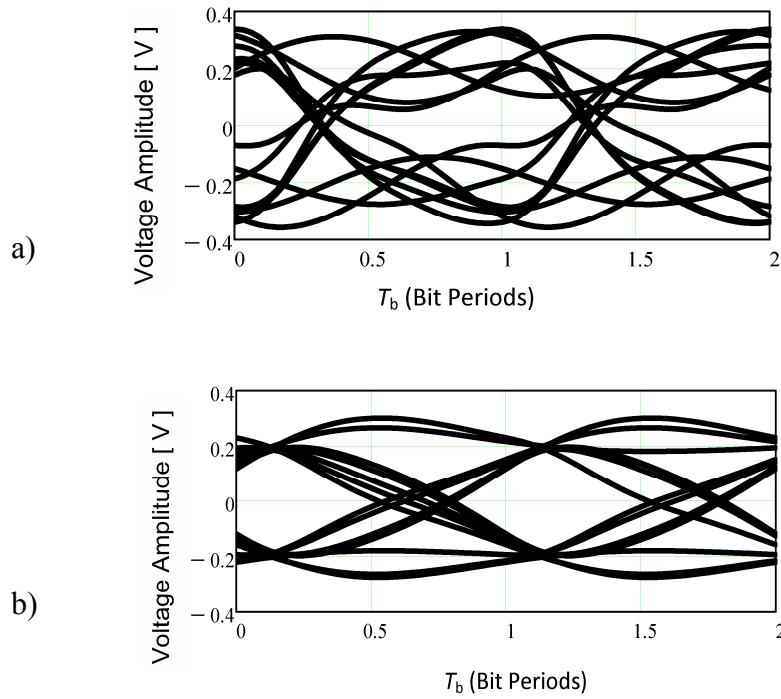


Fig. 6.10: Eye diagram analysis: a) output eye pattern when signal jumping across a ground plane, b) output eye pattern when signal jumping across a power plane

6.3 Summary

In this chapter was clearly demonstrated outputs from advanced modeling of signal integrity issues based on the developed models. Selected signal integrity issues clearly demonstrate the potential channel discontinuities which can affect the overall channel response. Especially for higher channel transfer function it is necessary to accurately identify the source of potential problems which can occur during the design of high speed interconnects. In the other future related work during the participation on research project which is focused on research of signal integrity at high-speed interconnects, the other practical measurements will be performed according to the proposed simulation models. The main objective is to better understand how the discontinuities which occur in higher order transmission channels impact the overall performance of the proposed equalization technique.

7 IMPLEMENTATION OF BOTH PWM AND PWM-2 SIGNALING TECHNIQUES

In this chapter practical implementations of both PWM and PWM-2 pulse-width techniques are demonstrated. Due to the maximal transmission speed restriction of the digital signal with regard to the currently available development kit the effect of equalization is realized for 300 Mbps and 450 Mbps.

7.1 Channel Properties

For the demonstration of higher order transmission channel a low cost 150 m length coaxial cable is used. As can be seen from the measured channel transfer characteristic in Fig. 7.1 the channel losses are significant since units of MHz. Thus, the ratio between the maximum transfer rate and channel losses at 3 dB signal level is similarly as in the case of simulation with higher transfer rates. For example if we take into the account the Nyquist frequency for above listed transfer rates it can be deduced Nyquist frequency 100 MHz for lower transfer rate 200 Mbps. In the case of higher transfer ratio 450 Mbps the Nyquist frequency is 225 MHz. In MathCAD simulation for channel losses are used mainly transfer rates from 6 Gbps to 10 Gbps. It corresponds with Nyquist frequencies from 3 GHz to 5 GHz. BW_{3dB} coefficient is set to values from 150 MHz to 500 MHz. Thus, the ratio for 4 GHz Nyquist frequency and $BW_{3dB} = 250$ MHz is 1:16. For Nyquist frequencies deducted from practically implemented transfer rates and $BW_{3dB} = 12$ MHz the ratio varies from 1:8 to 1:19. Moreover as was pointed out in previous analyses the mainly destructive effect on signal shaping have conductive losses as a dominant factor of overall channel losses. Thus, the realized measurements have high predictive value for overall performance evaluation of compared equalization techniques.

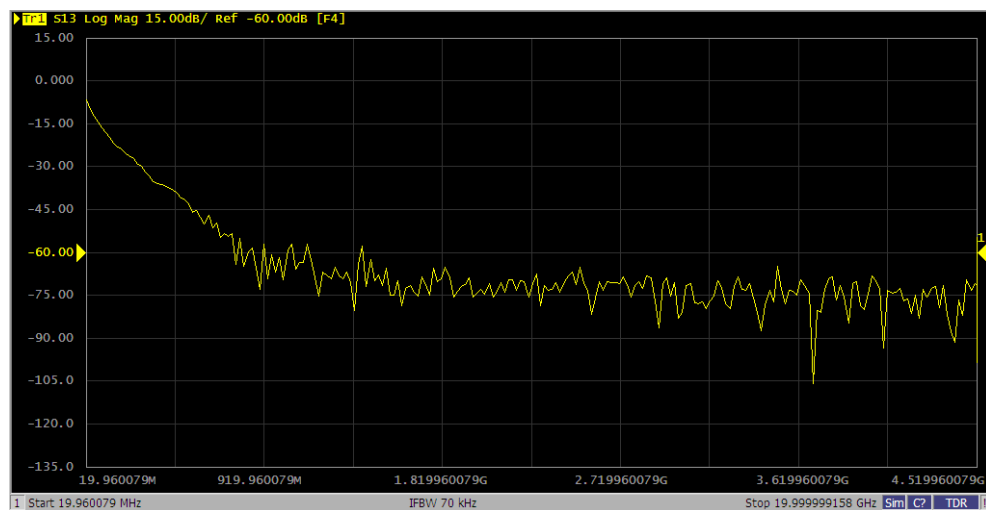


Fig. 7.1: Channel transfer function of analyzed low cost coaxial cable.

From the output eye diagrams it is clearly seen the effect of increasing of the transmission rate by 50%. The output eye diagram for lower transmission rate is shown in Fig. 7.2a. It is obvious that the eye opening is detectable. After the increasing of the transmission rate there is complete eye closure and the transmission channel is unusable for reliable data transfer from transmitter to receiver. For demonstration of signal attenuation effect of analysed transmission channel a configuration of input signal is listed in Fig. 7.2c. In this case a conventional signalling method is applied.

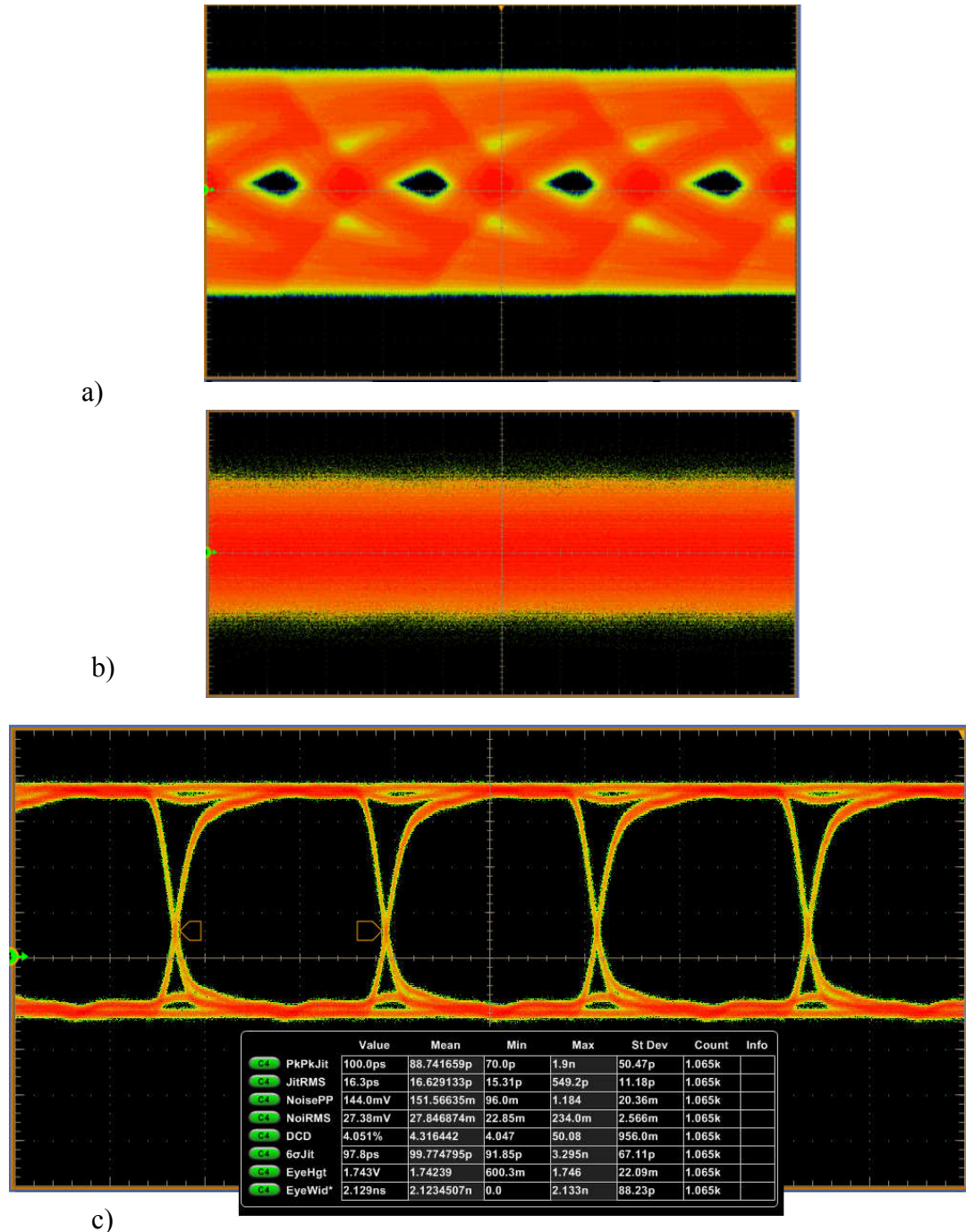
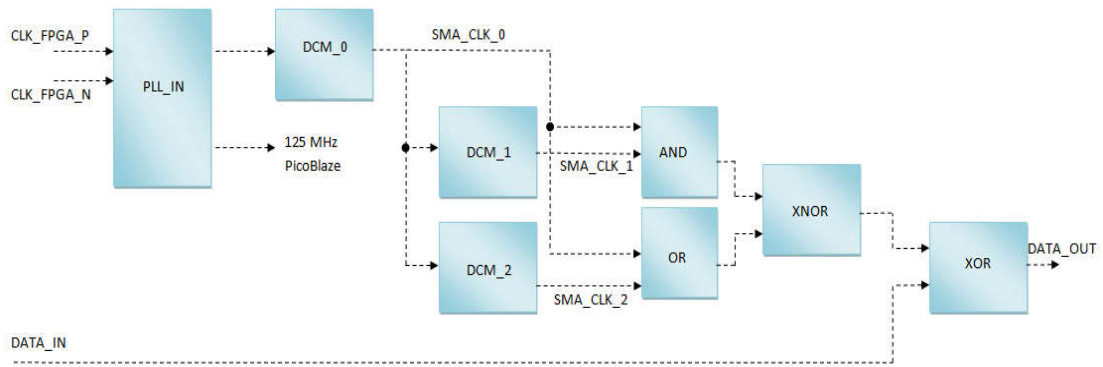


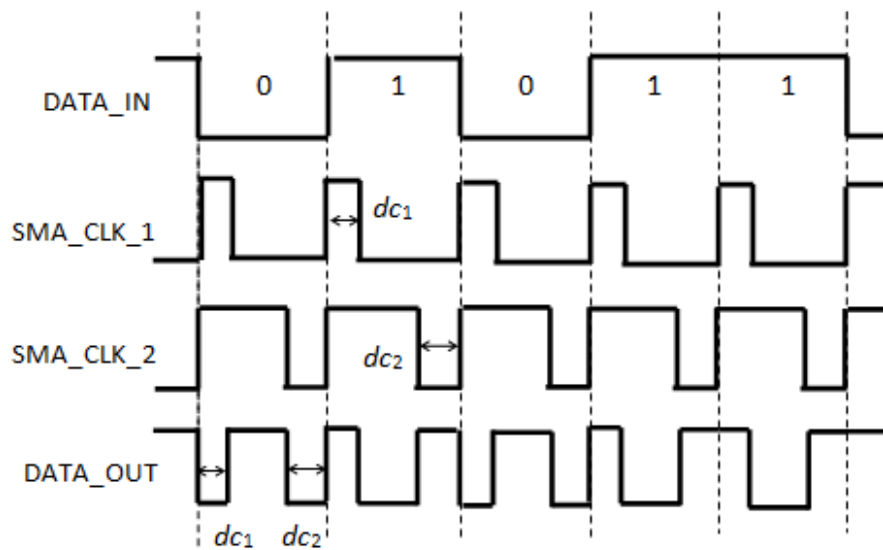
Fig. 7.2: Channel output eye diagrams: a) 300 Mbps data transfer rate enabled, b) 450 Mbps data transfer rate enabled, c) input signal definition - conventional signalling.

7.2 Signal Generation Circuits

FPGA implementation was used for general realization of signalling PWM techniques. In Fig. 7.3a the principle of FPGA implementations is illustrated. Development board with XUPV5 circuit Virtex-5 (XC5VLX110T) was configured. DCM (digital clock manager) represent an electronic component available on FPGAs (notably produced by Xilinx producer). Mainly used for manipulating with clock signals inside the FPGA and to avoid clock skew which would introduce errors in the circuit. Main functions of DCM are multiplying or dividing an incoming clock from external source to the FPGA, for example from a Digital Frequency Synthesizer. Thus, SMA_CLK_0 clock is adjusted in two steps to generate SMA_CLK_1 clock and SMA_CLK_2 clock. For the first order PWM signalling only SMA_CLK_1 clock is needed. For the second order PWM-2 signalling an additional SMA_CLK_2 clock is added. Finally input data stream DATA_IN is merged through XOR with both PWM clocks.



a)



b)

Fig. 7.3: Principle of PWM-2 equalization technique: a) signalling circuit concept for FPGA implementations, b) signal diagram.

7.3 Performance of Equalization

In the first case the performance of both PWM and PWM-2 equalization methods for lower transmission rate 200 Mbps are compared. In this case it can be expected lower high frequency content attenuation which mainly defines sharp signal transitions, especially during long sequences of alternating symbols ...1010101... generated by transmitter. After comparing of both eye diagrams for PWM and PWM-2 data streams it can be found that due to the better possibility to set appropriate pulse shaping in PWM-2 configuration higher eye opening is achieved. Note that the jitter and noise parameters are worst for PWM-2 signalling.

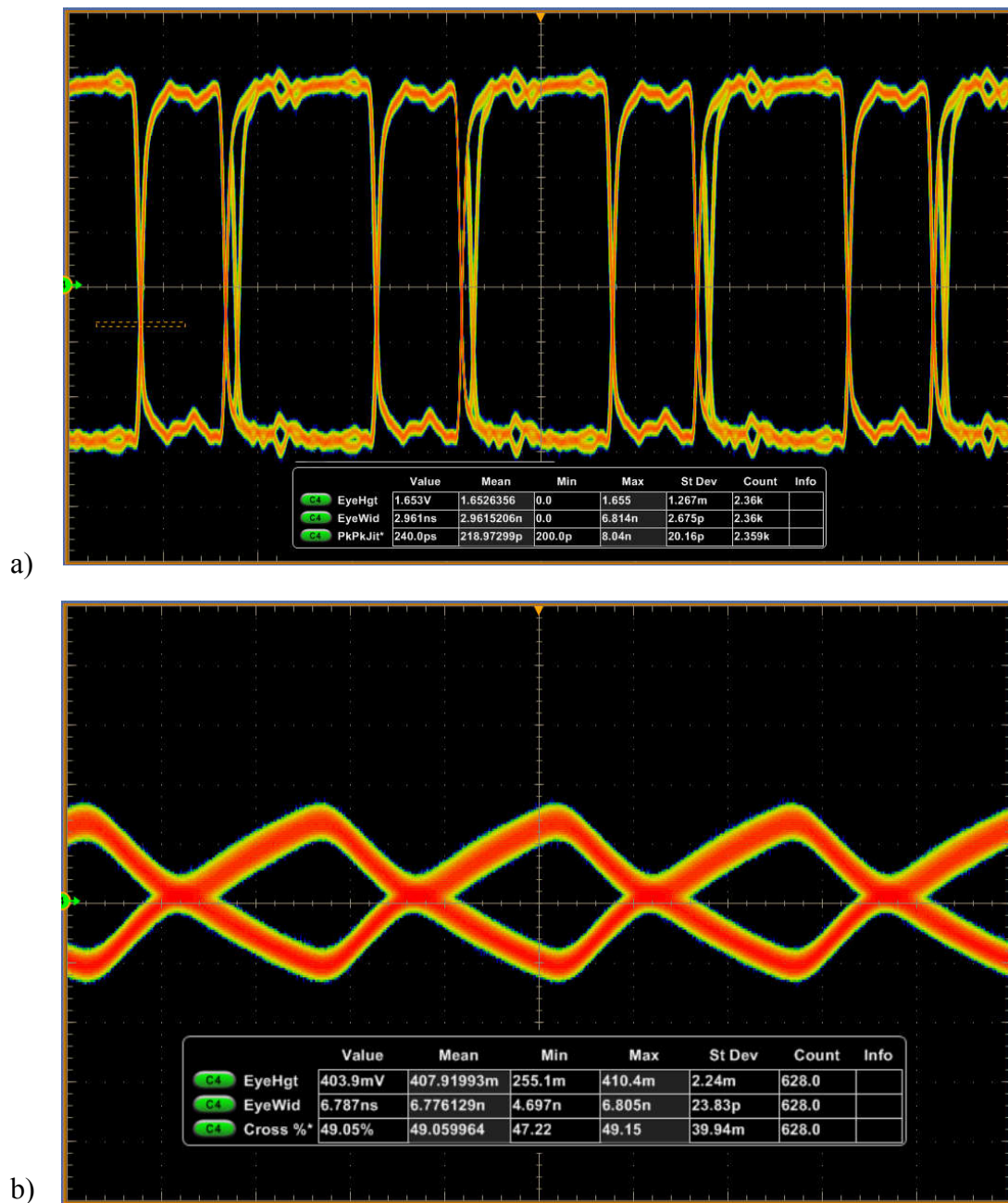


Fig. 7.4: Eye diagrams for PWM signalling (200 Mbps): a) input signal, b) channel output signal.

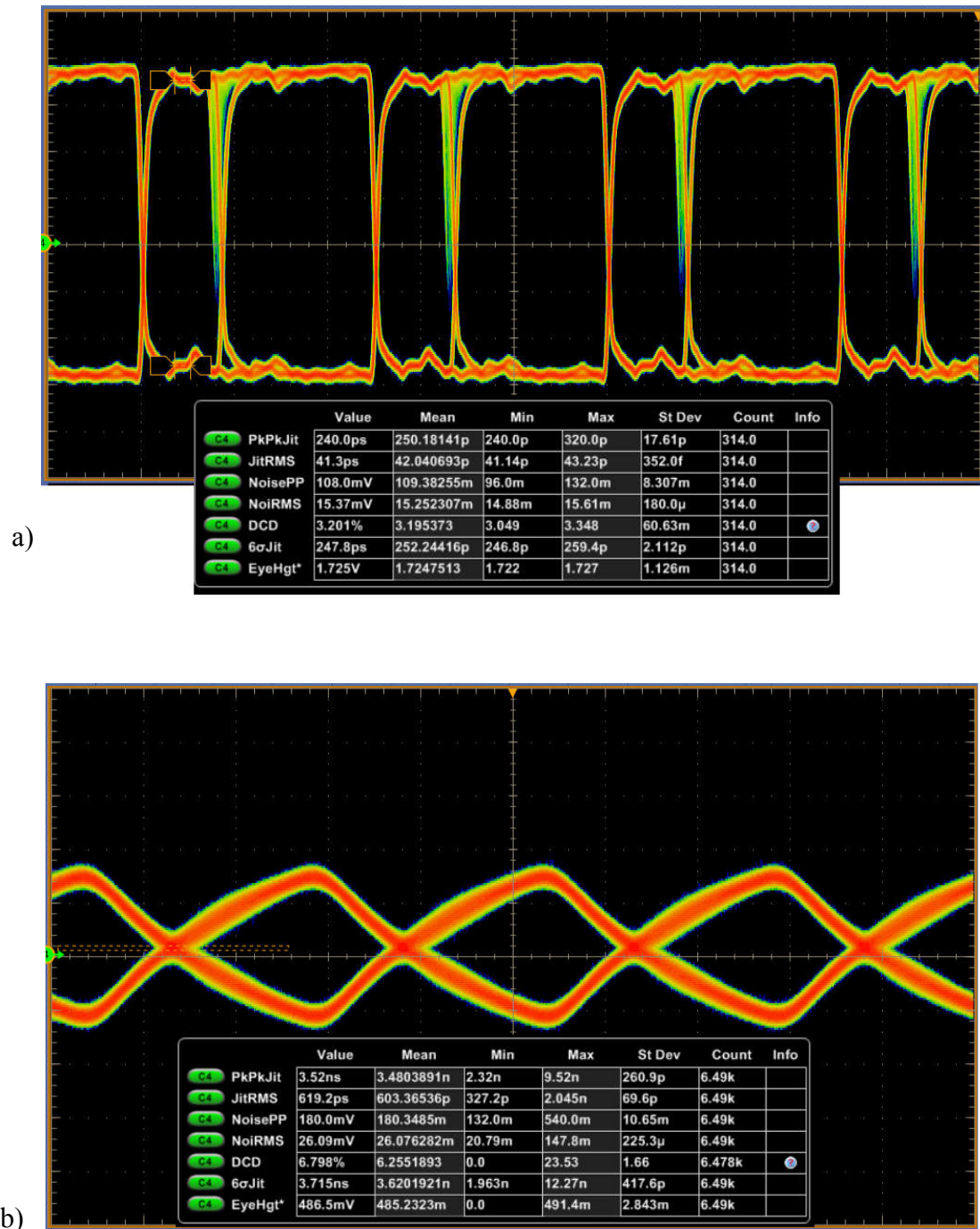


Fig. 7.5: Eye diagrams for PWM-2 signalling (200 Mbps): a) input signal, b) channel output signal.

In the second case the transmission rate was increased by more than 50 %. It is necessary to keep in mind that transmission channel completely closes eye diagram for conventional NRZ signalling. It is obvious that Nyquist frequency for higher transmission rates is situated in an area where channel losses reach almost 30 dB. A comparison of the performance of both signalling techniques show better results for PWM-2 pulse. Note that the eye height, eye width, jitter and noise parameters are completely better than in the case of PWM pulse, see Tab. 7.1 and 7.2. If both input pulses for PWM techniques are compared (only PCB trace from transmitter affects the

data signal) it can be seen that the basic parameters like the eye height and jitter are very similar. However, it is obvious that PWM-2 signal has signal amplitude reduction from initial 1.800 V to 1.497 V (16.83 % reduction) and PWM signal has signal amplitude reduction from initial 1.800 V to 1.520 V (15.56 % reduction). On the other hand comparison of both outputs eye diagrams brings better performance (+6,4 %) in eye height for PWM-2 signal. This confirms the correctness or reasoning that PWM-2 filter adjust signal shaping similarly as raised cosine approximation applied on PWM signal and thus signal goes through the channel with the same parameters with lower losses.

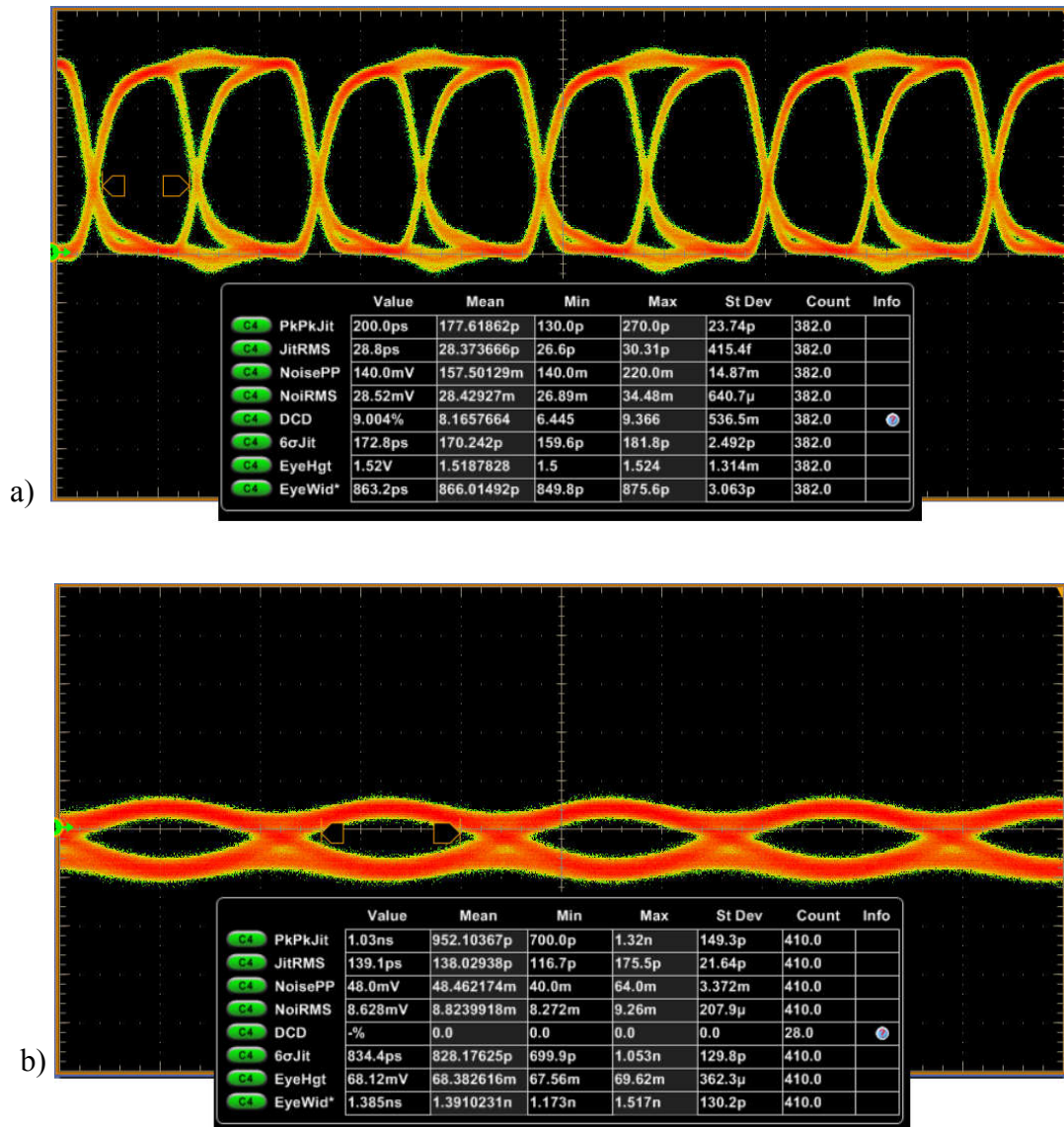
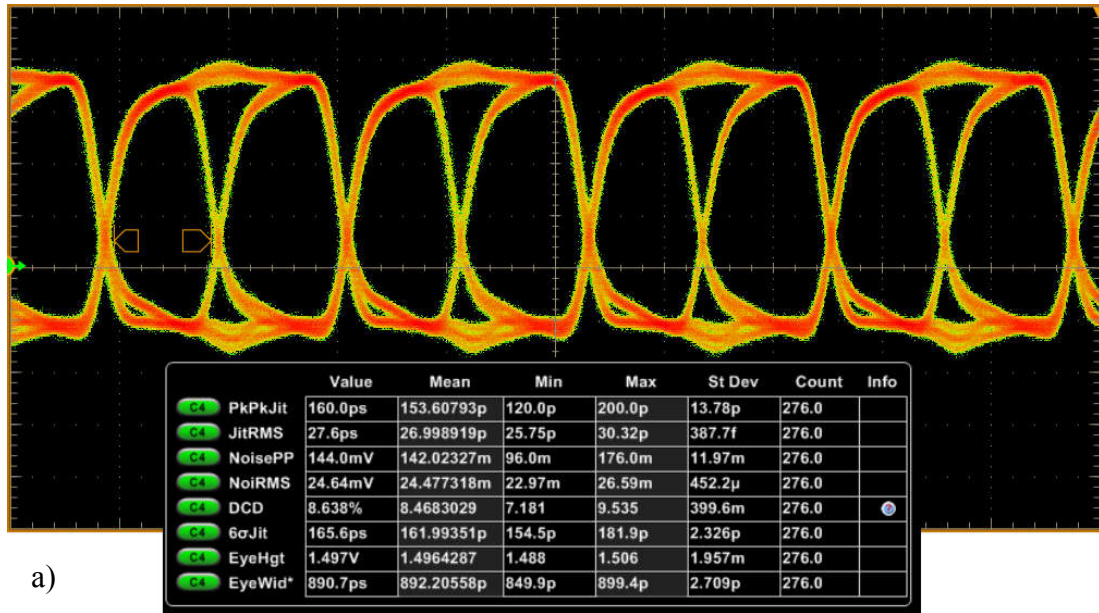
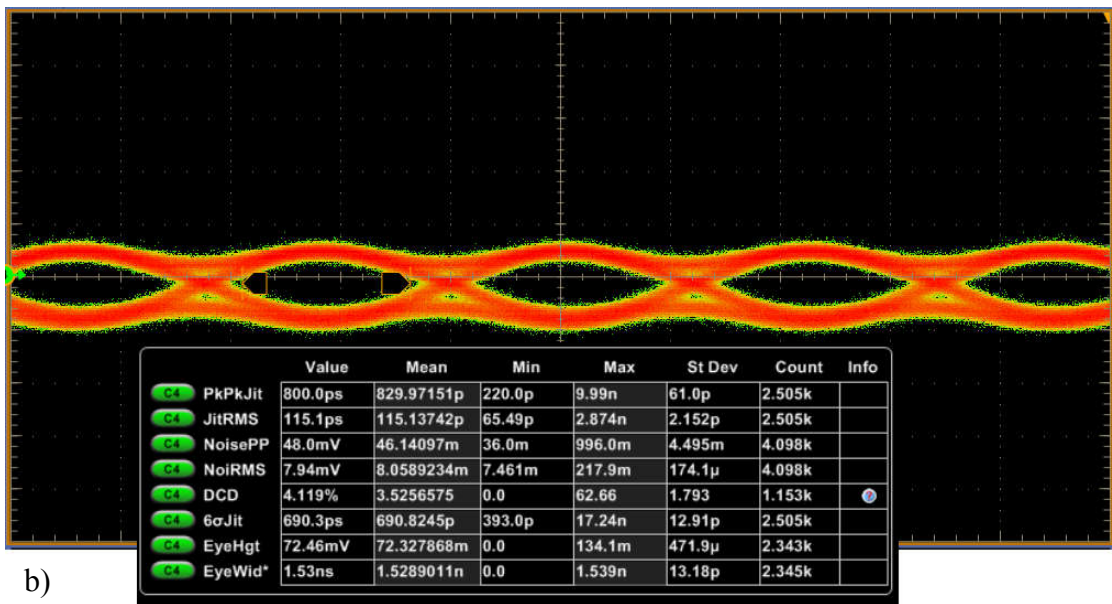


Fig. 7.6: Eye diagrams for PWM signalling (450 Mbps): a) input signal, b) channel output signal.



a)



b)

Fig. 7.7: Eye diagrams for PWM-2 signalling (450 Mbps): a) input signal, b) channel output signal.

Into the total overview of the equalization techniques performance there are also listed specific examples of strong pre-emphasis and 3-Tap FIR filter analysis. In the case of 3-Tap FIR filter built-in function of network analyzer to configure own setting for the filter was used. Thus, the overall performance of FIR filtering in comparison with PWM signaling techniques is a little bit impacted by fact that PWM signal generator is not situated directly at the analyzed channel input. Thus, a certain part of a PCB trace should be taken into the account as a part of transmission channel during analysis. In the case of FIR filtering the generated signal has parameters directly adjusted according to user setting in the built-in interface and increasing of transmission rate has no impact on

the pulse shaping at the input of the analyzed transmission channel. The effect of different signal shaping is obvious from comparison of input data streams for different transmission rates. Figure 7.8 illustrates the effect of strong pre-emphasis which can cause additional noise content in the data signal. Note how the noise RMS parameter has increased from 8.6 mV to 13.84 mV (increase by almost 61 %) while eye height parameter was strongly reduced from 68.1 mV to 42.8 mV (decrease by 37 %). The same worsening effect is observed also on other parameters of eye diagram like jitter increase by almost 25 %). It is obvious that result of better equalization is impacted by the quality of used clock circuits because ensuring of good synchronization of clock signals with input data signals play key role in the overall equalization performance.

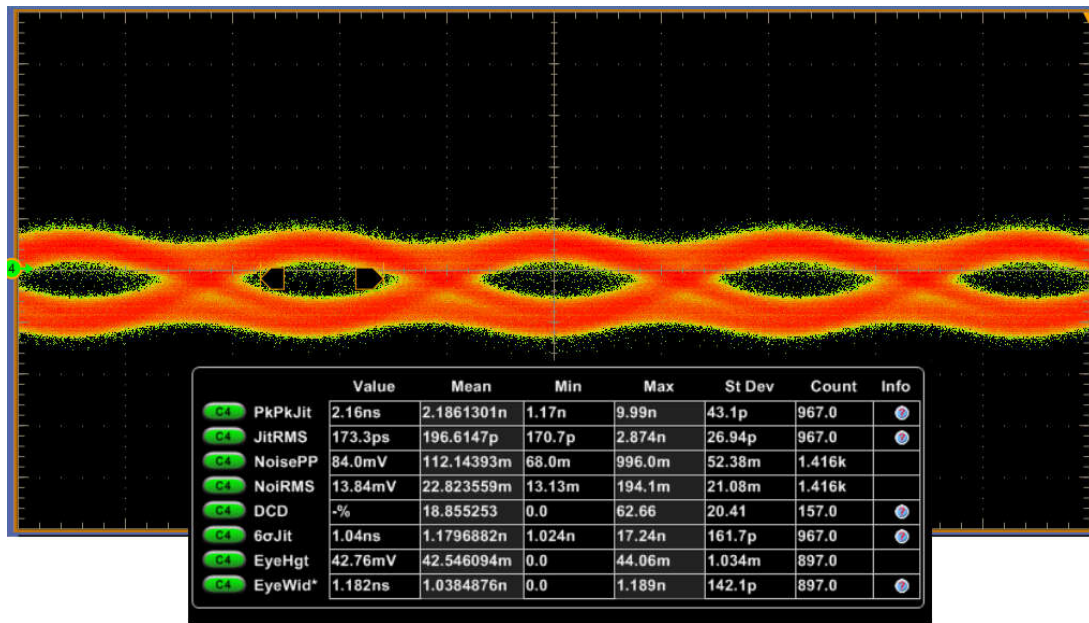


Fig. 7.8: Eye diagram for PWM signalling (450 Mbps) - strong pre-emphasis $dc = 50\%$.

The last eye diagram listed in Fig. 7.9 shows the channel output if the built-in 3-TAP FIR filter is used. Eye diagram shows better performance for jitter and eye width parameter than in the case of PWM signaling techniques. Eye height is relatively worse. It confirms the considerations that channel with higher losses on lower frequencies has no such impact on the rise of signal spreading over the more bit periods than in the case of channel usable for multi gigabits transmission rates where high frequency signal content is significantly more suppressed. It can be estimated better performance of PWM techniques in comparison with FIR filter during signaling over the multi gigabits transmission channel. Thus, another practical analysis in future will be focused also on research of effect of multi gigabits higher order channel on final equalization performance.

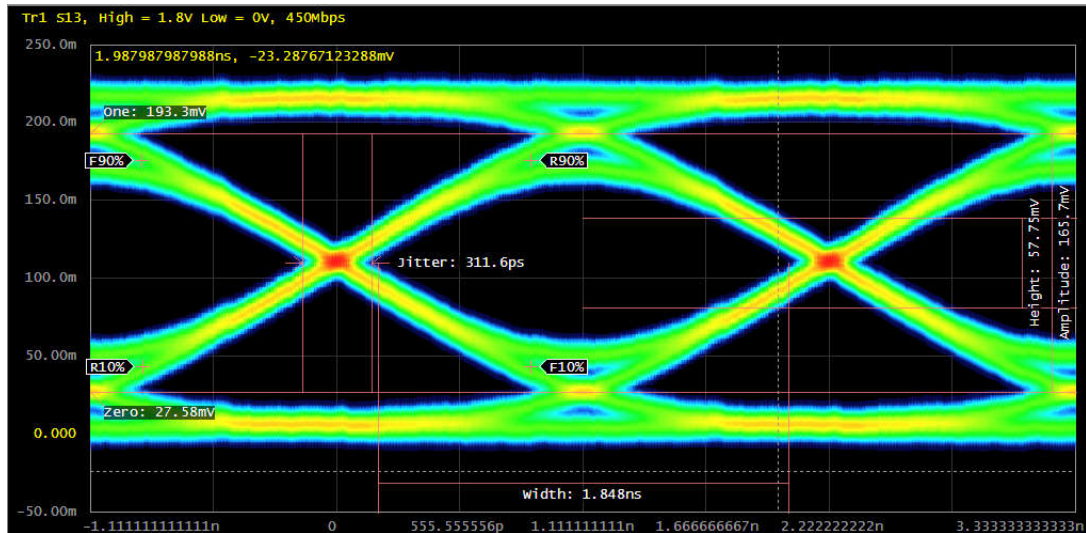


Fig. 7.9 Eye diagram for 3-TAP FIR signalling (450 Mbps) - optimal setting

Tab. 7.1: Performance of analyzed equalization techniques - 200 Mbps

	$dc = 64 \%$	$dc_1 = 28 \%, dc_2 = 90 \%$	
200 Mbps	PWM	PWM-2	PWM-2 Performance
Eye width [ps]	6787	7892	+ 16.3 %
Eye height [mV]	403.9	486.5	+ 20.6 %
Jitter RMS [ps]	580	619.2	- 6.8 %
Noise RMS [mV]	25.2	26.9	- 6.7 %

Tab. 7.2: Performance of analyzed equalization techniques - 450 Mbps

	$dc = 53 \%$	$dc_1 = 29 \%, dc_2 = 76 \%$	$dc = 50 \%$		
450 Mbps	PWM	PWM-2	PWM	3-TAP FIR	PWM-2 Performance
Eye width [ps]	1385	1530	1182	1848	+10.5 %
Eye height [mV]	68.12	72.46	42.76	57.75	+ 6.4 %
Jitter RMS [ps]	139.1	115.1	173.3	62.31	+17.3 %
NoiseRMS [mV]	8.63	7.94	13.84	11.24	+8 %

7.4 Summary

In this chapter there were practically implemented both PWM and PWM-2 signaling methods and the final performance was compared together with conventional FIR filtering method. From the overall performance comparison better properties of PWM-2 technique during the overcoming of transmission channel losses can be deducted. In this case the conductive losses dominate in the transmission channel, see Fig. 7.10 for illustration of practical realization.

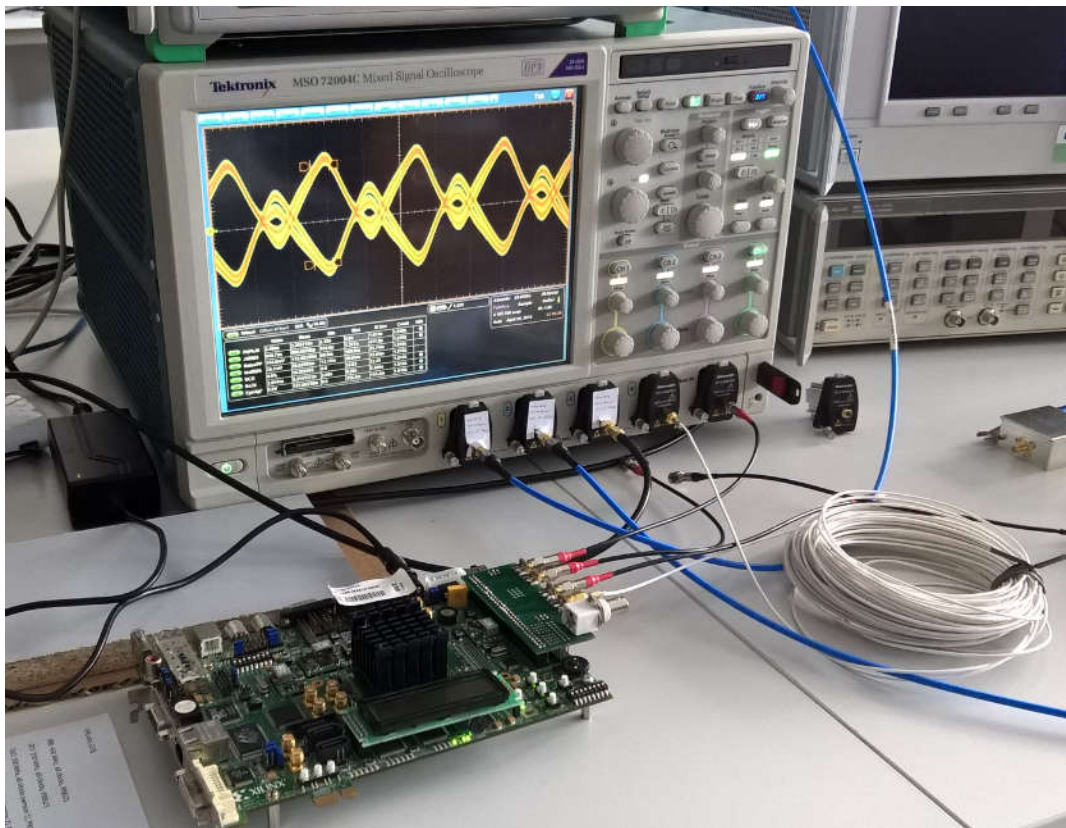


Fig. 7.10: Practical implementation - eye diagram for PWM signalling (450Mbps) - weak pre-emphasis $dc = 85\%$

In Tab. 7.1 is clearly demonstrated that during the lower transmission rates, where can be expected less channel low pass effect, the performance of PWM-2 techniques is not better in all parameters. Especially higher jitter and noise content due to the more transitions in the PWM-2 signal is obvious. After increasing of transmission rate the low pass effect of transmission channel was increased significantly. Subsequently it can be seen that PWM-2 signaling is better adjusted for the higher channel losses.

8 RESEARCH CHALLENGES AND CONCLUSION

In this chapter doctoral thesis is summarized. The main goals of the doctoral thesis are divided into the following points:

- Development of perspective adaptive pre-emphasis techniques that are feasible to implement in modern high-speed CMOS processes according to new trends in low power consumption design. [88], [89].
- Optimization of the first order time-domain equalization techniques to achieve higher crosstalk immunity to achieve higher loss compensation in real PCB high-speed communication channels.
- Equalization of higher-order transmission channel with more complex transfer functions. Development of complex models of transmission channels which reflect the signal integrity issues that occur during high speed interconnection signaling. Extension of the new proposed scheme of PWM-RC equalization technique to the second order realization.
- Implementation of developed pre-emphasis algorithms to one complex MathCAD model for effective pre-design simulations of equalization techniques performance applicable in practice during high-speed interconnection design.
- Experimental implementations of proposed solutions and optimization of models based on the practical findings.

The first chapters of the doctoral thesis are focused on signal integrity problems which can occur during high-speed data transfer. A several models of high speed transmission channels have been analyzed. Based on the practice measurement on the development board from Texas Instruments the real channel characteristics for a few types of high speed transmission lines were obtain. It is obvious that PCB copper channels suffer from attenuation and dispersion effects which may ultimately reduce the quality of a transmitted signal. Especially for low cost PCB transmission lines is typically use of inexpensive materials for dielectric and low quality fabrication of micro strip lines. Thus, the channel losses can achieve fairly soon tens of decibels at frequencies which correspond with Nyquist frequencies for data rates from gigabits to tens of gigabits, see practice results achieved in Fig. 2.8 where PCB channels primarily for testing of performance of conventional techniques are analyzed. It is evident that there is a very small border between sufficient signal quality at the channel output and the maximum achievable bit rate. Seemingly sufficient transmission channel e.g. for 5 Gbps rate may be unusable for higher transmission rate e.g. 30 % higher transmission rate. It is important to realize that this is not just about overcoming the exponentially growing losses but additional signal discontinuities effects can occur at higher frequencies. Thus, the data signal must overcome far more lossy environments with additional signal integrity issues such as additional reflections or resonant frequency notches in detail analyzed in Chapter 6.

Other part of the doctoral thesis deals with perspective time-domain pre-emphasis technique usable as an adequate substitute of conventional equalization technique which are not compatible with current requirements for low power CMOS design. Thus, the timing resolution instead of an amplitude resolution is used. The beginning of the work is greatly inspired by the results achieved in [16]. However, the conventional time-domain equalization technique due to the exhibition of more high frequency noise content in data signal can be in practice less powerful than expected results from theoretical simulations. These assumptions were verified during the practical implementations where strong pre-emphasized conventional PWM pulse was tested. It was found that additional loss compensation is not possible because eye diagram opening was significantly reduced by the own noise produced by PWM filter. The additional content of many high-frequency harmonic components which is strongly dependent on low-frequency content in the data signal can cause problems with implementation in high-speed channels with crosstalk susceptibility. Thus, in the main part of the Chapter 4, the novel PWM-RC scheme is proposed, original own contributions are listed in [82], [83]. In comparison with the conventional PWM method, the frequency-domain analysis shows better performance of proposed method for equalization of transmission channels where the attenuation is not monotonically increasing. Additional variability due to the possibility of edge pulse shaping allows to achieve higher frequency loss compensation. This key findings can play a critical role for optimal pre-emphasis setting to achieve better eye opening at the channel output. For example, the weak pre-emphasis can be sufficient to low-frequency content compensation but the compensation for high-frequency content is not still sufficient. The solution for the conventional PWM method is to increase the amount of pre-emphasis and it also boosts high-frequency noise. Furthermore, a better signal to noise ratio (SNR) is required. Using an advanced model of higher-order PCB channel based on measured results with differential transmission line implemented in Agilent ADS studio, successful transmission of a 2-PAM 5 Gbps data signal is demonstrated for PWM-RC scheme. The proposed equalization method triples the frequency at which the eye closes completely from 0.8 GHz to 2.5 GHz,. In the case of conventional PWM filter the reduction in the loss variation allows only shifting the frequency at which the eye closes completely from 0.8 GHz to 1.8 GHz. From the practical implementations realized in Chapter 7 it can be concluded that the PWM pre-emphasis is capable to compensate almost 30 dB of channel loss at $f_N=200$ MHz. It is obvious that pulse edge shaping may ultimately improve jitter parameters of output signal after passing through a lossy channel. It was confirmed during practical measurement was confirmed that the major effect on the overall eye diagram opening has just final pulse shaping on the channel output. Thus, the jitter parameter can be significantly reduced and better eye opening can be achieved with lower overall signal amplitude. Note that it was also found that raised cosine pulse and exponential pulse have tendency to increase BER during increasing of sampling error. Thus, the modified exponential edge pulse shaping was proposed and demonstrated. It is necessary to have in mind the fact that the overall performance of pulse-width modulation technique is strongly dependent on quality of synchronization of PWM clock signal with data signal. Especially, during the increasing of data rates, the synchronization problem can cause additional sampling error, which can be significantly reduced to a certain extent just by using optimized pulse edge shaping, see eye diagram outputs and results in section 4.8. The own publication focused on the pulse shaping optimalization and higher order channel functions are listed in [90], [91] and [92].

In Chapter 5 the novel pulse second order shaping was firstly introduced for high-speed chip-to-chip interconnects. The proposed signalling scheme is based on the results published in the connection with the search for the optimum edge pulse shaping. As can be listed in Fig. 5.2a using the second order PWM-2 scheme it is possible to achieve the channel output signaling which just corresponds with the proposed PWM-RC scheme. Especially during the fast signal transitions the effect of raised cosine shaping allows to achieve better results during the higher order channel compensation. In [93] is published similar idea which was coming out of author's original ideas published two years before in the works [90], [92]. In this paper it seems that some practical measurements were performed not quite right. The output simulation models of eye diagrams are not correspond with PWM shaping. The testing Xilinx kit listed in the work is not able to produce such high data transmission rates with pulse width modulated scheme. The outputs from the practical measurements show unreliable eye diagrams with additionally drawn axes. It confirms the fact mentioned in the previous sentence. In fact, the true measured results from implementation of PWM-2 scheme and detailed information from the performance analysis in the time-domain and frequency domain are listed only in this doctoral thesis. The presented results in Chapter 7 clearly show the parameters of the analyzed transmission channel and the presented eye diagrams show clearly the parameters of the analyzed signal. Also Fig. 7.10 clearly demonstrates that the proposed PWM-2 scheme was truly implemented. As can be seen from the performance comparison of PWM techniques listed in Tab. 7.1 and Tab. 7.2 the proposed PWM-2 scheme is able to achieve better eye opening at the Nyquist frequency of the transmitted pulse which corresponds with current channel losses about 35 dB. It is obvious that conventional PWM scheme does not achieve higher loss compensation than 30 dB and during the compensation of the 35 dB channel losses the eye diagram shows worse result than in the case of PWM-2 filter. In Fig. 7.8 is clearly demonstrated that additional strong pre-emphasis is not able to improve the eye opening and additional noise content is generated. The PWM-2 scheme shows additional potential in future testing because the maximum dc coefficients settings are not achieved, especially dc_2 coefficient set to only 76% has a reserve for compensation of pulses with longer tails. According to realized simulation, the maximum limit of loss compensation should be around more than 40 dB.

The original contributions of the doctoral thesis are

- The discovery that by applying modified PWM-RC scheme to wireline equalization the maximal achievable loss compensation during the channel equalization can be improved by an average of 2 dB.
- The discovery that PWM-RC scheme can be optimized by using additional edge pulse shaping with achievable better endurance to the sampling errors.
- Advanced simulation scheme which shows better performance of eye opening if pulses based on raised cosine shaping are produced at the channel output.

- Implementation of previous findings into the new proposed second order PWM-2 signaling scheme with detail analysis of second order PWM-2 scheme in time domain and frequency domain.
- Practical experimental implementations of proposed PWM-2 scheme together with PWM scheme which confirms the discovery realized in the third point and realized simulations.
- 35 db channel loss compensation achieved by using higher order transmission channel

Recommendations for future work

- Practical implementations of PWM-2 pulse scheme on higher transmission rates together with higher order channel loss compensation.
- Possibility to extend PWM pre-emphasis to the systems which use multilevel signaling scheme.
- Other simulation work on the proposed higher order transmission channel which reflects possible signal integrity issues.

REFERENCES

- [1] HALL, S.H., HECK, H. Advanced Signal Integrity for High-Speed Digital Design. John Willey & Sons. New Yersey, 2009.
- [2] LUCKY, R.W., SALZ, J., WELDON, E.J. Principles of Data Communication. McGraw-Hill, 1968.
- [3] SANJAY, K., WINTERS, J. Techniques for high-speed implementation of nonlinear cancellation. *IEEE Journal on Selected Areas in Communications*, June 1991, vol. 9, no. 5, pp. 711–717.
- [4] YUMINAKA, Y., YAMAMURA, K. Equalization Techniques for Multiple-Valued Data Transmission and Their Application. *IEEE Proc. 37th International Symposium on Multiple-Valued Logic*, 2007, Freiburg im Breisgau, Germany, pp. 26 – 29.
- [5] CANIGGIA, S., MARADEI, F. Signal Integrity and Radiated Emission of High-Speed Digital Systems. John Willey & Sons. New Delhi, 2008.
- [6] HIGASHI, H., MASAKI, S., KIBUNE, M., MATSUBARA, S., CHIBA, T., DOI, Y., YAMAGUCHI, H., TAKAUCHI, H., ISHIDA, H., GOTOH, K., AND TAMURA, H. 5- 6.4 Gbps 12 Channel Transceiver with Pre-Emphasis and Equalizer. *Symposium on VLSI circuits*, June 2004, Honolulu, Hawaii, pp. 130-133.
- [7] JIN, L., LING, X. Equalization in High-Speed Communication Systems. *IEEE Circuits and Systems Magazine*, 2004, vol. 4, no. 2, pp. 4–17.
- [8] RUIFENG, S., PARK, J., O’MAHONY, F., AND YUE, C. P. A Low-Power, 20-Gb/s Continuous-Time Adaptive Passive Equalizer. *IEEE Symposium on Circuits and Systems*, May 2005, Cincinnati, Ohio, pp. 920–923.
- [9] GAI, W., HIDAKA, Y., KOYANAGI, Y., JIANG, J.H., OSONE, H., AND HORIE, T. A 4-Channel 3.125 Gb/s/ch CMOS Transceiver with 30dB Equalization. *Symposium on VLSI Circuits, Digest of Technical Papers*, 2004, Honolulu, Hawaii, pp. 138-141.
- [10] FARJAD-RAD, R., YANG, C. K., HOROWITZ, M., LEE, T. A 0.3- μ m CMOS 8-Gb/s 4-PAM Serial Link Transceiver. *IEEE Journal of Solid-State Circuits*, May 2000, vol. 35, no. 5, pp. 757-764.
- [11] YANG, C. K., FARJAD-RAD, R., HOROWITZ, M. A 0.5- μ m CMOS 4.0-Gbit/s Serial Link Transceiver With Data Recovery Using Oversampling. *IEEE Journal of Solid-State Circuits*, May 1998, vol. 33, no. 5, pp. 713-722.

- [12] ŠEVČÍK, B. High-Speed Serial Differential Signaling Links with Commercial Equalizer. In *Proceedings of 20th International Conference Radioelektronika 2010*, 2010, Brno, pp. 191-194.
- [13] MAXIM INTEGRATED PRODUCTS, Designing a Simple, Small, Wide-band and Low-Power Equalizer for FR4 Copper Links. *Proceedings of DesignCon 2003*, 2003, Santa Clara, California, pp. 1-14.
- [14] ŠEVČÍK, B., BRANČÍK, L. Signal Integrity Problems in the Design of High-Speed Serial Communication Device. In *33rd International Conference on Telecommunications and Signal– 2010*, 2010, Baden near Vienna, Austria, pp. 426-431.
- [15] YUMINAKA, Y., TAKAHASHI, Y., AND HENMI, K. “Multiple-Valued Data Transmission Based on Time-Domain Pre-Emphasis Techniques in Consideration of Higher-Order Channel Effects,” *IEEE Proc. 39th International Symposium on Multiple-Valued Logic*, 2009, Okinawa, Japan, pp. 250-255.
- [16] SCHRADER, J. H. R. Wireline Equalization using Pulse-Width Modulation, Ph. D. Thesis, 2007, Netherlands.
- [17] GOODMAN, J. “High-Speed Inter-chip Signaling in CMOS,” Annual research report, Microsystems Technology Laboratories, Massachusetts, USA, 2000.
- [18] WENDEMAGEGNEHU, T. B, ALEKSIC, M. ”A Study of Optimal Data Rates of High-Speed Channels,” *DesignCon 2011*, Santa Clara, California, USA, 2011.
- [19] THIREAUF, S. C. High-Speed Circuit Board Signal Integrity. Artech House, Inc. London, 2004.
- [20] HATAMKHANI, H., YANG C. “A study of the optimal data rate for minimum power of I/Os,” *IEEE Trans. on CAS-II*, Vol. 3, no. 11, Nov. 2006
- [21] STOJANOVIC, V., HOROWITZ, M. Modeling and Analysis of High-Speed Links. *IEEE Custom Integrated Circuits Conference*, September 2003, San Jose, pp. 589-594.
- [22] ZERBE, J., WERNER, C., KOLLIPARA, R., STOJANOVIC, V. A Flexible Serial Link for 5-10Gb/s in Realistic Backplane Environments. *Proceedings of DesignCon 2004*, 2004, California, USA, pp. 215-286.
- [23] ŠEVČÍK, B, BRANČÍK, L. Analysis and Modeling of Signal Integrity Problems in the Serial Communication Devices. In *Proceedings of International Conference Mathematical Models for Engineering Science MMES'10*, November 2010, Puerto De La Cruz, Tenerife, Canary Islands (Spain): IEEE.AM, pp. 172-178.
- [24] KOLLIPARA, R., YEH, G. J, CHIA, B., AGARWAL, A. Design, Modeling and Characterization of High-Speed Backplane Interconnects. *Proceedings of DesignCon 2003*, 2003, California, USA, pp. 256-263.

- [25] WU, S. *ET AL*, Design of a 6.25-Gbps Backplane SerDes with Top-Down Design Metodology. *Proceedings of DesignCon 2004*, 2004, California, USA, pp. 115-123.
- [26] BRANČÍK, L., ŠEVČÍK, B. Time-Domain Simulation of Nonuniform Multiconductor Transmission Lines in Matlab. *International Journal of Mathematics and Computers in Simulation*, 2011, vol. 5, no. 2, pp. 77-84.
- [27] BRANČÍK, L., ŠEVČÍK, B. Modeling of Nonuniform Multiconductor Transmission Lines via Wendroff Method. In *Proceeding of the International Conference on Mathematical Models for Engineering Science (MMES 10)*, 2010, Puerto De La Cruz, Tenerife, Canary Islands, Spain, pp. 130-133.
- [28] BRANČÍK, L., ŠEVČÍK, B. Computer Simulation of Nonuniform MTLs via Implicit Wendroff and State-Variable Methods. *Radioengineering*, 2011, Brno, vol. 20, no. 1, pp. 221-227.
- [29] BRANČÍK, L., ŠEVČÍK, B. Simulation of MTLs via Wendroff Method Combined with Modified Nodal Analysis. In *Proceedings of 21st International Conference Radioelektronika 2011*, 2011 Brno, Czech Republic, pp. 207-210.
- [30] ŠEVČÍK, B. Modeling Adaptive Techniques in High-Speed Communication Systems. In *Proceedings of the 16th Conference Student EEICT*, 2010, Brno, Czech Republic, vol. 4, pp. 42-47.
- [31] ULRYCH, J. Problematika integrity signálů ve smíšených elektronických systémech. Brno: Vysoké učení technické v Brně, Fakulta elektrotechniky a komunikačních technologií, 2007. 71 s. Vedoucí diplomové práce doc. Ing. Lubomír Brančík, CSc.
- [32] LEE, M. J. E., DALLY, W. J., AND CHIANG, P. Low-Power Area-Efficient High-Speed I/O Circuit Techniques. *IEEE Journal of Solid-State Circuits*, November 2000, vol. 35, pp. 1591-1599.
- [33] DALLY, W. J. AND POULTON, J. Transmitter Equalization for 4 Gb/s Signaling. *IEEE Micro*, Jan.-Feb. 1997, vol. 17, no. 1, pp. 48-56.
- [34] V. BALAN, V., J. CAROSELLI, J., CHERN, J.-G, CHOW, C. ET AL. A 4.8-6.4Gbps Serial Link for Backplane Applications Using Decision Feedback Equalization. *IEEE Journal of Solid-State Circuits*, September 2005, vol. 40, no. 9, pp. 1957-1967.
- [35] STONICK, J. T., WEI, G. Y., SONNTAG, J. L., AND WEINLADER, D. K. An Adaptive PAM-4 5-Gb/s Backplane Transceiver in 0.25 μm CMOS. *IEEE Journal of Solid-State Circuits*, March 2003, vol. 38, no. 3, pp. 436-443.

- [36] ZERBE, J. L., WERNER, C.W., STOJANOVIC, V., CHEN, F. ET AL. Equalization and Clock Recovery for a 2.5–10-Gb/s 2-PAM/4-PAM Backplane Transceiver Cell. *IEEE Journal of Solid-State Circuits*, Sep. 2003, vol. 38, no. 12, pp. 2121–2130.
- [37] KUDOH, Y., FUKAISHI, M., AND MIZUNO, M. A 0.13- μm CMOS 5-Gb/s 10-m 28 AWG Cable Transceiver with No-Feedback-Loop Continuous-Time Post-Equalizer. *IEEE Journal of Solid-State Circuits*, May 2003, vol. 38, no. 5, pp. 741–746.
- [38] CHOI, J. S., HWANG, M. S., AND JEONG, D. K. A 0.18- μm CMOS 3.5-Gb/s continuous-time adaptive cable equalizer using enhanced low-frequency gain control method. *IEEE Journal of Solid -State Circuits*, Mar. 2004, vol. 39, no. 3, pp. 419–425.
- [39] MAILLARD, X. Novel circuits and principles for inter-chip communication. PhD. thesis, Vrije Universiteit Brussel, 2005.
- [40] PROAKIS, J. G. Digital Communications. 3rd ed. New York: McGraw-Hill, 1995.
- [41] STOJANOVIC, V., HO, A., GARLEPP, B., CHEN, F. ET AL. Adaptive Equalization and Data Recovery in a Dual Mode (2PAM/4) Serial Link Transceiver. In *Symposium on VLSI Circuits, Dig. Tech. Papers*, Honolulu, Hawaii, Jun. 2004, pp. 348–351.
- [42] ŠEVČÍK, B., BRANČÍK, L., KUBÍČEK, M. Analysis of Pre-Emphasis Techniques for Channels with Higher-Order Transfer Function. *International Journal of Mathematical Models and Methods in Applied Sciences*, vol. 5, 2011, pp. 433–444.
- [43] SCHRADER, J., KLUMPERINK, E., AND NAUTA, B. Wireline Equalization Using Pulse-Width Modulation. In *Proceedings of 2006 Custom Integrated Circuits Conference (CICC)*, San Diego, California, 2006, pp. 591–598.
- [44] COUCH, L. W. Digital and analog communication systems. Prentice-Hall, 2001.
- [45] ŠEVČÍK, B., DVOŘÁK, R., ŠPORIK, V. Analysis of Time-Domain Pre-Emphasis Method for High-Speed VLSI systems. In *Proceedings of the 17th Conference Student EEICT*, Brno, Czech Republic, vol. 4, 2011, pp. 42–47.
- [46] NORTE, D. The Impact of Signal Jumping from a Reference Ground Plane to a Different Reference Ground Plane on Signal Integrity with a High-Impedance Load. *The Signal and Power Integrity Institute*, 2008.
- [47] JOHNSON, H., GRAHAM, M. High-Speed Digital Design: A Handbook of Black Magic. Prentice Hall, 1993

- [48] ŠEVČÍK, B., BRANČÍK, L. Comparative Study of Transmitter Pre-Emphasis Methods for More Complex Channel Transfer Function. In *Proceedings of Electronic Devices and Systems EDS11 IMAPS CS International Conference 2011*, Brno, 2011.
- [49] ŠEVČÍK, B., BRANČÍK, L. Application of Pulse-Width Modulated Pre-Emphasis in Closely-Spaced Transmission Lines with Additional Discontinuities. In *Proceedings of International Conference on Computer as a Tool Eurocon 2011*, Lisboa, Portugal, 2011, pp. 110-114.
- [50] ŠEVČÍK, B., BRANČÍK, L. Adaptive Time-Domain Pre-Emphasis Techniques for High-Speed VLSI Systems. In *Proceedings of 21st International Conference Radioelektronika 2011, Brno, Czech Republic*, 2011, pp. 315-318.
- [51] SCHINKEL, D., MENSINK, E., KLUMPERINK, M., TUIJL, A. M., AND NAUTA, B. A 3-Gb/s/ch Transceiver for 10-mm Uninterrupted RC-Limited Global On-Chip Interconnects. *IEEE Journal of Solid-State Circuits*, vol. 41, no.1, Jan. 2006, pp. 297–306.
- [52] RAZAVI, B. Design of analog CMOS integrated circuits. McGraw-Hill, 2001.
- [53] WESTERGAARD, P., DICKSON, T.O., AND VOINIGESCU, S.P. A 1.5V 20/30 Gb/s CMOS Backplane Driver with Digital Pre-Emphasis. In *Proc. IEEE Custom Integrated Circuits Conf. (CICC)*, Oct. 2004, pp. 23–26.
- [54] PROKOP, R. Modular approach to design of modern analog devices in CMOS technology. *Doctoral (Ph.D.) Thesis*. Dept. Of Microelectronics FEEC BUT Brno, Czech Republic, 2009, p. 1-98.
- [55] YUMINAKA, Y., HENMI, K. Data-Dependent Time Domain Pre-emphasis Techniques for High-Speed Data Transmission. International Symposium on Communications and Information Technologies (ISCIT), Tokio, Japan, 2010, pp. 1103-1107.
- [56] BIOLEK, D., SENANI, R., BIOLKOVA, V., KOLKA, Z. Active Elements for Analog Signal Processing: Classification, Review, and New Proposal. *Radioengineering*, 2008, vol. 17, no. 4, pp. 15 – 32.
- [57] ŠOTNER, R., ŠEVČÍK, B., SLEZÁK, J., PETRŽELA, J., BRANČÍK, L. Sinusoidal Oscillator based on Adjustable Current Amplifier and Diamond Transistors with Buffers. *Przegląd Elektrotechniczny*, 2011, vol. 87, no. 1, s. 266-270.
- [58] ŠOTNER, R., ŠEVČÍK, B., BRANČÍK, L., DOSTÁL, T. Multifunctional Adjustable Biquadratic Active RC Filters: Design Approach by Modification of Corresponding Signal Flow Graphs. *Przegląd Elektrotechniczny*, 2011, vol. 87, no. 2, p. 225-229.

- [59] ŠOTNER, R.; JEŘÁBEK, J., ŠEVČÍK, B.; DOSTÁL, T., VRBA, K. Novel Solution of Notch/ All-pass Filter with Special Electronic Adjusting of Attenuation in the Stop Band. *Elektronika Ir Elektrotechnika*, 2011, vol. 16, no. 4. Accepted. To be published in November 2011.
- [60] ŠEVČÍK, B., BRANČÍK, L. Application of Digital Potentiometers in Multifunctional Active Filters at Frequencies above 1 MHz. *International Journal of Microelectronics and Computer*, 2010, vol. 1, no. 2, pp. 138-146.
- [61] ŠEVČÍK, B. Modeling and Signal Integrity Testing of Digital Potentiometers. In *Proceedings of the 17th International Conference Mixed Design of Integrated Circuits and Systems MIXDES 2010*. 2010. s. 570-575.
- [62] ŠEVČÍK, B., BRANČÍK, L., KUBÍČEK, M., ŠOTNER, R. Adaptive Time Domain Pre-Emphasis Technique for Multi-Gigabit VLSI Systems Modeling and Signal Integrity Testing of Digital Potentiometers. In *Proceedings of the 18th International Conference Mixed Design of Integrated Circuits and Systems MIXDES 2011*. 2011. s. 560-565.
- [63] TEXAS INSTRUMENT, "3.125 Gbps LVDS Single Channel Buffers with Transmit Pre-emphasis and Receive Equalization family," User manual r01 16Mar07, Dallas, USA 2007 [Online]. Available: <http://www.ti.com/tool/ds25br100evk>.
- [64] ZHANG, L., WILSON, J., BASHIRULLAH, R., FRANZON, P., "Driver Pre-emphasis Techniques for On-Chip Global Bus," Int. Symp. on Low Power Electronics and Design, pp. 186-191, Aug. 2005
- [65] LIU, H., MOHAMMAD, I., FAN, Y., MORGAN, M. AND LIU, J., "A HDMI Cable Equalizer with Self-Generated Energy Ratio Adaptation Scheme," *IEEE Transactions on Circuits and Systems II*, vol. 56, pp. 595-599, Jul. 2009.
- [66] JOHNSON, H., GRAHAM, M.. *High-Speed Digital Design: A Handbook of Black Magic*. Prentice Hall, 1993.
- [67] HAMMERSTAD AND JENSEN, "Accurate models for microstrip computer aided design", IEEE MFTT-S Int. Microwave Symp. Dig., pp. 407- 409, May 1980.
- [68] DJORDJEVIC, A. R., BILJIC, R.M., LIKAR-SMILJANIC, VD., and T.K. Sarkar, "Wideband frequency-domain characterization of FR-4 and time domain causality," *IEEE Trans. Electromagnetic Compatibility*, vol. 43, no. 4, pp. 662-667, November 2001.
- [69] COPERICH, K.M., MORSE, J. Y, AND CANGELLARIS, A.C., "Physically consistent transmission line models for high-speed interconnects in lossy dielectric," *IEEE Trans. Adv. Packaging*, vol.25, no.2, pp. 129-135, May 2002.

- [70] BOIS, K, KIRK B., TSUK M. AND QUINT D. "Simple and accurate determination of complex permittivity and skin effect of FR4 material in Gigahertz regime," Proc. 2003 Electronic Components and Technology Conference, pp. 1277-1282, 2003.
- [71] BRIST, G., CLOUSER, S., HALL, S. AND LIANG, T. "Non-Classical Conductor Losses due to Copper Foil Roughness and Treatment," 2005 IPC Electronic Circuits World Convention, February 2005.
- [72] HALL, S., LIANG, T., HECK, H. AND SHZKIND, D. "Modelling requirements for transmission lines in Multi-Gigabit systems," 13' Tropical Meeting on Electrical Performance of Electronic Packaging, pp. 67- 70, October 2004.
- [73] SHLEPNEV, Y., NWACHUKWU, C., Roughness characterization for interconnect analysis. - Proc. of the 2011 IEEE International Symposium on Electromagnetic Compatibility, Long Beach, CA, USA, August, 2011, p. 518-523.
- [74] SHLEPNEV, Y., System and method for identification of conductor surface roughness model for transmission lines, Patent Pending, App. #14/045,392 filed on Oct. 3, 2013.
- [75] BEYENE, W., HAHM, Y.-C., REN, J., SECKER, D., MULLEN, D., SHLEPNE, Y. Lessons learned: How to Make Predictable PCB Interconnects for Data Rates of 50 Gbps and Beyond, DesignCon 2014.
- [76] LIANG, T., HALL, S., HECK, H. AND BRIST, G. "A Practical Method for Modeling PCB Transmission Lines with Conductor Surface Roughness and Wideband Dielectric Properties," *2006 IEEE MTT-S International Microwave Symposium Digest*, San Francisco, CA, 2006, pp. 1780-1783.
- [77] AUDET, J., CRANMER, G., ET AL, "Design Optimization for Isolation in High Wiring Density Packages with High Speed SerDes Links" Proc 56th Electronic Components and Technology Conf, May 2006.
- [78] ROWLANDS M. AND DAS R.N., "Manufacture and Characterization of a Novel FlipChip Package Z- interconnect Stack-up with RF Structures" IMAPS (International Microelectronics and Advanced Packaging Society) 40th International Symposium on Microelectronics, November, 2007.
- [79] ROWLANDS, M. "How Long is Too Long? A Via Stub Electrical Performance Study," DesignCon2009, Santa Clara, CA, February 2-5, 2009
- [80] DREWNIAK, JAMES L., ET AL, "Developing a "Physical" Model for Vias - Part II: Coupled and Ground Return Vias" Proc DesignCon 2007, February 2007.
- [81] ROWLANDS, M. AND DAS, R.N., "Electrical Performance of an Organic, Z- interconnect, Flip- Chip Substrate" 57th Electronic Components and Technology Conference proceedings, May 2007.

- [82] ŠEVČÍK, B. "Time-Domain Predistortion Method Based on Raised Cosine Signaling in Real Transmission Channels," *Active and Passive Electronic Components*, vol. 2012, no. 1, pp. 1-5, 2012.
- [83] ŠEVČÍK, B., BRANČÍK L. "Time-Domain Pre-Distortion Technique Using Raised Cosine Shaping for High-Speed Serial Signaling," *ElectroScope*, vol. 2011, no. 4, pp. 1-6, 2011.
- [84] BASHIRULLAH, R., LIU, W., CAVIN, R. "Cross-talk reduction for interconnect limited bus based on raised cosine signaling," *IEEE Interconnect Technology Conference*, pp. 66-68, 2001.
- [85] BEAULIEU, N. C., TAN, C. C. AND DAMEN, M. O., "A "better than" Nyquist pulse," *IEEE Commun. Lett.*, vol. 5, pp. 367–368, Sept. 2001.
- [86] ASSALINI, A., TONELLO, A. M. "Improved Nyquist Pulses," *IEEE Commun. Lett.*, vol. 8, pp. 87–89, Feb. 2004.
- [87] YUMINAKA, Y. "High-speed data transmission techniques using raised cosine signaling," *Key Engineering Materials*, vol. 459, pp.252-259, 2011.
- [88] FAYNEH, E. *et al.*, "4.1 14nm 6th-generation Core processor SoC with low power consumption and improved performance," *2016 IEEE International Solid-State Circuits Conference (ISSCC)*, San Francisco, CA, 2016, pp. 72-73.
- [89] HOMAYOUN, A. AND RAZAVI, B. "A Low-Power CMOS Receiver for 5 GHz WLAN," in *IEEE Journal of Solid-State Circuits*, vol. 50, no. 3, pp. 630-643, March 2015.
- [90] ŠEVČÍK, B., BRANČÍK, L., KUBÍČEK, M. Analysis of Pre-Emphasis Techniques for Channels with Higher-Order Transfer Function. *International Journal of Mathematical Models and Methods in Applied Sciences*, vol. 5, 2011, pp. 433-444.
- [91] ŠEVČÍK, B., BRANČÍK, L. Signaling Technique Using Inverse Exponential Function for High-Speed On- Chip Interconnects. *WSEAS TRANSACTIONS on COMMUNICATIONS*, 2015, roč. 14, č. 54, s. 470-476. ISSN: 1109- 2742.
- [92] ŠEVČÍK, B.; BRANČÍK, L.; ŠOTNER, R.; KUBÍČEK, M. Signaling Optimization Techniques to Reduce Jitter and Crosstalk Susceptibility. *International Journal of Microelectronics and Computer Science* (<http://www.journal.dmcs.pl/web/guest/home>), 2011, roč. 2, č. 3, s. 113-120. ISSN: 2080- 8755.
- [93] YUMINAKA, Y., ISHIDA S., HENMI, K. "A 2nd-Order PWM Pre-Emphasis Technique and its Experimental FPGA Implementation", *Key Engineering Materials*, Vol. 534, pp. 227-232, 2013.

CURRICULUM VITAE

MSc. Bretislav SEVCIK

Date of Birth: 06.04.1985
Place of Birth: Prostějov
Country of citizenship: Czech Republic
Marital status: Single
Disabled with special needs: None

Contact info:

Telephone: +420731692228
E-mail: bretislavsevcik@seznam.cz
Contact address: Jedovnická 6, 62800, Brno, Czech Republic

Work experience:

- 10/2011 - present** **ABB s. r. o. (Technology centre - sensor development)**
Profession: Project Manager, Sensor Designer
Country: Czech republic
- 10/2014 - 10/2016** **ABB s. r. o. and FEEC BUT Brno**
Systém chránění sítě VN s využitím senzorů proudu a
napětí se standardizovaným digitálním výstupem IEC
61850-9-2
(GAČR no. TA03010444)
Profession: Sensor Designer
Country: Czech republic
- 01/2015 - present** **FEEC BUT Brno**
Research of signal integrity at high-speed interconnects
(GAČR no. 15-18288S)
Profession: Singal integrity engineer
Country: Czech republic
- 01/2012 - 12/2012** **FEEC BUT Brno**
**Innovation of computer exercises in the subject Analog
Electronic Circuits**
(FRVŠ no. 2442/2012/G1)
Profession: Electrical Engineer, Project Leader
Country: Czech republic
- 01/2011 - 12/2014** **FEEC BUT Brno**
Innovative approaches to design communication chain
(FEKT-S-11-13)
Profession: Electrical Engineer
Country: Czech republic

01/2011 - 12/2011	FEEC BUT Brno Laboratory extension - modern analog circuits for the signal generation (FRVŠ no. 450/2011/G1) Profession: Electrical Engineer Country: Czech republic
01/2010 - 12/2010	FEEC BUT Brno Research of robust hardware solutions for wireless communication systems (FEKT-S-10-9) Profession: Electrical Engineer Country: Czech republic

Education:

2009 - present	Doctor of Philosophy (PhD), FEEC BUT Brno Electrical engineering, telecommunications and computer technologies Postgraduate studies at the Department of Radio Electronics, Study Programme: Electrical, Electronic, Communication and Control Technology Topic of dissertation thesis: Signal integrity optimization techniques for high-speed chips signalling.
2007 - 2009	Master's degree (MSc.) - inženýr (Ing.), FEEC BUT Brno Electrical engineering, telecommunications and computer technologies, Department of Radio Electronics, Study Programme: Electrical, Electronic, Communication and Control Technology Topic of master's thesis: Digitally controlled active second order electrical filters
2004 - 2007	Bachelors's degree (BSc) - bakalář (Bc.), FEEC BUT Brno Electrical engineering, telecommunications and computer technologies Department of Radio Electronics, Study Programme: Electrical, Electronic, Communication and Control Technology Topic of bachelor's thesis: Digitally television planimeter

Certificates/Licenses:

50/78Sb. Certificate

Knowledge and skills:

Czech Proficient / native speaker
 English Intermediate (B2)
 IT knowledge: Knowledge of Microsoft office programs (Word, Excel...), knowledge of electrical and machinery engineering programs (Altium Designer, Eagle, PSpice, Matlab, Mathcad, SolidWorks, ProEngineering...)
 Driving license: B

Interests: I'm interest in literature and software development

Selected publications in scientific journals:

ŠEVČÍK, B.; BRANČÍK, L. Signaling Technique Using Inverse Exponential Function for High-Speed On-Chip Interconnects. *WSEAS TRANSACTIONS on COMMUNICATIONS*, 2015, vol. 14, no. 54, pp. 470-476.

ŠEVČÍK, B. "Time-Domain Predistortion Method Based on Raised Cosine Signaling in Real Transmission Channels," *Active and Passive Electronic Components*, 2012, vol. 2012, no. 1, pp. 1-5.

ŠEVČÍK, B., BRANČÍK, L. "Time-Domain Pre-Distortion Technique Using Raised Cosine Shaping for High-Speed Serial Signaling," *ElectroScope*, 2011, vol. 2011, no. 4, pp. 1-6.

ŠEVČÍK, B.; BRANČÍK, L.; ŠOTNER, R.; KUBÍČEK, M. Signaling Optimization Techniques to Reduce Jitter and Crosstalk Susceptibility. *International Journal of Microelectronics and Computer Science* (<http://www.journal.dmcs.pl/web/guest/home>), 2011, vol. 2, no. 3, pp. 113-120.

BRANČÍK, L.; ŠEVČÍK, B. Computer Simulation of Nonuniform MTLs via Implicit Wendroff and State- Variable Methods. *Radioengineering*, 2011, vol. 20, no. 1, pp. 221-227.

ŠEVČÍK, B., BRANČÍK, L., KUBÍČEK, M. Analysis of Pre-Emphasis Techniques for Channels with Higher-Order Transfer Function. *International Journal of Mathematical Models and Methods in Applied Sciences*, 2011, vol. 5, pp. 433-444.

Selected publications in international conferences:

ŠEVČÍK, B., BRANČÍK, L. Application of Pulse-Width Modulated Pre-Emphasis in Closely-Spaced Transmission Lines with Additional Discontinuities. In *Proceedings of IEEE Region 8 International Conference on Computer as a Tool Eurocon 2011*, Lisboa, Portugal, 2011, pp. 110-114.

ŠEVČÍK, B.; BRANČÍK, L. Adaptive Time-Domain Pre-Emphasis Techniques for High-Speed VLSI systems. In *Proceedings of 21st International Conference Radioelektronika 2011*. Brno, Czech Republic, IEEE, 2011. pp. 123-126.

ŠEVČÍK, B.; BRANČÍK, L.; KUBÍČEK, M.; ŠOTNER, R. Adaptive Time-Domain Pre-Emphasis Technique for Multi-Gigabit VLSI Systems. In *Proceedings of the 18th International Conference MIXDES 2011 MIXED DESIGN OF INTEGRATED CIRCUITS AND SYSTEMS*. Gliwice, Poland: 2011. pp. 1-5.

ŠEVČÍK, B.; BRANČÍK, L. Comparative Study of Transmitter Pre-Emphasis Methods For More Complex Channel Transfer Function. In *Proceedings of IMAPS CS International Conference EDS 2011*. Brno, Czech Republic: 2011. pp. 115-121.

Patents and utility models:

PARAMETRIZABLE MERGING UNIT FOR SENSOR-BASED MEASUREMENT, AND METHOD TO OPERATE SUCH UNIT, European patent application no. 15174648.4-1560, 2015

IMPEDANCE MATCHING ELEMENT FOR VOLTAGE AND/OR CURRENT SENSING DEVICES, U.S. application number 14/713,625, online to find here: <https://patentscope.wipo.int/search/en/detail.jsf?docId=EP153335750&redirectedID=true>

CURRENT AND/OR VOLTAGE SENSING DEVICE FOR INTEGRATIVE USE, International Application no.: PCT/EP2013/003127, online to find here: <https://patentscope.wipo.int/search/en/detail.jsf?docId=WO2014060106>

